Verification of Large Industrial Circuits Using SAT Based Reparameterization and Automated Abstraction-Refinement

Pankaj P. Chauhan

May 2007

CMU-CS-07-123

School of Computer Science
Carnegie Mellon University
Pittsburgh, PA 15213

Submitted in partial fulfillment of the requirements for the degree of Doctor of Philosophy.

Thesis Committee:
Prof. Edmund M. Clarke, Chair
Prof. Randal E. Bryant
Prof. James Hoe
Dr. Jin Yang, Intel

Copyright © 2007 Pankaj P. Chauhan

This research was sponsored by the Semiconductor Research Corporation (SRC) under contract no. 99-TJ-684, the National Science Foundation (NSF) under grant no. CCR-9803774, the Office of Naval Research (ONR), the Naval Research Laboratory (NRL) under contract no. N00014-01-1-0796, and the Army Research Office (ARO) under contract no. DAAD19-01-1-0485.

The views and conclusions contained in this document are those of the author and should not be interpreted as representing the official policies, either expressed or implied, of SRC, NSF, ONR, NRL, ARO, or the U.S. government.

Keywords: Model Checking, Image Computation, Quantification Scheduling, SAT, Bounded Model Checking, Parametric Representation, Abstraction-Refinement

For my parents.

Abstract

Automatic formal verification of large industrial circuits with thousands of latches is still a major challenge today due to the state space explosion problem. Moreover, BDD based algorithms are very sensitive to the variable ordering. Satisfiability (SAT) procedures have become much more powerful over the last few years, and hence they have been used in formal verification of large circuits with techniques like automated abstraction refinement and ATPG.

This thesis addresses the capacity challenge at multiple levels. First, at the core, I provide new algorithms for both BDD based and SAT based image computation. Image computation involves efficient quantification of variables from Boolean functions. I propose BDD based algorithms that use various combinatorial optimization techniques to obtain better quantification schedules, and in the later part, consider novel non-linear quantification schedules. The SAT based image computation uses algorithms for efficiently enumerating satisfying assignments to a Boolean formula, and for storing the enumerated assignments. Building upon this enumeration algorithm, I propose a novel SAT based reparameterization algorithm that increases the capacity of symbolic simulation by large extent. The reparameterization algorithm recomputes a much smaller representation for the set of states, whenever the size of the representation of state set becomes too large in symbolic simulation. These improvements help in bounded model checking of large systems, by allowing for much deeper depths. I demonstrate a 3x improvement in the runtime and space requirement over existing BMC algorithm and BDD based symbolic simulator on large industrial circuits. Finally, the reparameterization algorithm is incorporated in a SAT based automated abstraction-refinement framework. The reparamaterization algorithm can simulate much longer abstract counterexamples than previously possible. I then extract the refinement information from the simulation, completing the abstraction-refinement loop. Thus, contributions beginning at the core problem of image computation, through state space travesals and continuing all the way up to the abstraction-refinement are addressed in this thesis.

Acknowledgments

The old adage that your thesis advisor is the only adult besides your parents who mentors you for the longest period of time could not be truer in my case. Right from the beginning when Ed visited my undergraduate institution, he has been a constant source of inspiration and motivation. He would always have many problems you could work on, without worrying overly about the chance of success. The greatest virtue of Ed's group was the continued interaction with the brilliant group of visitors, post-doctoral students and graduate students that he would assemble from all over the world. Above all, Ed has always believed in me through out my long graduate studentship, and has been always there when I needed him in various ups and downs. I would like to express the deepest gratitude towards my *guru*, for everything that he blessed me with.

Any mention of Ed is incomplete without Martha. She has always been taking keen interested in the well being of Ed's students, and I was no exception, so I would like to say, thank you Martha. Thanks to the excellent support staff that Ed had, especially Keith and Denny, who made the life of Ed's group much easier. My heartfelt thanks to Sharon Burks, without whom CMU SCS is incomplete. She ties the whole school together, and is a "mother figure" for graduate students, faculty and every one else alike. Thanks also to Catherine Copetas and Deb Cavlovich.

Thanks to Somesh Jha and Helmut Veith for getting me started on real research at CMU. My work on BDD based image computation wouldn't have been possible without Somesh's suggestion and Helmut's guidance. Yuan got myself and Dong Wang started on abstraction refinement, to result in the first approach for automated abstraction refinement based on SAT. Helmut was again a mentor in that work. Thanks to Jim Kukula, Synopsys, we had a credible set of benchmarks for both image computation and abstraction-refinement. The core of my thesis, SAT based quantification procedure and the reparameterization algorithm, however were born out of discussions with and the subsequent guidance of Daniel Kröning. Thanks are also due to Amit Goel, whose DATE paper was a starting point for SAT-based reparameterization. He was a joy to collaborate with in the work we did on consistency of specifications, apart from being a good friend. Thanks also to Dong Wang, Samir Sapra, Shuvendu Lahiri, Ofer Strichman, and many others for enlightining discussions.

I would also like to thank my thesis committee members, Randy, Jin and James, for providing helpful and timely feedback throughout. Randy has always amazed me and I am sure most others with his sharp insight. Summer internships have always provided me with a varied and challenging learning environment, so thanks to my mentors Bob Kurshan at the then Bell Labs, Aarti Gupta and Pranav Ashar at NEC Labs, and Jin Yang at Intel. Special thanks to Sharad Malik, for his continued concern

and encouragement. Deep gratitude is also due to my funding sources, NSF, GSRC, SRC and CMU CSD, who made my studentship possible.

I have been fortunate enough to have great teachers, starting from my poor inner city primary school, through high-school, my undergraduate institute IIT Kharagpur, all the way to CMU. Most sincere thanks to my teachers and the institutes, without whom I would simply not be here.

My current employer Calypto also deserves a very special thanks. Anmol, Gagan, Nikhil, Deepak and others have provided a very stimulating, productive and supportive environment, not to mention the continued encouragement to finish up my thesis.

On a personal level, words can not describe my gratitude towards my parents. They always allowed me freedom to choose my own course in life, despite having many differences of opinions. I can never forget when dad helped me sneak to the train station to get to the IIT admissions counseling, where my fruitful higher education began. I also want to thank my brother Ashish and sister Priti for their love and support.

Thanks so much to Maithili, the woman behind this man, for always being there, taking care of Atharva, our son, and other things, and for making many sacrifices to put my research before everything.

I can never forget my friends and co-conspirators Chirag Parikh, Pragnesh Tewar, Malay Haldar, Sagar Chaki and others for putting up with me through and through.

Lastly, I am sure I am forgetting many who made a difference in my life, so apologies and sincere thanks to them.

Contents

1 Introduction **1**

1.1 Formal Verification Challenges 3

1.2 Image Computation and Reachability Analysis 6

1.3 Bounded Model Checking 9

1.4 Parametric Representation 11

1.5 Abstraction Refinement 14

1.6 Scope of the Thesis 15

1.6.1 Image Computation 16

1.6.2 SAT Based Reparameterization 17

1.6.3 Reparameterization for Abstraction-Refinement 19

1.7 Outline of the Dissertation 19

2 Image Computation and Reachability Analysis **21**

2.1 Heuristic Methods and Dependency Matrices 27

2.1.1 Minimizing λ is NP-complete 32

2.1.2 Ordering Clusters by Hill Climbing 33

2.1.3 Ordering Clusters by Simulated Annealing 34

2.1.4 Ordering Clusters Using Graph Separators 35

2.2 Non-linear Quantification Scheduling 38

2.3 Results for BDD Based Image Computation 44

2.4 SAT Procedures 51

2.5 SAT Procedures for Reachability Analysis 53

2.5.1 Efficient Implementation of SAT Based Reachability 56

2.5.2 Cube Enlargement 58

2.5.3 Efficient Set Representation 61

2.5.4 Complexity of the Set Representation 63
2.6 Results for SAT Based Reachability Analysis 66
2.7 Related Work 68
2.8 Summary 71

3 SAT Based Reparameterization Algorithm for Symbolic Simulation 73
3.1 Introduction 73
3.2 Parametric Representation 75
3.3 Reparameterization using SAT 80
3.3.1 Background 80
3.3.2 Computing h_i^1 and h_i^c 82
3.3.3 Computing h_i^0 and h_i^1 in a single SAT run 86
3.3.4 Incremental SAT 87
3.3.5 Extensions to Handle General Transition Relations 88
3.4 Checking Safety Properties 91
3.4.1 Safety Property Checking 91
3.4.2 Counterexample Generation 92
3.5 Experimental Results 93
3.6 Fixed-Points with Reparameterization 95
3.6.1 Set Union with an Auxiliary Variable 96
3.6.2 Fixed-Points by Using *Stall* Signal 97
3.7 Summary 99

4 SAT Based Reparameterization in an Abstraction-Refinement Framework 101
4.1 Introduction 101
4.2 SAT Based Abstraction-Refinement 104
4.2.1 Abstraction in Model Checking 104
4.2.2 Generation of Abstract State Machine 108
4.2.3 Bounded Model Checking in Abstraction-Refinement 113
4.2.4 Refinement Based on Scoring Invisible Variables 116
4.2.5 Refinement Based on Conflict Dependency Graph 117
4.3 Reparameterization in Abstraction-Refinement 122

4.4 Experimental Results for Refinement 123
4.5 Summary 129

5 Conclusions and Future Directions **131**

A Proof of Theorem 1 **135**

B Proof of Theorem 3 **139**

C Proof of Theorem 4 **149**

List of Figures

1.1 A counter state machine. 7

1.2 A circle in the xy plane. 12

2.1 Reachability algorithm 22

2.2 Hill climbing algorithm for minimizing λ 33

2.3 Simulated annealing algorithm to minimize λ 35

2.4 An ordering algorithm based on graph separators 37

2.5 Kernighan-Lin partition 37

2.6 Basic step of the VarScore algorithms 40

2.7 Dynamic VarScore algorithm in action. The dotted lines represent the BDDs in the set F at different iterations of the VarScoreBasicStep. 42

2.8 Basic DPLL backtracking search (used from [61] for illustration purposes) 52

2.9 Outline of the SAT based reachability algorithm 55

2.10 Procedure *ComputeSignature*. 62

2.11 Procedures *AddCube*. 64

3.1 High Level Description of the Reparameterization Algorithm 83

4.1 A counter state machine to illustrate abstraction and refinement. . . . 107

4.2 The counter state machine of Figure 4.1 encoded with 3 bits. 109

4.3 Approximation to the abstract state machine of Figure 4.2(B) obtained by pre-quantifying invisible variable v_3. 112

4.4 A spurious counterexample showing failure state [25]. No concrete path can be extended beyond failure state. 114

4.5 Two dependent conflict graphs. Conflict B depends on conflict A, as the conflict clause ω_9 derived from the conflict graph A produces conflict B. 118

4.6 The unpruned dependency graph and the dependency graph (within dotted lines) 119

4.7 Scatter plots of simulation time and total time. A point above the $y = x$ line (diagonal) is a win for the new algorithm, and a point below the line is a win for the FMCAD02 algorithm. 127

A.1 (a) An instance of Optimal Linear Arrangement, (b) its reduction to $\lambda - OPT$. The permutation v_1, v_2, v_3, v_5, v_4 is a solution to both. . . . 136

List of Tables

2.1 Correlation between various lifetime metrics and runtime/space for a representative sample of benchmarks. 45

2.2 Comparing FMCAD00, Kernighan-Lin separator (KLin) and Simulated annealing (SA) algorithms. (**MOut**)–Out of memory, (†)–SFEISTEL, (*)–8 reachability steps, (**)–14 reachability steps, (#)–13 reachability steps. The lifetimes reported are after the final ordering phase. 47

2.3 Comparing lifetimes for various methods 49

2.4 Comparing our three static algorithms VS-I, VS-II and VS-III against FMCAD00 and Simulated annealing (SA) algorithm. (**MOut**)–Out of memory, (†)–SFEISTEL, (*)–after 8 reachability steps, (**)–after 14 reachability steps. 50

2.5 Experimental results on a set of circuits from various sources including ISCAS'89 and Synopsys. The comparison is against [57]. Note: (*)-reachability was not complete. Empty boxes denote results N/A. . . . 67

3.1 Notations and Conventions. 78

3.2 Experimental Results on Large Industrial Benchmarks comparing plain BMC against SAT-based reparameterization. 94

4.1 Circuits used for abstraction-refinement experiment. 125

4.2 Comparison of SAT based reparameterization against plain SAT based simulation in abstraction-refinement framework. 126

Chapter 1

Introduction

Formal verification of hardware and software systems has come a long way over the years to become an integral part of the product life cycle. There are numerous examples of well publicized hardware and software errors, such as the historically famous FDIV bug in the Pentium processors (1994), the software glitch that led to the destruction of the NASA Orion-3 rocket (1998), the shutdown of the north-eastern US power grid (2003), or the shutdown of the BART commuter rail system in San Francisco Bay area (2005). It is then no surprise that formal analysis has found its most prominent use in finding errors in the systems. Apart from finding errors, formal analysis is used for proving the correctness of the system under consideration, for diagnosis of errors, for design, for planning and discovery, or to prove that the system meets certain specifications, such as timing requirements of various components on a chip. Hardware verification has already become an industry unto itself, with established EDA vendors, startups and internal R&D groups of chip makers providing tools for property verification, equivalence checking, directed simulation, and so on. The attractiveness of formal verification for hardware designers comes from the completeness of the formal verification with respect to state space exploration. Unlike

simulation and testing, formal verification analyzes each and every possible behavior of the system to provide an all inclusive proof of correctness. In the software verification, tools range from light weight static analysis tools such as Java Pathfinder and Coverity, to full blown model checkers such as SPIN, SLAM, and to classical Hoare style deductive proof engines such as NuPrl.

Formal methods [8, 29, 71] fall broadly under two categories, deductive methods, such as theorem proving [9, 41] and inductive methods such as model checking [24]. In theorem proving, a system and the specifications to be verified are modeled as axioms in a mathematical theory, and following a set of well founded inference rules, a deductive proof of the correctness is obtained, either automatically or by some human guidance. Theorem proving has traditionally been very effective in proving that a system satisfies certain specifications, and in dealing with infinite state systems. Hoare style proofs are used to prove the correctness of many fundamental algorithms, such as quick-sort. However, theorem proving usually requires a lot of human expertise. Moreover, if there is actually a bug in the system, demonstrating an error trace from the failure of the proof is often difficult. Model checking on the other hand is a technique where the state space of the system under considers is explored systematically in its entirety to reason about the property being verified. The system being verified is modeled as an automata, and the property to be verified is specified using certain mathematical logics, such as *linear temporal logic (LTL)* or *computation tree logic (CTL)*. Model checking is an automated method, that requires little or no user guidance. Moreover, model checking methods actually provide a counterexample trace if the property being verified does not hold for the system. This is a very useful diagnosis tool for system designers. Unlike theorem proving, an incomplete specification is easily accepted by model checking, allowing for an incremental development of both the model and the properties hand in hand with verification. However, model

checking techniques usually do not work well with infinite state systems. There have been many successful applications of model checkers, both industrial and academic.

1.1 Formal Verification Challenges

In spite of all the advances in formal verification, many challenges still need to be actively addressed. Active research, both from academia and industry alike, is being pursued on the following axes. As the primary focus of this thesis is on model checking, we will bias the discussion toward model checking.

Capacity

With ever increasing complexity of the systems, the size of the problems that need to be solved by formal verification tools grows exponentially. The increase in complexity results in the *state explosion* problem for model checking. Formal verification tools run on for days without producing any results, or run out of memory for many modern designs. The capacity limitations of model checkers and equivalence checkers often restrict their use to block level or even sub-block level verification. Moreover, it is often difficult to predict in advance whether a problem is tractable for formal verification tool or not. For example, a model checker may be able to prove some localized properties on a very large design, but may not be able to make progress on a much smaller design that has some *hard* operators, such as multipliers. The lack of predictability and capacity limitations of model checkers make it difficult to replace traditional simulation and testing from the design flow. Instead, formal verification is used to complement existing simulation and testing.

Usability

Another complaint against formal verification is the difficulty of use. Specifically, building a specification for the system, which will form the basis of verification often proves to be a daunting task for even the experienced users. The designers of the system are usually most knowledgeable about the system and its intended behavior, but they tend to be averse to using formal logics for specifying properties. The verification engineer on the other hand has the expertise of formal verification, but does not have the detailed system knowledge or specification. Efforts are being made to make easier to specify properties using derivatives of temporal logics such as IBM Sugar, PSL, or assertions in the hardware domain. In the software domain, executable specification languages such as Z and state charts are gaining popularity. Lightweight tools for software verification usually focus on certain classes of properties, such as null pointer dereference, or violation of locking discipline. These comprise more than 90% of errors found in software.

Lack of Completeness

Theorem proving and model checking both rely on a set of properties being specified, and the correctness of the system is checked with respect to those properties. However, the set of properties specified may not capture the full intent of the system specification. Formal verification tools only verify the system against given properties. For example, a verification engineer may specify all the properties related to the arithmetic and logical unit of a processor, but may not have enough specifications about the instruction fetch unit. The process of completely and faithfully translating an English language specification into a set of properties is a nontrivial task, often requiring substantial human expertise. Coverage metrics are used in the testing and

simulation domain, such as the number of lines covered by the simulation. However, given an LTL property, the coverage achieved by the property is difficult to define. One can think of a fraction of reachable states that satisfy a given property as a reasonable metric, but it does not relate well directly to the source code.

Lack of Diagnosis

Even though model checking provides a counterexample trace if a property fails, it is often difficult to pin-point the cause of the error. It would be very helpful to indicate a location or a set of locations in the source code that cause the error. Analysis of a counterexample to find the source of the error, and to fix the error, is usually a manual effort intensive process, requiring many iterations. Moreover, many a times, the error is usually caused by under-constrained environment. In that case, the environment constraints need to be refined.

Active research is being pursued to address all the challenges mentioned. In order to address the capacity issues, the following directions are being pursued. First, the fundamental data structures and algorithms used for state space exploration, such as BDDs [10] and SAT [63] engines, are continuously being improved. In *compositional reasoning* [42, 51], a large verification problem is broken down into smaller subproblems, and the proofs of correctness of the subproblems are assembled together to derive the correctness of the whole system. *Abstraction* has always been used to focus only on the relevant portion of the design for verifying a property. Abstraction has been a manual process, but significant advances [23] have been made to make the process of abstraction, and refinement of abstractions completely automatic. Next, bounded model checking [5] is used to verify that the system satisfy a given property for a bounded number of steps. If the bound is sufficiently large, than bounded model checking suffices to conclude that the property is always true. If one uses equivalence

checking for proving the functional correctness, one does not need to specify properties. However, a golden model needs to be established to compare a given design against. Establishing a golden model is a one time process, however, and one can devote enough resources to specify the correctness of the golden model in a complete manner. One a golden model is achieved, subsequent implementations can be checked for equivalence against the golden model, leveraging the effort spent in establishing the golden model in subsequent runs. In order to ease the diagnosis, sophisticated error trace analyzers [37] are used to pinpoint the cause of the error.

Next, we describe few important aspects of a successful verification tool, and briefly highlight the shortcomings in existing approaches.

1.2 Image Computation and Reachability Analysis

Consider the state transition system depicted in Figure 1.1. The transition system is a simple counter that counts from 0 to 3, upon receiving the input *count*. Let the counter begin in the state 0. After one transition, the counter could be either at state 1, or state 0, depending upon whether the input *count* was received or not. The *image* of a set of states under a transition relation is the set of states reachable from the given set of states in one transition. Thus, $\{0, 1\}$ is the image of the set of states $\{0\}$. Similarly, $\{0, 1, 2\}$ is the image of the set of states $\{0, 1\}$. *Pre-image* is the reverse of image. In the example, the pre-image of the set of states $\{0, 1, 2\}$ is $\{2, 1\}$. Intuitively, it denotes the set of states that can reach the given set of states in one transition. Formally, given a transition system $M = (S, R, S_0)$, where S is the set of states, $R(s, s')$ is the transition relation, and S_0 is the initial set of states, the

image of a set of states S_i is

$$\mathbf{Img}(S_i) = \{s' | \exists s \in S_i . R(s, s')\}. \tag{1.1}$$

Analogously, the *pre-image* operation is defined as

$$\mathbf{PreImg}(S_i) = \{s | \exists s' \in S_i . R(s, s')\}. \tag{1.2}$$

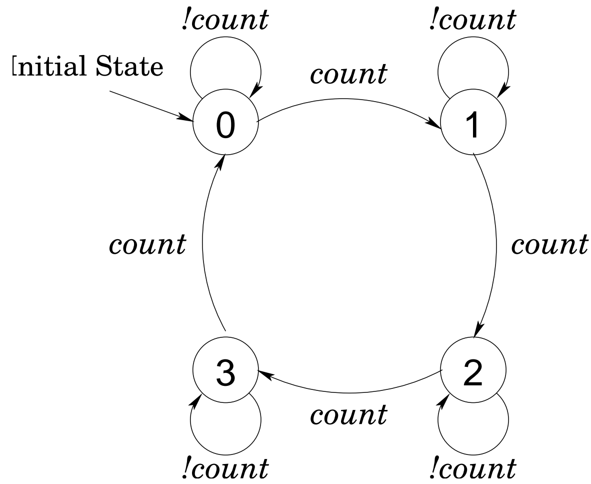

Figure 1.1: A counter state machine.

Image computation forms the core of all the state space traversal engines, including model checking and inductive invariant proofs. The foremost application that comes to mind is that of reachability, i.e., computing the set of states reachable from the set of initial states S_i. In out counter example, we can see that after one more image computation, we get the set of states $\{0, 1, 2, 3\}$, which is all the states in the state machine. Thus, we reach a fixed point, in fact, a least fixed point. In general, we keep on computing the union of the set of states after every image computation, and this process terminates when we reach a fixed point. Obviously, if the state space is infinite, a fixed point may never be reached. Formally, we can define the reachable

set of states as the fixed point of the following function.

$$f(x) = x \cup \mathbf{Img}(x).$$

To denote a least fixed point of a function $f(x)$, the notation $\mu x.f(x)$ from μ-calculus is often used. So, the set of reachable states is the fixed point

$$\mu x.(x \cup \mathbf{Img}(x)).$$

In model checking, there exists a fixed point characterization of all temporal logic operators. For example, the set of states satisfying the CTL property $\mathbf{EF}\, p$ is given by the following least fixed point at S_p, which is the set of states satisfying the atomic predicate p.

$$\mu x.(x \cup \mathbf{PreImg}(x)).$$

Since image computation is at the heart of model checking algorithms, it needs to be as efficient as possible. The algorithm used for image computation obviously depends on the underlying representation of the set of states and the transition relation, used by a model checker. However, one needs to provide an efficient quantification procedure for (pre) image computation, as per Equation 1.1 or Equation 1.2, no matter what representation is used. For BDD based image computation, one needs to quantify present (next) state variables and input variables for image (pre-image) computation. Moreover, instead of building a single monolithic BDD for the transition relation, implicitly conjoined BDDs for transition relations of individual state variables are commonly used. This is mostly done for capacity reasons, as building a single monolithic BDD for transition relation is often infeasible in practice. This representation is known as *conjunctively partitioned transition relation*. Synchronous systems, e.g., hardware designs, readily yield such conjunctively partitioned transition relations. For image computation, one needs to conjoin all the individual transition

relations and conjoin it with the BDD for the present state set. In order to avoid blow up in BDD sizes during image computation, state variables are quantified as soon as possible, in *early quantification*. We propose many new procedures for early quantification, that are superior to existing, static approaches for early quantification.

It is well known that while BDDs are compact representations of many functions, they unfortunately suffer from size explosion for many circuits. A BDD based model checker is like a black box. A slight change in circuit or variable order can make model checking infeasible. Moreover, there are some functions like multipliers, where the BDDs are always exponentially large in the number of variables. BDD based model checkers do not have a gradual degradation in performance, and the performance is often not predictable. Modern SAT solvers have become very powerful over the years, and thus provide an alternative to BDDs. Thus, we also offer a SAT based image computation and reachability procedure that is robust and degrades gradually. The runtime of our algorithm depends only on the size of the input circuit and on the longest shortest path between an initial state and any reachable state, commonly referred to as the diameter of the circuit. The existential quantification needed for image computation is carried out by enumerating satisfying assignments to SAT formulas and storing them in an efficient manner. The enumeration procedure for computing existential quantification is central to the SAT based image computation algorithm. This procedure also forms the core of reparameterization algorithms we propose later.

1.3 Bounded Model Checking

In regular model checking, image or pre-image computation is carried out until a fixed point, corresponding to the property being verified, is reached. Bounded model

checking on the other hand searches for counterexamples to a given LTL property within a certain bound k. For the simple counter shown earlier in Figure 1.1, let us consider the LTL property $\mathbf{AG}(counter < 3)$. This property is obviously false, and the path $0, 1, 2, 3$ is a counterexample to it. However, note that the shortest length of a counterexample is 4. If we were bounded model checking the LTL property with a bound of 3, we would not find a counterexample to the property. Bounded model checking was proposed by Biere et al. [5] to overcome the limitations of BDDs, just at the time when SAT procedures were becoming more powerful. In their formulation of bounded model checking for safety property $\mathbf{AG}\, p$, a propositional formula is built that corresponds to the given transition relation $R(s, s')$ being unwound for k transitions (the depth of the bounded model checking), starting from initial states $I(s_0)$, and the failure of the property is checked after the k time steps, i.e., the following propositional formula is built,

$$I(s_0) \wedge R(s_0, s_1) \wedge R(s_1, s_2) \wedge \ldots \wedge R(s_{k-1}, s_k) \wedge \neg p(s_k)$$

The formula above is satisfiable if and only if there exists a counterexample to the property of length k. A satisfying assignment to the above formula provides a trace in the state variables at times $0, 1, ..., k$ that violates the property. If there doesn't exist a counterexample to the property within k transition, the bound k is increased, and the same process is repeated, until either the SAT procedure runs out of resources, or sufficient depth is reached. The sufficient depth for a given transition relation and the given property is called *completeness threshold* [27, 28], which could be quite large in practice. The basic technique above can be extended to do inductive proofs as well. The inductive methods, such as proposed by Sheeran *et al.* [67], prove that if the property holds for k transitions starting from any state, then the property holds for $k + 1$ transitions as well. Coupling this with the proof of the property for the first k transitions, i.e., the transitions from the initial states, we get a complete

proof of the property.

Since the original paper on bounded model checking, apart from the sophistication in the bounded model checking itself, SAT solvers have come a long way. This has increased the scope of bounded model checking many fold. SAT based techniques outperform BDD based techniques for many classes of verification problems. Therefore, SAT based bounded model checking has become the preferred method for bug finding. A comprehensive survey of bounded model checking and SAT based verification techniques can be found in [6, 63]. A detailed comparison of various SAT based bounded and unbounded model checking techniques in an industrial setting is provided in [2].

Despite all the advances, certain limitations are still encountered in practice for bounded model checking. The main problem is that the difficulty of SAT problems keeps on increasing as the bound k for bounded model checking is increased. This limits the depth of the bounded model checking runs to a few tens of transitions at most in practice. The usefulness of BMC as a complete verification technique is jeopardized in the light of the fact that the completeness thresholds for most realistic designs are large. Sometimes, computing the completeness thresholds of the design is as hard as BMC itself. The technique of reparameterization that forms a large part of this thesis attempts to alleviate the problem of deeper BMC depths by re-encoding a set of states exactly as soon as the unrolled circuit becomes large.

1.4 Parametric Representation

Consider a circle of radius R in a 2-dimensional plane, centered at co-ordinates $(0, 0)$, shown in Figure 1.4. All the points (x, y) on the circle are described by the following

constraint.

$$x^2 + y^2 = R^2 \tag{1.3}$$

Even though this constraint describes the circle completely, it is not straight forward

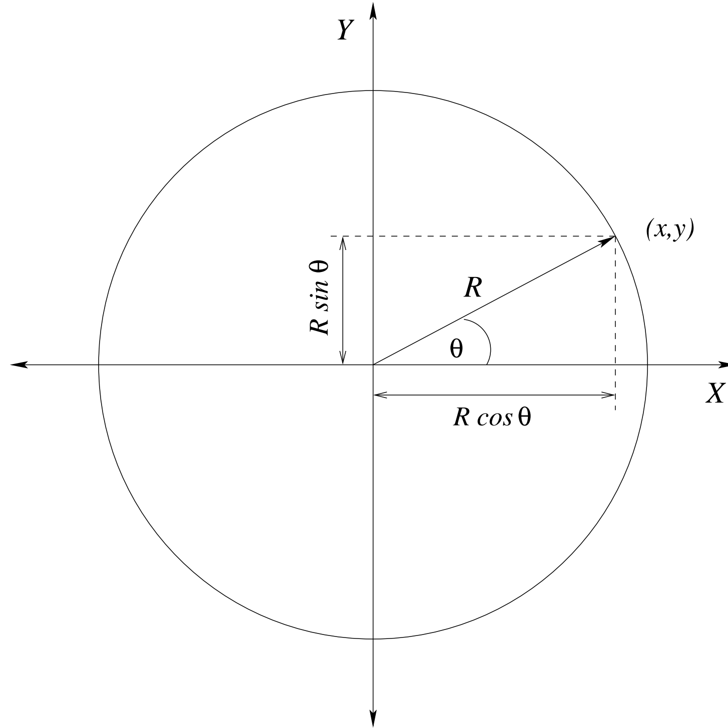

Figure 1.2: A circle in the xy plane.

to actually compute various points that lie on the circle. One can also view the Equation 1.4 above defining a set of points in a real plane that make up a circle. In that sense, Equation 1.4 can be referred to as a characteristic function of the circle.

On the other hand, circle is also described by the following two equations, which directly compute the value of the x and y co-ordinates respectively. Parametric representations can also be very compact compared to the characteristic function representation.

$$\left.\begin{array}{rcl} x & = & R \cdot \cos\theta \\ y & = & R \cdot \sin\theta \end{array}\right\} 0 \leq \theta \leq 2\pi$$

The two representations can also be carried over to the Boolean domain. Consider the set of states $\{01, 10\}$, with x_1 and x_2 as the state variables. We can represent this set of states using the characteristic function

$$(x_1 \wedge \neg x_2) \vee (\neg x_1 \wedge x_2).$$

The same set of states can be given by the parametric representation

$$x_1 = p, x = \neg p.$$

Here, p is a Boolean parameter. Note that parametric representation is not unique. For the same set of states, we can also use

$$x_1 = q_1 \wedge q_2, x_2 = \neg q_1 \vee \neg q_2,$$

which is not as compact as the first parametric representation. It can be easily shown that one can always have a parametric representation with n or fewer parameters for a set of vectors of n Boolean variables.

Parametric representations arise naturally in symbolic simulation, where a set of expressions describing the values of state variables is built by unrolling the circuit, as is done in BMC. After unrolling a circuit for k transitions, we have an expression for each state variable. Primary inputs for each transition, and state variables of each transition are the variables present in each expression. These variables can be seen as the parameters that make up the parametric representation for the set of states after k transitions. This parametric representation however is not compact, and it grows linearly with the number of transitions. The same set of states could be described compactly using n parameters or less, where n is the number of state variables. Coming up with compact, efficient parametric representations is a major part of this thesis. We propose novel SAT based method for reparameterizations. We show that using SAT based reparameterization, one can perform much deeper depth

BMC. The existing approaches to parametric representation are based on BDDs, and they suffer the usual drawbacks of BDD based methods. Specifically, as the number of transitions in an unrolling increases, the number of BDD variables increases. BDDs are much less robust to number of variables compared to SAT based methods, which is the primary advantage of our method.

1.5 Abstraction Refinement

Symbolic model checking has been successful at automatically verifying temporal specifications on small to medium sized designs. However, the inability of BDD based model checking to handle large state spaces of "real world" designs hinders the wide scale acceptance of these techniques. There have been advances on various fronts to push the limits of automatic verification. On the one hand, improving BDD based algorithms improves the ability to handle large state machines, while on the other hand, various abstraction algorithms reduce the size of the design by focusing only on relevant portions of the design. It is important to make improvements on both fronts for successful verification.

A conservative abstraction is one which preserves all the behaviors of a concrete system. Conservative abstractions benefit from a *preservation* theorem which states that the correctness of any universal (e.g. ACTL*) formula on an abstract system automatically implies the correctness of the formula on the concrete system. On the other hand, a counterexample on an abstract system may not correspond to any real path, in which case it is called a *spurious* counterexample. To get rid of a spurious counterexample, the abstraction needs to be made more precise via refinement. It is obviously desirable to automate this procedure.

In *Counterexample guided abstraction refinement* (CEGAR) [3, 23, 25, 36, 49, 62],

an abstract counterexample is checked for validity on the original transition system. If it is found to be invalid, then the abstraction is refined. SAT-based Unbounded model checking [53, 54] combines the ideas of bounded model checking, and abstraction refinement. It uses BMC on the abstract system to infer that no counterexamples exist of a certain depth, and then unsatisfiability proofs of BMC to derive the refinement. This thesis presents one of the earlier methods for SAT based CEGAR. Most abstraction-refinement methods, including our method, rely on an effective procedure for symbolic simulation of the original circuit, which could be very large. The SAT reparameterization algorithm we present is used to make deeper symbolic simulation efficient.

1.6 Scope of the Thesis

This thesis addresses the capacity challenge on multiple fronts. First, at the core, I provide new algorithms for both BDD based and SAT based image computation. The SAT based image computation uses an algorithm for enumerating satisfying assignments to a Boolean formula, and an efficient representation of the enumerated assignments. Building upon this enumeration algorithm, I propose a novel SAT based reparameterization algorithm that increases the capacity of symbolic simulation by a large extent. These improvements help in bounded model checking of large systems. Finally, the reparameterization algorithm is incorporated in a SAT based abstraction-refinement framework, thus providing completeness for safety and liveness properties. Thus, improvements beginning at the core problem of image computation and continuing it way up to the abstraction-refinement are addressed in this thesis.

1.6.1 Image Computation

We begin with new algorithms for BDD based image computation. I evaluate several new heuristics, metrics, and algorithms for the problem of quantification scheduling, central to BDD based image computation. The algorithms use combinatorial optimization techniques such as hill climbing, simulated annealing, and ordering by recursive partitioning to obtain better results than was previously the case. Theoretical analysis and systematic experimentation are used to evaluate the algorithms. In the second part of the project, I provide non-linear quantification scheduling. Until then, quantification scheduling in image computation, with a conjunctively partitioned transition relation, had been restricted to a linear schedule. This results in a loss of flexibility during image computation. We view image computation as a problem of constructing an optimal parse tree for the image set. The optimality of a parse tree is defined by the largest BDD that is encountered during the computation of the tree. We present dynamic and static versions of a new algorithm, *VarScore*, which exploits the flexibility offered by the parse tree approach to the image computation. We show by extensive experimentation that our techniques outperform the best known techniques so far.

Satisfiability procedures have shown significant promise for symbolic simulation of large circuits, hence they have been used in many formal verification techniques, including automated abstraction refinement, ATPG etc. I describe how to use modern SAT solvers like Chaff and GRASP to compute images of sets of states and how to efficiently detect fixed point of the sets of states during reachability analysis. Our method is completely SAT based, and does not use BDDs at all. The sets of states and transition relation are represented in clausal form, which can be processed by SAT checkers. The SAT checker subsequently generates the set of newly reached states in a clausal form as well. At the heart of our engine lie two efficient

algorithms. The first algorithm shortens the cubes that the SAT checker generates, which significantly reduces the number of cubes the SAT checker needs to enumerate. The second algorithm reduces the space required to store sets of states as a set of cubes by a recursive cube-merging procedure. The effectiveness of the SAT based image computation procedure is demonstrated on ISCAS sequential benchmarks for reachability. In particular, the algorithm does not have BDD size explosion surprises and deteriorates in a predictable manner. There are many improvements to be done to the enumeration procedure. A major improvement will be the use of non-clausal representation for state sets. The interpolation proof based approach [54] provides one possibility to explore.

1.6.2 SAT Based Reparameterization

I describe a SAT-based algorithm to perform the reparameterization step for symbolic simulation. The algorithm performs better than BDD-based reparameterization especially in the presence of many input variables. The algorithm takes arbitrary Boolean equations as input. Therefore, it does not require BDDs for the symbolic simulation. Instead, non-canonical forms that grow linearly with the number of simulation steps can be used. In essence, the SAT-based reparameterization algorithm computes a new parametric function for each state variable one at a time. In each computation, a large number of input variables are quantified by a single call to a SAT-based enumeration procedure [18, 53]. The advantage of this approach is two-fold: First, all input variables are quantified at the same time, and second, the performance of SAT-based enumeration procedure is largely unaffected by the number of input variables that are quantified. I demonstrate the efficiency of this new technique using large industrial circuits with thousands of latches. I compared it to both SAT-based Bounded Model Checking and BDD-based symbolic simulation. This new algorithm

can go much deeper than a standard Bounded Model Checker can. Moreover, the overall memory consumption and the run times are, on average, 3 times less than the values measured using a Bounded Model Checker. The BDD-based symbolic simulator could not even verify most of the circuits that we used. There are various research problems to be solved for using this algorithm for complete verification of safety and liveness properties.

Safety property checking requires generation of a SAT formula from reparameterized form. For the symbolic simulator, the counterexample generation is nontrivial, since we do not keep the whole simulation. Periodically, we reparameterize the representation and hence lose the information about input variables up to that point. I next provide algorithms for safety property checking and counterexample generation for the symbolic simulator. Invariant statements are often used to restrict the state space for verification. Such invariants are often called *verification conditions* [43]. The technique described so far assumes that the transition relation is given by a set of transition functions. It does not allow any arbitrary transition relation. I propose extensions to handle both invariant constraints and general transition relations.

The algorithm can also benefit from the improvements to the basic SAT-based enumeration algorithm. One limitation of the SAT-based enumeration algorithm is the clausal (CNF or DNF) representation it uses. There are certain class of Boolean functions which have no compact clausal representation. There has been some existing work in SAT based enumeration algorithms [44, 53, 68]. At present, the symbolic simulator handles only safety properties. Biere et al. [66] recently showed that checking for liveness properties can be done by a semantic translation to safety properties with auxiliary variables. I briefly explore the computation of fixed-points using my symbolic simulator.

1.6.3 Reparameterization for Abstraction-Refinement

Abstraction-refinement algorithms that simulate concrete systems benefit immensely from a powerful simulator. I use my symbolic simulation algorithm for simulating abstract counterexamples on concrete systems as in [19] or for doing BMC on concrete systems as in [55]. The refinement information in both approaches is obtained from the analysis of failed SAT instances (these correspond to spurious counterexamples, meaning the abstraction needs to refined). One issue with using reparameterization algorithm for refinement is that the SAT problem does not contain the information of the simulation from the initial state. The SAT problem only contains the trace from the last time frame when reparameterization was done to the length of the failed counterexample state. I investigate the effect of doing refinement based on such truncated counterexamples. Integrating my symbolic simulation with abstraction-refinement will allow complete model checking of safety properties. Along with the semantic translation of liveness properties to safety properties as in [66], handling liveness properties should also be possible.

1.7 Outline of the Dissertation

The first half of Chapter 2 proposes new algorithms for BDD based image computation that rely on novel quantification scheduling technique. In the second half of Chapter 2, we move on to SAT based image computation. The core of the SAT based forward image computation is a SAT based algorithm for existential quantification. The existential quantification algorithm is used as a building block for SAT based reparameterization for symbolic simulation, described in Chapter 3. The SAT based reparameterization algorithm allows us to simulate symbolically a circuit by periodically re-encoding the set of reachable states. Chapter 4 describes an impor-

tant application of the reparameterization algorithm, namely the simulation used to validate abstract counterexample on concrete machine in an automated abstraction-refinement framework. Finally, we conclude in Chapter 5, with directions for future research.

Chapter 2

Image Computation and Reachability Analysis

Computing the set of states reachable in one step from a given set of states under a transition relation forms the heart of many symbolic state exploration algorithms, including reachability analysis, model checking [21, 22, 24], etc. This operation is called *image computation*. Let us consider a state transition relation T over the set of states S. The set of states is defined by the set of valuations over a vector of state variables $\mathbf{x}$. We denote a set or a vector of variables in a boldface. The transition relation $T(\mathbf{x}, \mathbf{i}, \mathbf{x}')$ relates states defined by valuations of present state variables $\mathbf{x}$ and inputs $\mathbf{i}$ to states defined by valuations of next state variables $\mathbf{x}'$. Note that we are using characteristic functions $S(\mathbf{x})$ and $T(\mathbf{x}, \mathbf{i}, \mathbf{x}')$ to represent sets of states and sets of transitions respectively. The image of $S(\mathbf{x})$ under $T(\mathbf{x}, \mathbf{i}, \mathbf{x}')$ is given by the following equation.

$$Img(S(\mathbf{x}')) = \exists \mathbf{x}, \mathbf{i}. T(\mathbf{x}, \mathbf{i}, \mathbf{x}') \wedge S(\mathbf{x}) \tag{2.1}$$

Image computation is a major bottleneck in verification. In this chapter, we will present various methods for efficient computation of images, both with BDDs and with SAT solvers. For BDD based image computation, often it is infeasible to construct BDDs for the transition relation T and the set S. In SAT based image computation, we use propositional formulas in CNF with intermediate variables to represent these sets, often resulting in much a smaller representation. The definition of image computation involves evaluation of simple *quantified Boolean formulas* [18].

In reachability analysis, beginning with the set of initial states S_0, images are repeatedly computed until the set of states does not grow any more, in other words, the least fixed-point, beginning at S_0, given below is computed.

$$\mu X.(X \cup Img(X)) \tag{2.2}$$

Following simple algorithm computes this fixed-point.

REACHABILITY(S_0)

1 $S_{reach} \leftarrow \phi$

2 $S_0 \leftarrow \phi$

3 $i \leftarrow 0$

4 **while** ($S_i \neq \phi$) {

5 $\quad S_{reach} \leftarrow S_{reach} \cup S_i$

6 $\quad S_{i+1} \leftarrow Img(S_i) \backslash S_{reach}$

7 $\quad i \leftarrow i + 1$

8 }

9 **return** S_{reach}

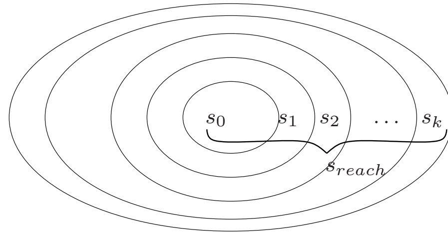

Figure 2.1: Reachability algorithm

In this algorithm, S_i denotes the set of newly discovered states in each iteration.

Once there are no more states to be discovered, we have reached a fixed-point.

As noted earlier, the sets of states and sets of transitions are traditionally represented by BDDs ([10,13,14,24]). Canonicity of BDDs and compactness of representation for many functions encountered in practice allows for very efficient fixed point checks. It is well known that while BDDs are compact representations of many functions, they unfortunately suffer from size explosion for many circuits. A BDD based model checker is like a black box. A slight change in circuit or variable order can make model checking infeasible. For example, arithmetic functions like adders need to have the inputs interleaved for linear sized BDD, while non-interleaved order leads to an exponential blowup in BDD size. BDD based model checkers do not have a gradual degradation in performance, and the performance is often not predictable. Thus, we also offer a SAT based image computation and reachability procedure that is robust and degrades gradually. The runtime of our algorithm depends only on the size of the input circuit and on the longest shortest path between an initial state and any reachable state, commonly referred to as the diameter of the circuit. An enumeration procedure for computing existential quantification is central to the SAT based image computation algorithm. This procedure also forms the core of reparameterization algorithms described in the next chapter.

BDD Based Image Computation

In this section, we describe BDD based image computation algorithms. First, we need to set up some preliminaries.

Notation: Every state is represented as a vector $b_1 \dots b_n \in \{0,1\}^n$ of Boolean values. The transition relation R is represented by a Boolean function $T(x_1, \dots, x_n, x'_1, \dots, x'_n)$. Note that we will drop the explicit mention of input variables. Variables $X = x_1, x_2, \dots, x_n$ and $X' = x'_1, x'_2, \dots, x'_n$ are called *current state* and *next state* variables respectively. $T(X, X')$ is an abbreviation for $T(x_1, \dots, x_n, x'_1, \dots, x'_n)$. Similarly, functions of the form $S(X) = S(x_1, \dots, x_n)$ describe sets of states. We will occasionally refer to S as the *set*, and to T as the *transition relation*. For simplicity we will use X to denote both the set $\{x_1, \dots, x_n\}$ and the vector $\langle x_1, \dots, x_n \rangle$. Then the set of variables on which f depends is denoted by $Supp(f)$.

Example 1 [3 bit counter. (Running Example)] *Consider a 3-bit counter with bits x_1, x_2 and x_3. x_1 is the least significant and x_3 the most significant bit. The state variables are $X = x_1, x_2, x_3$, $X' = x'_1, x'_2, x'_3$. The transition relation of the counter can be expressed as*

$$T(X, X') = (x'_1 \leftrightarrow \neg x_1) \wedge (x'_2 \leftrightarrow x_1 \oplus x_2) \wedge (x'_3 \leftrightarrow (x_1 \wedge x_2) \oplus x_3).$$

In later examples, we will compute the image $\mathbf{Img}(S)$ *of the set $S(X) = \neg x_1$. Note that $S(X)$ contains those states where the counter is even.*

Partitioned BDDs: For most realistic designs it is impossible to build a single BDD for the entire transition relation. Therefore, it is common to represent the transition relation as a conjunction of smaller BDDs $T_1(X, X'),\ T_2(X, X'),\ \dots,\ T_l(X, X')$,

i.e.,

$$T(X, X') = \bigwedge_{1 \leq i \leq l} T_i(X, X'),$$

where each T_i is represented as a BDD. The sequence $T_1, \ldots, T_l$ is called a *partitioned transition relation*. Note that T is *not actually computed*, but only the T_i's are kept in memory.

Example 2 [3 bit counter, ctd.] *For the 3 bit counter, a very simple partitioned transition relation is given by the functions* $T_1 = (x'_1 \leftrightarrow \neg x_1), T_2 = (x'_2 \leftrightarrow x_1 \oplus x_2)$ *and* $T_3 = (x'_3 \leftrightarrow (x_1 \wedge x_2) \oplus x_3)$.

Partitioned transition relations appear naturally in hardware circuits where each latch (i.e., state variable) has a separate transition function. However, a partitioned transition relation of this form typically leads to a very large number of conjuncts. A large partitioned transition relation is similar to a CNF representation. So as the number of conjuncts increases; the advantages of BDDs are gradually lost. Therefore, starting with a very fine partition $T_1, \ldots, T_l$ obtained from the bit relations, the conjuncts T_i are grouped together into *clusters* $C_1, \ldots, C_r$, $r < l$ such that each C_i is a BDD representing the conjunction of several T_i's. The image $\mathbf{Img}(S)$ of S is given by the following expression.

$$\begin{aligned}
\mathbf{Img}(S(X)) &= \exists X \cdot (T(X, X') \wedge S(X)) && (2.3)\\
&= \exists X \cdot (\bigwedge_{1 \leq i \leq l} T_i(X, X') \wedge S(X)) && (2.4)\\
&= \exists X \cdot (\bigwedge_{1 \leq i \leq r} C_i(X, X') \wedge S(X)) && (2.5)
\end{aligned}$$

Note that in general, an existential quantifier does not distribute over conunction. Consequently, to compute $\mathbf{Img}(S(X))$, formula 2.5 instructs us to compute first a BDD for $\bigwedge_{1 \leq i \leq r} C_i(X, X') \wedge S(X)$. As argued above, partitioned transition relations have been introduced to *avoid* computing this potentially large BDD.

Early Quantification: Under certain circumstances, existential quantification can be distributed over conjunction using *early quantification* [13,70]. Early quantification is based on the following observation: if we know that α *does not contain* x, then $\exists x(\alpha \ \ \& \ \ \beta)$ is equivalent to $\alpha \ \ \& \ \ (\exists x \beta)$. In general, we have l conjuncts and n variables to be quantified. Since loosely speaking, clusters correspond to semantic entities of the design to be verified, it is expected that not all variables appear in all clusters. Therefore, some of the quantifications may be shifted over several C_i's. For a given sequence $C_1, \ldots, C_r$ of clusters, we obtain

$$\begin{aligned} \mathbf{Img}(S(X)) &= \exists X_1 \cdot (C_1(X, X') \wedge \exists X_2 \cdot (C_2(X, X') \ldots \\ &\quad \exists X_r \cdot (C_r(X, X') \wedge S(X)))) \end{aligned} \tag{2.6}$$

where X_i is the set of variables which do not appear in $Supp(C_1) \cup \ldots \cup Supp(C_{i-1})$ and each X_i is disjoint from each other. Existentially quantifying out a variable from a formula f reduces $|\,Supp(f)|$, which usually results in a reduced BDD size. The success of early quantification strongly depends on the order of the conjuncts $C_1, \ldots, C_r$. If we look at the parse tree of this equation, we see that it is a linear chain of conjunctions and quantifications. Generalizing this for an arbitrary parse tree, a variable can be quantified away at a subtree node as soon as it does not appear in the rest of the tree.

Quantification Scheduling. The size of the intermediate BDDs in image computation can be reduced by addressing the following two questions:

Clustering: How to derive the clusters $C_1, \ldots, C_r$ from the bit-relations $T_1, \ldots, T_l$?

Ordering: How to order the clusters so as to minimize the size of the intermediate BDDs?

These two questions are not independent. In particular, a bad clustering results in a bad ordering. Moon and Somenzi [60] refer to this combined problem as the *quantification scheduling* problem. The ordering of clusters is known as the *conjunction schedule*. Traditionally, only linear conjunction schedules have been considered. Later on, we generalize this concept to arbitrary parse trees of the image computation equation.

2.1 Heuristic Methods and Dependency Matrices

In this section, we propose algorithms for BDD based image computation that follow traditional linear quantification schedules. The main contributions of this work are the following:

• We extend and analyze image computation techniques previously developed by Moon *et al.* [59]. These techniques are based on the *dependence matrix* of the partitioned transition relation. We explore various *lifetime metrics* related to this representation and argue their importance in predicting costs of image computation. Moreover, we provide effective heuristic techniques to optimize these metrics.

• We show that the problem of minimizing the lifetime metric of [59] is NP-complete. More importantly, the reduction used to prove this NP-completeness result explains the close connection between efficient image computation and the well studied problem of computing the *optimal linear arrangement* for an undirected graph.

• We model the interaction between various sub-relations in the partitioned transition relation as a weighted graph and introduce a new class of heuristics called *ordering by recursive partitioning*.

• We have performed extensive experiments which indicate the effectiveness of our techniques.

The main conclusion to be drawn from our analysis is the following: For complicated industrial designs, the effort initially spent on ordering algorithms is clearly amortized during image computation. In other words, the benefits of good orderings outweigh the cost of slow combinatorial optimization algorithms.

Our algorithms are based on the concepts of *dependence matrices* (introduced in [59, 60]) and *sharing graphs*.

Definition 1 (Moon et al) *The* ***dependence matrix*** *of an ordered set of functions* $\{f_1, f_2, \ldots, f_m\}$ *depending on variables* $x_1, \ldots, x_n$ *is a matrix* D *with* m *rows and* n *columns such that* $d_{ij} = 1$ *if function* f_i *depends on variable* x_j*, and* $d_{ij} = 0$ *otherwise.*

Thus, each row corresponds to a formula, and each column to a variable. For image computation, we will associate the rows with the conjuncts of the partitioned transition relation, and the columns with the state variables. For example, $f_m = S(X), f_{m-1} = C_r, \ldots$. Thus, different choices for $f_i, 1 \leq i \leq m$ correspond to different orderings.

We will assume that the conjunction is taken in the order $f_m, f_{m-1}, \ldots, f_2, f_1$, i.e., we consider an expression of the form $\exists X\ (f_1\ \&\ (f_2\ \&\ \cdots\ \&\ (f_{m-1}\ \&\ f_m)))$. If a variable occurs *only* in f_m, we can quantify the variable early by pushing it to the right just before f_m.

Example 3 [3 bit counter, ctd.] *For* $f_4 = S(X)$*,* $f_3 = T_3$*,* $f_2 = T_2$*,* $f_1 = T_1$*, as described in example 2 earlier, the dependency matrix for our running example looks as follows:*

	v_1	v_2	v_3	v_1'	v_2'	v_3'
$f_1 = T_1$	*1*	*0*	*0*	*1*	*0*	*0*
$f_2 = T_2$	*1*	*1*	*0*	*0*	*1*	*0*
$f_3 = T_3$	*1*	*1*	*1*	*0*	*0*	*1*
$f_4 = S(X)$	*1*	*0*	*0*	*0*	*0*	*0*

In the matrix above, the rows are numbered from top to bottom, and the columns are numbered from left to right. The cojunction order is given by the row order. In general, for a variable x_j, let l_j denote the smallest index i in column j such that $d_{ij} = 1$. Analogously, h_j denotes the largest index. We can quantify away the variable x_j as soon as the conjunct corresponding to the row l_j has been considered. This is because the variable x_j does not appear in any conjunct after the conjunct for row j has been considered. For example, if we look at the variable v_2 in the dependency matrix above, it can be quantified as soon as the conjunct T_2 has been applied. Moreover, the variable x_j does not appear in any conjuncts after h_j. Hence, $h_j - l_j$ can be viewed as the *lifetime* of a variable. Moon, Kukula, Ravi and Somenzi [59] define the following metric and use it extensively in their algorithms.

Definition 2 (Moon, Kukula, Ravi, Somenzi) *The **normalized average lifetime** of the variables in a dependence matrix $D_{m\times n}$ is given by*

$$\lambda = \frac{\sum_{1\leq j\leq n}(h_j - l_j + 1)}{m \cdot n}$$

Note that the definition of λ assumes that $S(X)$ is given. Therefore, since λ *depends* on $S(X)$, the ordering has to be recomputed in each step of the fixpoint computation. We are considering static ordering techniques here, which are computed independently of any particular $S(X)$, so it is necessary to make assumptions about the structure of $S(X)$. We obtain two lifetime metrics λ_U and λ_L depending on

whether we assume $Supp(S) = X$ or $Supp(S) = \emptyset$. It is easy to see that $\lambda_L \leq \lambda \leq \lambda_U$. The terms *average active lifetime* and *total active lifetime* are also used to denote λ_L and λ_U respectively. Moon and Somenzi argue in favour of using λ_L. We will evaluate the effectiveness of each of these metrics to predict image computation costs.

Moon and Somenzi argue in favor of using λ_L as follows :

> If we have a conjunction of two functions $S(x_1, x_2, \ldots, x_n)$ and $T(x_1, x_2, \ldots, x_k)$ such that these x_k variables are the first k variables among $x_1, \ldots, x_n$ in the BDD variable order, then the recursion depth of BDD conjunction operation is never more than k and the variables $x_{k+1}, \ldots, x_n$ don't affect the size or running time. Consider two functions $f(x_1, \ldots, x_n)$ and $g(x_1, \ldots, x_k)$, $k < n$, with the variable order $x_1 < \ldots < x_n$. In the computation of $f \wedge g$ the recursion is never deeper than k. Even though all n variables appear in the operands, and may appear in the result, only k of them are *active*....."

However the situation described in the argument used by Moon and Somenzi occurs with very low probability. It is reasonable to assume that the BDD variable ordering and the support sets of the conjuncts are independent. An easy combinatorial argument shows the following:

Proposition 1 *Let K be a k-element random subset of the variable set X of n elements. Then the expected value of the largest variable index in K is $\frac{k(n+1)}{k+1}$.*

Proof: Let the elements of the set X be indexed $1, 2, \ldots, n$. The total number of choices for a k-element subset is $\binom{n}{k}$. Clearly, the largest index in any k-element subset of X can not be less than k. Now, the number of choices when the largest

index is i is $\binom{i-1}{k-1}/\binom{n}{k}$. So the expected value of the largest index is:

$$\sum_{i=k}^{i=n} i \cdot \frac{\binom{i-1}{k-1}}{\binom{n}{k}} = \sum_{i=k}^{i=n} k \cdot \frac{\binom{i}{k}}{\binom{n}{k}} = \sum_{i=k}^{i=n} k \cdot \frac{\binom{n+1}{k+1}}{\binom{n}{k}}.$$

The last equality follows from a well known binomial identity. Simplifying this we get $\frac{k(n+1)}{k+1}$.

Note that already for $k = 9$, this amounts to $0.9(n+1)$ which is very close to n. Suppose that there are two functions f and g such that f depends on all n variables, and g depends on only k variables. Then the proposition says that with high probability g will contain variables which are close to x_n, and therefore, the recursion depth will be close to n. Because of Proposition 1, we use λ_U in our experiments instead of λ_L. We ran a few experiments and computed actual λ at each image computation. We found that the actual λ is close to λ_U rather than λ_L.

Algorithms for Ordering Clusters

The algorithms we propose also follow the order-cluster-order strategy. The ordering algorithms that we present in this section are used before and after clustering. Our clustering strategy is as in [64], called IWLS95. For the sake of clarity of notation, let us assume that the clusters $C_1, C_2, \ldots, C_r$ have been constructed and we are ordering them. But the discussion applies equally well to ordering the initial conjuncts $T_1, \ldots, T_n$.

We present two classes of algorithms. The first one is based on dependence matrix and the other one on *sharing graphs*.

Earlier, we defined a dependence matrix D corresponding to the set of clusters $C_1, \cdots, C_r$. As already pointed out, the number of support variables provides a good estimate of the size of a BDD. Therefore, we seek a schedule in which the lifetime of

variables is low. Moon and Somenzi [60] provide a method to convert a dependence matrix into bordered block triangular form with the goal of reducing λ_L.

2.1.1 Minimizing λ is NP-complete

The main result of this subsection (Theorem 1) motivates the use of various combinatorial optimization methods.

Let λ-OPT be the following decision problem: given a dependence matrix D and a number r, does there exist a permutation σ of the rows of D such that $\lambda < r$? The following theorem shows that $\lambda - OPT$ is NP-complete. The reduction is from the *optimal linear arrangement problem (OLA)* [32, page 200]. Due to space limitations the proof is given in Appendix A.

Theorem 1 *λ-OPT is NP-complete.*

The complexity of this problem was not explored by Moon and Somenzi [60]. There exists a variety of heuristics for solving the optimal linear arrangement problem and related problems in combinatorial optimization. Some of these heuristics are based on hill climbing and simulated annealing. There are two important characteristics of this class of algorithms. First of all, they all try to minimize an underlying cost function. Second, these heuristics use a finite set of *primitive transformations* on potential solutions, which are used to move from one solution to another. In our case, swapping two rows of the dependence is a primitive transformation and the cost function can be chosen to be either λ_L or λ_U. Our experimental results (Section 2.3) confirm that λ_L correlates with image computation costs much better than λ_U does, in accordance with the claim of [60]. Simulated annealing is a more general and flexible strategy than hill climbing.

2.1.2 Ordering Clusters by Hill Climbing

Hill climbing is the simplest greedy strategy in which at each point, the solution is improved by choosing two rows to be swapped in such a manner as to achieve best improvement in the cost function. This process is repeated until no further move improves the solution. Since the best move is chosen at each point, this strategy is also called *steepest descent hill climbing*. However, the greedy steepest descent algorithm can easily get stuck in local optima. Randomization is used to alleviate this problem as follows: The best move that improves the solution is accepted only with some probability p, and with probability $1 - p$, a random move is accepted. Note that with $p = 1.0$, we get the steepest descent hill climbing. The algorithm can be run multiple number of times, each time beginning with a random permutation, and the best solution that is achieved after a few runs is accepted.

HillClimbOrder(D)
1. $\lambda_{best} = 2$ // any number greater than 1 will do, since λ is always less than 1
2. **for** $i = 1$ to $NumStarts$
3. let σ' be a random permutation of conjuncts.
4. **while** there exists a swap in σ' to reduce λ
5. make the best swap with probability p,
6. or make a random swap with probability $1 - p$ to update σ'.
7. **if** $\lambda' < \lambda_{best}$
8. $\lambda_{best} = \lambda'$
9. $\sigma_{best} = \sigma$
10. **endif**
11. **endfor**

Figure 2.2: Hill climbing algorithm for minimizing λ

Figure 2.2 describes the algorithm in exact terms. The hill climbing procedure is repeated *NumStarts* times. In the algorithm, σ denotes a permutation of the rows of the dependency matrix. Hill climbing is performed until no further improvement in λ is possible.

2.1.3 Ordering Clusters by Simulated Annealing

The physical process of annealing involves heating a piece of metal and letting it cool down slowly to relieve stresses in the metal. The simulated annealing algorithm (introduced by Metropolis *et al.* [56]) mimics this process to solve large combinatorial optimization problems [46]. Drawing analogy from the physical process of annealing, the algorithm begins at a high "temperature", where the set of moves is essentially random. This allows larger jumps from local to global optima. Gradually, the temperature is decreased and the moves become less random, favoring greedy moves over random moves for achieving a global optimum. Finally, the algorithm terminates at "freezing" temperatures where no further moves are possible. At each stage, the temperature is kept constant until "thermal quasi-equilibrium" is reached. While random moves help in the beginning when the algorithm has a greater tendency to get stuck in local optima, the greedy moves help to achieve a global optimum once the solution is in the proximity of one global optimum. In practice, simulated annealing has been successfully used to solve optimization problems from several domains.

The probability of making a move that *increases* the cost function is related to the temperature t_i at the i-th iteration, and is given by $e^{-\Delta\lambda/t_i}$. Thus at higher temperatures, the probability of accepting random moves is high. The gradual decrease of temperature is called the *cooling schedule*. If the temperature is decreased by a fraction r in each stage, we get a simple *exponential cooling schedule*. Thus beginning with an initial temperature of t_0, the temperature in the i-th iteration is $t_0 r^i$. It has

been shown that a logarithmic cooling schedule is guaranteed to achieve an optimal solution with high probability [4, 40]. However, logarithmic schedule is an extremely slow cooling schedule and simple cooling schedules like exponential schedules perform well for many problems. Figure 2.3 describes our algorithm. The parameter $NumStarts$ controls the number of times the temperature is decreased. The parameter $NumStarts2$ controls the number of iterations at a fixed temperature t_i.

```
    SimAnnealOrder(D)
    for i = 1 to NumStarts
1     t_i ← t_0 r^i
2     for j = 1 to NumStarts2
3         permute two random rows of D to get D_i
4         if (λ_i < λ)    // greedy move
5             λ ← λ_i; D ← D_i
6         else // random move
7             with probability e^(-(λ_i - λ)/t_i), set λ ← λ_i; D ← D_i
8         endif
9     endfor
10  endfor
```

Figure 2.3: Simulated annealing algorithm to minimize λ

2.1.4 Ordering Clusters Using Graph Separators

In this section, we describe the use of graph separator algorithms for ordering clusters. First, we define *sharing graphs* below to model interaction between clusters.

Definition 3 *A **sharing graph** corresponding to a set of Boolean functions* $\{f_1, f_2, \ldots, f_m\}$ *is a weighted graph* $G(V, E, w_e)$*, where* $V = \{f_1, f_2, \ldots, f_m\}$*,* $E = V \times V$ *and* $w_e : E \rightarrow \Re$ *is a real-valued weight function.*

Informally, the vertices of sharing graph are the clusters, and the edges denote the interaction between the clusters. We shall use heuristic weight functions to express interaction between clusters. Intuitively, the stronger the interaction between two clusters, the closer they should be in the ordering. IWLS95 and Bwolen Yang's heuristics order the conjuncts based on this type of interaction between conjuncts. We propose to use graph separator algorithms on sharing graphs to order the conjuncts. We define the weight $w(T_i, T_j)$ of an edge (T_i, T_j) in the sharing graph as

$$w(T_i, T_j) = W_1 \times \frac{|\,Supp(T_i) \cap Supp(T_j)|}{|\,Supp(T_i)| + |\,Supp(T_j)|} + W_2 \times \frac{BddSize(T_i \wedge T_j)}{BddSize(T_i) + BddSize(T_j)}$$

The first factor ($W_1 \geq 0$) denotes the relative weight of sharing of support between two conjuncts, while the second factor ($W_2 \leq 0$) denotes the weight of the relative growth in the sizes of BDDs if these two conjuncts are conjoined. Therefore, a higher edge weight between two conjuncts indicates a higher degree of interaction and consequently these conjuncts should appear "close" in the ordering.

A separator partitions the vertices of a weighted undirected graph into two sets such that the total weight of the edges between two partitions is "small". Formally, an *edge separator* is defined as follows:

Definition 4 *Given a weighted undirected graph* $G(V, E)$ *with two weight functions* $w_e : E \rightarrow \Re$ *and* $w_v : V \rightarrow \Re$*, and a positive constant* $\gamma < 0.5$*, an* edge separator *is a collection of edges* E_s *such that removing* E_s *from* G *partitions* G *into two disconnected subgraphs* V_1 *and* V_2*, and* $\frac{|\sum_{v \in V1} w_v(v) - \sum_{v \in V2} w_v(v)|}{\sum_{v \in V} w_v(v)} < \gamma$*.*

Usually, γ is chosen very close to zero so that the size of the two sets is approximately the same. The weight of the edge separator E_s is simply the sum of the weight

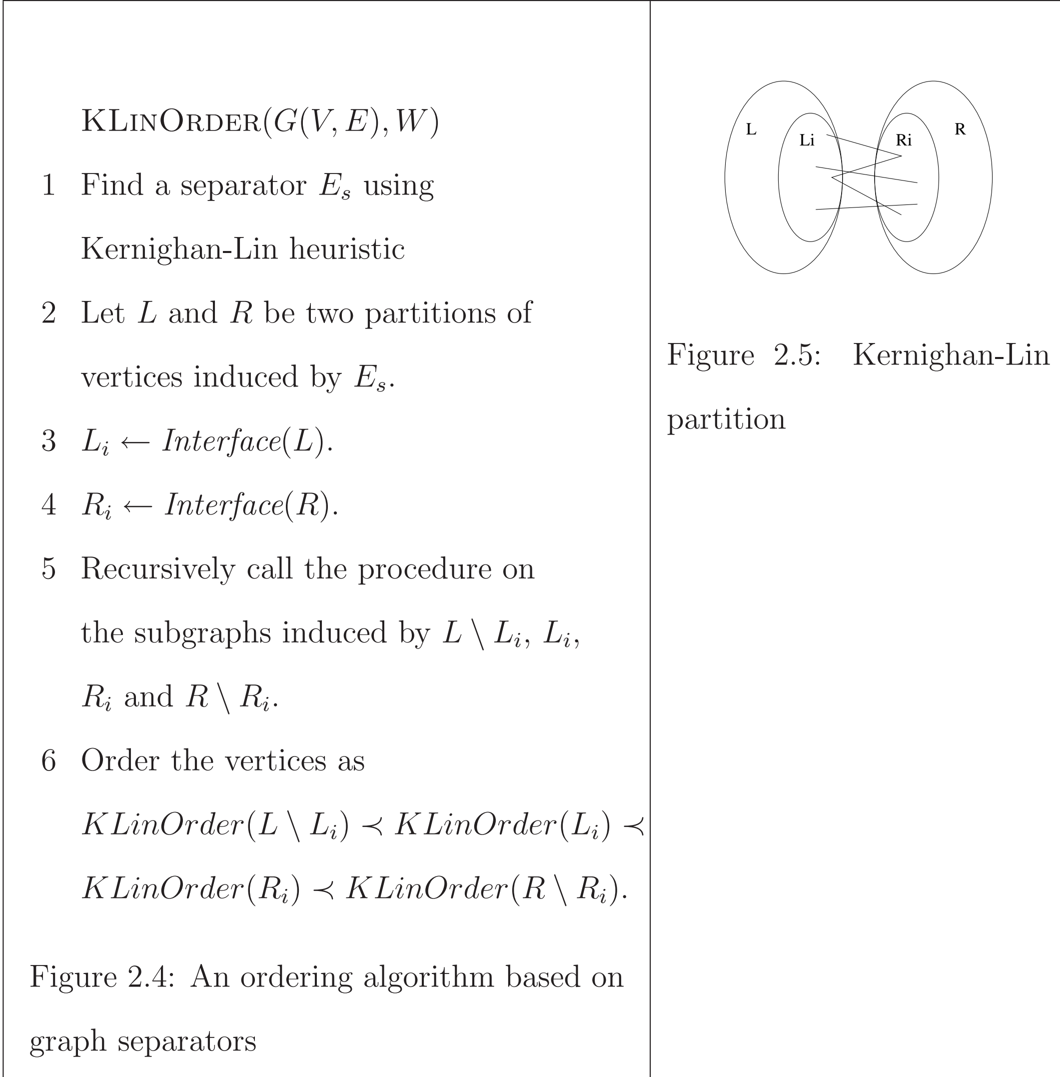

KLinOrder($G(V, E), W$)

1 Find a separator E_s using Kernighan-Lin heuristic
2 Let L and R be two partitions of vertices induced by E_s.
3 $L_i \leftarrow Interface(L)$.
4 $R_i \leftarrow Interface(R)$.
5 Recursively call the procedure on the subgraphs induced by $L \setminus L_i$, L_i, R_i and $R \setminus R_i$.
6 Order the vertices as $KLinOrder(L \setminus L_i) \prec KLinOrder(L_i) \prec KLinOrder(R_i) \prec KLinOrder(R \setminus R_i)$.

Figure 2.4: An ordering algorithm based on graph separators

Figure 2.5: Kernighan-Lin partition

of the edges in E_s. It has been shown that finding an edge separator of minimum weight is NP-complete [32, pp. 209], in fact finding an approximation is NP-hard, too [11]. The problem of finding a good separator occurs in many different contexts and a wide range of application areas. A large number of heuristics have been proposed for the problem. One of the most important heuristics is due to Kernighan and Lin [45]. Variations of this heuristic [31] have been found to work very well in practice.

By finding a good edge separator of the sharing graph, we obtain two sets of vertices with a low level of interaction between them. Thus the vertices of these two sets can be separated in the ordering. A complete ordering is achieved by recursively invoking the separator algorithm on the two halves. Since this ordering respects the interaction strengths between conjuncts, we expect to achieve smaller BDD sizes.

We use the Kernighan-Lin algorithm for finding a good edge separator E_s. Figure 2.4 describes the complete algorithm for ordering clusters based on the Kernighan-Lin separator algorithm. This produces two sets of vertices L and R. A vertex $v \in L$ that has an edge of non-zero weight to a vertex in R is called an *interface vertex*. L_I denotes the set of interface vertices in L. Similarly, R_I denotes the set of interface vertices in R. We invoke the algorithm to recursively order $L \setminus L_I$, L_I, R_I, and $R \setminus R_I$. Finally, the order on the vertices is given by the order on $L \setminus L_I$ followed by the order on L_I, followed by the order on R_I, and followed by the order on $R \setminus R_I$.

2.2 Non-linear Quantification Scheduling

In this section, we propose a more flexible approach to image computation by viewing the image computation equation as a *symbolic expression evaluation* problem. The main contributions are as follows:

- We formulate the problem of image computation as an expression evaluation problem where the goal is to reduce the size of the intermediate BDDs. This approach provides significantly more flexibility than the traditional *linear* approach for ordering BDDs during image computation. We show how this approach subsumes the *linear* approaches.
- We provide heuristics, called *VarScore heuristics*, for evaluating the parse tree

of image computation equation to reduce the size of the intermediate BDDs. Our heuristics are based on scoring the variables that need to be quantified and restructuring the parse tree according to the heuristic. We provide *dynamic* and *static* versions of our *VarScore* heuristics. In the dynamic version, the parse tree is built for each image computation, while in the static version, a single parse tree is built in the beginning and is used for all subsequent image computations.

- We compare our dynamic and static heuristics to the best known techniques based on linear ordering of BDDs. We show that even with a simple heuristic such as *VarScore*, we achieve impressive results.

We have demonstrated that our simple yet flexible approach yields better experimental results for many reachability analysis and model checking problems.

VarScore Algorithms

We describe the *VarScore* heuristic algorithms for the quantification scheduling problem. First, we describe the dynamic version of *VarScore* algorithm, where a parse tree is built for each image computation. Next, we describe static versions of *VarScore* algorithm, where the parse tree is built only once and used for all the image computations that follow. Since we don't have the information about the state set $S(X)$ (Equation 2.6), the heuristic scores are approximations.

The basic step of our algorithms is described in Figure 2.6.

The input to VarScoreBasicStep is a set of variables to be quantified, Q, and a collection of BDDs, F. First, any variable that appears in the support of only one BDD is quantified away immediately and the sets F and Q are adjusted accordingly

```
    VarScoreBasicStep(F, Q)
 1  if there exists a variable q ∈ Q such that q appears in
    the support of only one BDD T ∈ F
 2      F ← F \ {T} ∪ {∃q.T}
 3      Q ← Q \ {q}
 4  else
 5      compute heuristic score VarScore for
        each variable in Q
 6      let q ∈ Q be the variable with the lowest score
 7      let T1, T2 ∈ F be the two smallest BDDs such
        that q ∈ Supp(T1) ∩ Supp(T2)
 8      if q ∉ ⋃_{Ti ∈ F \ {T1,T2}} Supp(Ti)
                // use BDDAndExists for efficiency
 9              F ← F \ {T1, T2} ∪ {∃q.T1 ∧ T2}
10              q ← Q \ {q}
11      else
12              F ← F \ {T1, T2} ∪ {T1 ∧ T2}
13      endif
14  endif
15  return(F, Q)
```

Figure 2.6: Basic step of the VarScore algorithms

(lines 1–3). Otherwise a heuristic score is computed for the variables in Q. The variable with the lowest score, say q, is chosen next and the two smallest BDDs in whose support that variable appears are conjoined next. For efficiency reasons, if q appears in the support of only those two BDDs, then *BDDAndExists* operation is used to conjoin and quantify away that variable.

In the **dynamic version** of the algorithm, this step is called repeatedly for each image computation, beginning with $F = \{T_1, \ldots, T_l, S\}$ and $Q = X \cup W$. Just to remind the reader, $T_1, \ldots, T_l$ are the transition functions, S is the set of state whose image we are interested in, X is the set of present state variables, and W is the set of input variables. F can also be seen as a collection of subtrees of the parse tree (or a *forest*) where the BDD operations are carried out at the roots of the subtrees. When all the variables are quantified ($Q = \emptyset$), remaining BDDs from F are conjoined in any arbitrary order to compute $\mathbf{Img}(S)$. The scoring algorithm that we use is very simple: *we sum up the sizes of the BDDs in which a particular variable appears.* However, we are also investigating other more complex scoring algorithms. Figure 2.7 illustrates the dynamic algorithm on our 3-bit counter example.

First Static Approach: If there are multiple image computations to be done, e.g., in reachability analysis where we compute images until we reach a fixed-point, a lot of work is repeated. This is especially true if the circuit partitioning is fine. In traditional linear conjunction schedules, *clustering* is done so that most of the BDDs are conjoined once and for all before any image computations, however, very few quantifications are carried out at that time. In the dynamic version, all the subtrees that do not quantify away any present state variables can be evaluated in the beginning (subject to the BDD size growth constraint). This is because $S(X)$ only depends upon present state variables. Since we don't have any information about which particular $S(X)$ is going to be used, we can conservatively assume that

Figure 2.7: Dynamic VarScore algorithm in action. The dotted lines represent the BDDs in the set F at different iterations of the VarScoreBasicStep.

$S(X)$ contains all X variables in the support. So, the overall approach is to begin with $F = \{T_1, \ldots, T_l\}$, $Q = W$ and repeatedly call VarScoreBasicStep until either $Q = \emptyset$ or no BDD operation can be done without exceeding the size limit. This will leave some F_{rem} and Q_{rem}. Then for each image computation, we call VarScoreBasicStep repeatedly beginning with $F = F_{rem} \cup S$ and $Q = Q_{rem} \cup X$, until all the variables are quantified away. We just conjoin all the BDDs in the final F to get $\mathbf{Img}(S)$.

Second Static Approach: Note that in the first static approach, we cannot quantify away any present state variable as we do not have information about S. Thus the parse tree that is built in the beginning does not take into account the effects of those variables and S at all. However, introducing S as early in the Equation 2.6 restricts the conjunct BDDs, often reducing their sizes [39, 59]. Moreover, the bulk of the variables affecting the computation are these present state variables. In fact, if we remove the BDD size constraint, we end up with a monolithic representation of the

transition relation! To alleviate this problem, we propose a second static approach that takes into effect the present state variables. We build an approximation of the parse tree but not the tree itself. Instead of working with the actual BDDs, we work only with the support sets of BDDs. The size of a BDD T_i is estimated to be some function of $|\,Supp(T_i)|$. The linear function $size(T_i) = |\,Supp(T_i)|$ is an optimistic choice, while the exponential function $size(T_i) = 2^{|\,Supp(T_i)|}$ is too pessimistic. We have determined experimentally that a quadratic function $size(T_i) = |\,Supp(T_i)|^2$ is a good estimate. The following identities are used for adjusting the support sets after conjunction/quantification.

$$\begin{aligned} Supp(\exists q.T_i) &= Supp(T_i) \setminus \{q\} \\ Supp(T_i \wedge T_j) &= Supp(T_i) \cup Supp(T_j) \end{aligned}$$

So we build the pseudo-parse tree with these approximations by calling VARSCORE-BASICSTEP repeatedly until $Q = \emptyset$. The remaining subtrees in F are conjoined in arbitrary order to get a single parse tree. Here F will denote the forest of the subtrees. We assume that $Supp(S) = X$. After building this pseudo-parse tree, we can see that all the subtrees not on the path from S to the root can be evaluated right at the beginning. Moreover, we do not need to take into account the BDD size constraint, because those same BDDs will have to be evaluated anyway. So we evaluate the remaining subtrees and get a linear chain from S to the root. The quantifications for X variables are scheduled anew for each image computation.

Third Static Approach: This approach is similar to the second static approach, but instead of working with the support sets, we work with actual BDDs. This provides a more accurate estimate of the sizes (compared to approximating the sizes of BDDs as some function of the size of support set). The BDD for S is taken to be some reasonably complex BDD resembling the state set. For example, we could

use the BDD for the set of states after every few image computation iterations as a proxy for the set of states for the current iteration. This is the only approximation introduced. The tree is built statically and all the subtrees not in the path from S to the root are evaluated in the beginning. The quantifications along the path from S to the root are scheduled for each image computation using the actual S, as in the second approach.

2.3 Results for BDD Based Image Computation

In order to evaluate the effectiveness of our algorithms, we ran reachability and model checking experiments on circuits obtained from the public domain and industry. The "S" series of circuits are ISCAS'93 benchmarks, and the "IU" series of circuits are various abstractions of an interface control circuit from Synopsys. For a fair comparison, we implemented all the techniques in the NuSMV model checker. All experiments were done on a 200MHz quad Pentium Pro processor machine running the Linux operating system with 1GB of main memory. We restricted the memory usage to 900MB, but did not set a time limit. The two performance metrics we measured are *running time* and *peak number of live BDD nodes*. We provided a prior ordering to the model checker and turned off the dynamic variable reordering option. This was done so that the effects of BDD variable reordering do not "pollute" the result. We also recorded the fraction of time spent in the clustering and ordering phases. The cost of these phases is amortized over several image computations performed during model checking and reachability analysis.

In the techniques that we have described, several parameters have to be chosen. For example, the cooling schedule in the case of simulated annealing needs to be determined. We ran extensive "tuning experiments" to find the best value for these

parameters. Due to space constraints, we do not describe all those experiments. However, the choice of lifetime metric to optimize is a crucial one and hence in our first set of experiments, we evaluate the effectiveness of these metrics for predicting image computation costs.

Our algorithms for combinatorial optimization of lifetime metrics can choose to work with either upper or lower approximations of lifetimes. We ran the following experiment to estimate the correlation between the performance, and λ_L and λ_U respectively. We generate various conjunction schedules for a number of benchmarks by different ordering methods and by varying various parameters of the optimization methods. Each schedule gives us different values for lifetime metrics. We measure the running time and the peak number of live BDD nodes used for the model checking or reachability phase. For each circuit, this gives us four scatter plots for running time vs lifetime metric and space vs lifetime metric. A statistical correlation coefficient between runtime/space and lifetime metric indicates the effectiveness of a metric for predicting the runtime/space requirement. The following Table 2.1 concisely summarizes the correlation results.

Circuit	Runtime		Space	
	λ_L	λ_U	λ_L	λ_U
IU40	0.560	0.303	0.610	0.227
IU70	0.603	0.336	0.644	0.263
TCAS	0.587	0.366	0.628	0.240
S1269	0.536	0.402	0.559	0.345
S3271	0.572	0.350	0.602	0.297

Table 2.1: Correlation between various lifetime metrics and runtime/space for a representative sample of benchmarks.

It is clear from this data that the active lifetime (λ_L) is a much more accurate predictor of image computation costs than total lifetime (λ_U). Hence, simulated annealing and hill climbing techniques optimize λ_L.

In the following set of experiments (Table 2.2), we compare our techniques against the FMCAD00 strategy [60]. The first column indicates the total running time of the benchmark (including ordering/clustering and model checking/reachability phases), the second column indicates the peak number of live BDD nodes in thousands during the whole computation, the third column indicates time used by ordering phase, the next two columns indicate λ_L and λ_U achieved. From hill climbing and simulated annealing, we only report the results of simulated annealing, as both of them belong to the same class of algorithms. Moreover, we found out that in general, simulated annealing achieves better performance than hill climbing.

The algorithm KLin based on edge separators achieves lower peak live node count for several circuits than FMCAD00. For the 15 large benchmarks for which FMCAD'00 takes more than 100 secs to finish, KLin wins 10 cases in terms of Peak live BDD nodes, and 7 cases in terms of running time. In some cases, the savings in space is 40%.

The result for the simulated annealing algorithm that minimizes λ is shown in Table 2.2. Again, in comparison to FMCAD00, for the 15 non-trivial benchmarks, simulated annealing wins 14 cases and ties for the other in space, and wins 11 cases in time. In some cases, the savings in space is 55%. The simulated annealing algorithm can also complete 16 reachability steps for the S1423 circuit, which at that time was the largest number of reachability steps for this circuit. Comparing KLin and simulated annealing, simulated annealing achieves the better results for all the nontrivial benchmarks.

The improvements in execution times are less than the improvements in space,

Circuit	#FF	#inp.	log_2 of #reach	Total Time (secs)			Peak Live BDD Nodes (K)			Ordering time (secs)			λ_L			λ_U		
				FMCAD	KLin	SA	FMCAD	KLin	SA	FMCAD	KLin	SA	FMCAD	KLin	SA	FMCAD	KLin	SA
IDLE	73	0	14.63	159	161	182	289	276	223	2	20	29	0.329	0.293	0.200	0.421	0.515	0.487
GUID	91	0	47.58	14	20	24	137	106	138	4	15	19	0.346	0.220	0.165	0.394	0.452	0.294
S953	29	16	8.98	1	2	3	15	13	15	1	1	3	0.290	0.290	0.271	0.507	0.485	0.410
IU30	30	138	18.07	28	104	63	290	563	290	3	24	34	0.360	0.368	0.324	0.459	0.522	0.634
IU35	35	183	22.49	13	29	11	257	366	202	4	24	6	0.364	0.373	0.304	0.573	0.360	0.308
IU40	40	159	25.85	13	37	14	353	384	232	5	21	5	0.326	0.336	0.302	0.508	0.326	0.334
IU45	45	183	29.82	**MOut**	11256	165	**MOut**	3952	483	10	32	39	0.360	0.353	0.300	0.465	0.663	0.569
IU50	50	615	31.57	476	522	540	1627	1599	1602	16	52	77	0.319	0.418	0.133	0.459	0.654	0.403
IU55	55	625	33.94	982	891	870	4683	3358	3298	14	90	84	0.384	0.386	0.324	0.583	0.432	0.515
IU65	65	632	39.32	**MOut**	1260	1083	**MOut**	7048	6793	18	81	100	0.389	0.353	0.353	0.659	0.448	0.423
IU70	70	635	42.07	5398	3033	2855	17355	9099	9964	38	95	129	0.303	0.296	0.286	0.424	0.393	0.486
IU75	75	322	46.59	5367	4218	3822	16538	12193	9404	45	115	140	0.398	0.371	0.349	0.731	0.692	0.526
IU80	80	350	49.80	**MOut**	6586	4824	**MOut**	22234	17993	49	127	136	0.372	0.335	0.322	0.570	0.628	0.345
IU85	85	362	52.14	**MOut**	**MOut**	6933	**MOut**	**MOut**	25661	59	141	154	0.332	0.303	0.287	0.623	0.597	0.591
TCAS	139	0	106.87	5058	5285	4598	11931	12376	9140	27	173	165	0.173	0.182	0.227	0.299	0.306	0.261
S1269	37	18	30.07	2109	2466	1875	1440	1736	893	10	19	24	0.584	0.622	0.449	0.659	0.929	0.589
S1512	57	29	40.59	799	1794	651	159	190	135	15	24	30	0.412	0.394	0.386	0.521	0.619	0.714
S5378	179	35	57.71*	18036	**MOut**	10168	1632	**MOut**	1279	42	49	67	0.124	0.114	0.099	0.219	0.164	0.152
S4863	104	49	72.35	3565	3109	3013	1124	947	910	38	45	56	0.102	0.103	0.086	0.251	0.109	0.179
S3271	116	26	79.83	4234	3286	3399	8635	6240	6203	33	30	30	0.224	0.185	0.184	0.366	0.306	0.226
S3330	132	40	86.64	23659	19533	24563	12837	9866	11381	69	123	150	0.214	0.217	0.227	0.299	0.335	0.378
SFE†	293	69	218.77	863	916	762	147	146	130	14	84	76	0.383	0.354	0.344	0.554	0.624	0.531
S1423	74	17	37.41**	23325	19265#	35876	65215	27653#	48366	10	17	35	0.486	0.501	0.301	0.622	0.622	0.460

Table 2.2: Comparing FMCAD00, Kernighan-Lin separator (KLin) and Simulated annealing (SA) algorithms. (**MOut**)–Out of memory, (†)–SFEISTEL, (*)–8 reachability steps, (**)–14 reachability steps, (#)–13 reachability steps. The lifetimes reported are after the final ordering phase.

especially for smaller circuits. This is because separator based algorithms spend more time in the ordering phase itself. However, for larger circuits, this cost gets amortized by the smaller BDDs achieved during analysis. An important observation that can be made is that in general, our algorithms spend more time in the initial ordering phase as compared to FMCAD00. This is to be expected since both KLin and simulated annealing are optimization methods.

The last two columns in Table 2.3 indeed demonstrate that our algorithms improve various λs with respect to FMCAD'00. The main objective of our algorithms was to improve λ_L, though we can see that they also result in better λ_Us in general.

The following table 2.3 indeed demonstrates that our algorithms improve various λs with respect to FMCAD'00. We report both λ_U and λ_L.

In Table 2.2, we compare the 3 static versions of the *VarScore* algorithm against FMCAD00 [60] and against simulated annealing based techniques from table 2.2.

We observe that *VarScore* algorithms win in most of the cases against best of the simulated annealing and FMCAD00 methods. The margin is more for space than for time. Also observe that we spend significantly more time in the initial ordering phase (some time about 20% of the total time). Thus we have very good results when the number of image computations to be done are large, so that the cost of the initial phase is amortized. The average time speedup we observe is about 20% over the best of FMCAD00 and simulated annealing, while space savings are even better, about 40% for VS-III and about 20-30% on average for VS-I and VS-II.

Circuit	λ_L			λ_U		
	FMCAD	KLin	SA	FMCAD	KLin	SA
IDLE	0.329	0.293	0.200	0.421	0.515	0.487
GUID	0.346	0.220	0.165	0.394	0.452	0.294
S953	0.290	0.290	0.271	0.507	0.485	0.410
IU30	0.360	0.368	0.324	0.459	0.522	0.634
IU35	0.364	0.373	0.304	0.573	0.360	0.308
IU40	0.326	0.336	0.302	0.508	0.326	0.334
IU45	0.360	0.353	0.300	0.465	0.663	0.569
IU50	0.319	0.418	0.133	0.459	0.654	0.403
IU55	0.384	0.386	0.324	0.583	0.432	0.515
IU65	0.389	0.353	0.353	0.659	0.448	0.423
IU70	0.303	0.296	0.286	0.424	0.393	0.486
IU75	0.398	0.371	0.349	0.731	0.692	0.526
IU80	0.372	0.335	0.322	0.570	0.628	0.345
IU85	0.332	0.303	0.287	0.623	0.597	0.591
TCAS	0.173	0.182	0.227	0.299	0.306	0.261
S1269	0.584	0.622	0.449	0.659	0.929	0.589
S1512	0.412	0.394	0.386	0.521	0.619	0.714
S5378	0.124	0.114	0.099	0.219	0.164	0.152
S4863	0.102	0.103	0.086	0.251	0.109	0.179
S3271	0.224	0.185	0.184	0.366	0.306	0.226
S3330	0.214	0.217	0.227	0.299	0.335	0.378
SFEISTEL	0.383	0.354	0.344	0.554	0.624	0.531
S1423	0.486	0.501	0.301	0.622	0.622	0.460

Table 2.3: Comparing lifetimes for various methods

Circuit	#FF	#inp.	log_2 of #reach	Total Time (secs)					Peak Live BDD Nodes (K)					Static phase time (secs)				
				FMCAD	SA	VS-I	VS-II	VS-III	FMCAD	SA	VS-I	VS-II	VS-III	FMCAD	SA	VS-I	VS-II	VS-III
IDLE	73	0	14.63	159	182	37	86	73	289	223	225	29	19	2	29	19	17	19
GUID	91	0	47.58	14	24	54	18	35	137	138	14	95	95	4	19	28	24	27
S953	29	16	8.98	1	3	4	2	2	15	15	14	19	16	1	3	2	1	1
IU30	30	138	18.07	28	63	25	46	38	290	290	324	250	226	3	34	12	10	10
IU35	35	183	22.49	13	11	25	17	19	257	202	183	241	222	4	6	19	15	15
IU40	40	159	25.85	13	14	38	13	18	353	232	292	214	170	5	5	15	10	12
IU45	45	183	29.82	**MOut**	165	186	158	157	**MOut**	483	566	564	439	10	39	24	20	22
IU50	50	615	31.57	476	540	701	427	561	1627	1602	1655	2020	2384	16	77	238	208	250
IU55	55	625	33.94	982	870	1011	614	585	4683	3298	4923	4189	3100	14	84	322	224	223
IU65	65	632	39.32	**MOut**	1083	1161	809	751	**MOut**	6793	6965	6711	5440	18	100	406	414	361
IU70	70	635	42.07	5398	2855	3596	2371	2947	17355	9964	8225	9619	8570	38	129	943	885	966
IU75	75	322	46.59	5367	3822	4911	2828	2522	16538	9404	1309	8707	6414	45	140	1395	1118	1057
IU80	80	350	49.80	**MOut**	4824	5418	4552	4302	**MOut**	17993	20193	16018	12062	49	136	1975	1728	1964
IU85	85	362	52.14	**MOut**	6933	**MOut**	5558	6289	**MOut**	25661	**MOut**	22938	23659	59	154	2633	1950	2704
TCAS	139	0	106.87	5058	4598	4139	3781	3646	11931	9140	8463	7792	6494	27	165	69	57	70
S1269	37	18	30.07	2109	1875	1939	1703	1540	1440	893	858	665	538	10	24	331	299	318
S1512	57	29	40.59	799	651	694	505	431	159	135	167	122	80	15	30	193	140	177
S5378	179	35	57.71*	18036	10168	10184	8862	8092	1632	1279	1039	936	889	42	67	4539	2958	3851
S4863	104	49	72.35	3565	3013	3630	2111	1747	1124	910	924	986	663	38	56	653	415	565
S3271	116	26	79.83	4234	3399	4723	2947	2838	8635	6203	9023	5601	4105	33	30	815	732	710
S3330	132	40	86.64	23659	24563	**MOut**	18893	16946	12837	11381	**MOut**	9927	7626	69	150	431	394	445
SFE[†]	293	69	218.77	863	762	892	519	438	147	130	153	101	71	14	76	94	92	88
S1423	74	17	37.41**	23325	35876	**MOut**	29916	**MOut**	65215	48366	**MOut**	**MOut**	49873	10	35	89	91	105

Table 2.4: Comparing our three static algorithms VS-I, VS-II and VS-III against FMCAD00 and Simulated annealing (SA) algorithm. (**MOut**)–Out of memory, (†)–SFEISTEL, (*)–after 8 reachability steps, (**)–after 14 reachability steps.

SAT Based Image Computation

2.4 SAT Procedures

A SAT solver reads a formula in conjunctive normal form (CNF) and finds a satisfying assignment if there is any. If not, the solver returns that the formula is unsatisfiable. SAT solving is one of the classical NP-complete problems. Over the last 4 years, propositional SAT checkers have demonstrated tremendous success on various classes of boolean formulas. The key to the effectiveness of SAT checkers like Chaff [61], GRASP [69], and SATO [75] is non-chronological backtracking, efficient conflict driven learning of conflict clauses, and improved decision heuristics.

SAT checkers have been successfully used for Bounded Model Checking (BMC) [7], where the design under consideration is unrolled and the property is symbolically verified using SAT procedures. BMC is effective for showing the presence of errors. However, BMC is not at all effective for showing that a specification is true unless the diameter of the state space is known. Moreover, BMC performance degrades when searching for deep counterexamples. The basic problem with BMC is that there is no mechanism to detect whether a fixed-point has been reached while exploring the state space. A more serious problem is that the transition relation is unrolled for a progressively increasing number of steps; hence, searching for deeper counterexamples becomes impractical. Our algorithm is used to detect fixed-points in image computations and the SAT checker never has to deal with multiple unrollings of the transition relation. In each SAT checker run, only one step of the image computation is done at a time.

The efficiency of SAT procedures has made it possible to handle circuits with several thousand of variables, much larger than any BDD based model checker is

able to do at present.

```
while(1) {
   if (decide_next_branch()) {        // Branching
      while (deduce() == conflict) {  // Propagate implications
         blevel = analyse_conflict(); // Learning
         if (blevel == 0)
            return UNSAT;
         else
            backtrack(blevel);        // Non-chronological
                                      // backtrack
      }
   }
   else                               // no branch means all vars
                                      // have been assigned
      return SAT;
}
```

Figure 2.8: Basic DPLL backtracking search (used from [61] for illustration purposes)

The basic framework for these SAT procedures, shown in Figure 2.8, is based on Davis-Putnam-Longeman-Loveland (DPLL) backtracking search. The function `decide_next_branch()` chooses the branching variable at current *decision level*. The function `deduce()` does *Boolean constraint propagation* to deduce further assignments. In the process, it might infer that the present set of assignments to variables does not lead to any satisfying solution. This is termed as a conflict, as at least one CNF clause remains unsatisfied. In case of a conflict, new clauses are learned by `analyze_conflict()` that hopefully prevent the same unsuccessful search in the

future. The conflict analysis also returns a variable for which another value should be tried. This variable may not be the most recent variable decided, leading to a *non-chronological* backtrack. If all variables have been decided, then we have found a satisfying assignment and the procedure returns. The strength of various SAT checkers lies in their implementation of constraint propagation, non-chronological backtracking, decision heuristics, and learning.

Modern SAT checkers work by introducing conflict clauses in the learning phase and by non-chronological backtracking. Implication graphs are used for Boolean constraint propagation. The vertexes of this graph are literals, and each edge is labeled with the clause that forces the assignment. When a clause becomes unsatisfiable as a result of the current set of assignments (decision assignments or implied assignments), a conflict clause is introduced to record the cause of the conflict, so that the same futile search is never repeated. The conflict clause is learned from the structure of the implication graph. When the search backtracks, it backtracks to the most recent variable in the conflict clause just added, not to the variable that was assigned last.

In our enumeration algorithm, we use the Chaff SAT checker [61], as it has been demonstrated to be the most powerful SAT checker on a wide class of problems.

2.5 SAT Procedures for Reachability Analysis

Following the outline of the basic reachability algorithm 2.1, we can use SAT procedures for image computation. The transition relation and the set of states is represented using a propositional formulas. SAT checkers like Chaff read propositional formulas represented in conjunctive normal forms (CNFs). We present an algorithm that does not use any BDDs. We assume that the transition relation $T(\mathbf{x}, \mathbf{i}, \mathbf{x}')$ is already represented in as a set of CNF clauses. It is customary to convert any transition

relation represented as a set of propositional formula to CNF form by introducing intermediate variables. This translation is polynomial in the size of the original circuit. We represent the set of newly reached states after each iteration of the reachability loop (S_i in Figure 2.1) as a set of disjunctive normal form (DNF) cubes. The set of all reachable states after each step (S_{reach}) is also represented in DNF. Since S_{reach} is in DNF, $\neg S_{reach}$ will be automatically in CNF. As Chaff needs CNF representation, we convert S_i from DNF to CNF by introducing intermediate variables. In each iteration i, we ask the SAT checker to find satisfying assignments to the formula below.

$$S_{i-1}(\mathbf{x}) \wedge T(\mathbf{x}, \mathbf{i}, \mathbf{x}') \wedge \neg S_{reach}(\mathbf{x}') \tag{2.7}$$

Formula 2.7 corresponds to step 5 of the basic reachability algorithm (Fig. 2.1). Any satisfying assignment to Formula 2.7 is such that the present state variables $\mathbf{x}$ and input variables $\mathbf{i}$ satisfy the predicate $S_{i-1}(\mathbf{x}) \wedge T(\mathbf{x}, \mathbf{i}, \mathbf{x}')$, i. e., the set of states reachable from the newly discovered states in the previous iteration. Furthermore, such a satisfying assignment also is in the negation of the set of all accumulated states so far ($\neg S_{reach}$), thus we ask the SAT checker to compute only the states that have not been seen so far. If the SAT checker concludes that the formula is unsatisfiable, then it means that the set of newly reached states S_i is empty, and we have reached fixed-point. On the other hand, if the SAT checker finds a satisfying assignment to this formula in present state $\mathbf{x}$, input $\mathbf{i}$, intermediate and $\mathbf{x}'$ variables, the projection of this assignment on $\mathbf{x}'$ variables gives a subset of newly reached states. Note that this partial assignment to $\mathbf{x}'$ is consistent with the full assignment that the SAT checker finds to the Formula 2.7. The Formula 2.7 describes all constraints on the next set of states. Therefore, the projection is a valid state reachable from S_{i-1} following the transition relation T. Thus, the following lemma easily follows.

```
    /* It is assumed that S_0 is given in DNF form */
    SatReachability(S_0)
1   i ← 1
2   S_reach ← S_0
3   while (S_{i-1} ≠ φ)
4       S_i ← φ
        /* DNFtoCNF converts a formula to CNF by
           introducing intermediate variables */
5       for (each satisfying partial assignment d in x' to
                DNFtoCNF(S_{i-1}(x)) ∧ T(x, i, x') ∧ ¬S_reach(x'))
                /* d contains only next state variables */
6               d' ← EnlargeCube(d)
7               Add ¬d' as a blocking clause
8               S_i ← AddCube(S_i, next2current(d'))
9               S_reach ← AddCube(S_reach, d')
10      endfor
11  endwhile
12  return next2current(S_reach)
```

Figure 2.9: Outline of the SAT based reachability algorithm

Lemma 1 *The projection of any partial satisfying assignment to Equation 2.7 in* $\mathbf{x}$, $\mathbf{i}$, $\mathbf{x}'$ *and intermediate variables to just* $\mathbf{x}'$ *is a valid partial assignment in* $\mathbf{x}'$ *describing a newly discovered state reachable from* S_{i-1} *following* T.

We add this state to $S_i(\mathbf{x})$ as a DNF cube $\mathbf{d}$, after translating the next state variables in the cube to present state variables. The negation of $\mathbf{d}$ is a CNF clause, which is added as a conflict clause in the SAT engine. This clause $\neg\mathbf{d}$ is called a *blocking clause*. Thus after finding each satisfying assignment, the set $S_{reach}(\mathbf{x}')$ grows.

We present the high level algorithm in Figure 2.9. The algorithm has two loops. The outer loop carries out different steps of image computation, while the inner loop is implicit in the SAT checker, and enumerates sets of the newly reached states in a particular step.

Each satisfying cube $\mathbf{d}$ is added to S_i and S_{reach} after enlarging it to $\mathbf{d}'$ in step 6. The addition of $\mathbf{d}'$ to S_{reach} is done in the SAT checker when the blocking clause $\neg\mathbf{d}'$ is added. As noted earlier, negation of S_{reach} is automatically in CNF. Step 6 of the algorithm is crucial to make our approach efficient and practical. We describe the efficiency issues, including step 6 of the algorithm, in the next subsection.

2.5.1 Efficient Implementation of SAT Based Reachability

Algorithm given in Figure 2.9, without step 6, is very inefficient and hence impractical. The first problem comes from the way the SAT checker computes satisfying assignments or cubes. The Chaff SAT checker gives values to all variables in any assignment. We then project this assignment to $\mathbf{d}$, which assigns values to all next state variables $\mathbf{x}'$. Therefore $\mathbf{d}$ describes only one newly reached state. Enumerating states one at a time is clearly very inefficient. However, most of the times, one does

not need to come up with a complete assignment to satisfy the CNF formula. A partial assignment to $\mathbf{x}'$ describes more than one state at a time, the larger the set, the fewer the number of assignments. This is advantageous in two ways, first the blocking clause for $\mathbf{d}$ prunes the SAT search space drastically, second, the number of state enumerations required go down considerably. Therefore, it is desired that the partial assignment be as small as possible. It is clearly to our advantage to get as small cubes as possible, since smaller cubes cover a larger number of assignments. Given a cube computed by Chaff, it may be possible to throw away certain assignments from the cube, and still get a satisfying cube. By a static analysis of the transition relation, we infer the unnecessary assignments in $\mathbf{d}$. This procedure *EnlargeCube*, described in the next sub-section, is called in line 6 on $\mathbf{d}$ to get a smaller cube $\mathbf{d}'$.

The second problem is that the representation of the sets S_{reach} and even S_i can grow too large. For example, if we consider a counter that counts up to 2^{30}, each iteration of the while loop will add only one state to S_{reach}. Thus we will have to represent 2^{30} clauses for S_{reach}. However, the DNF clause 1 represents all possible values of the counter. In other words, after a satisfying assignment to S_{reach} is found, we can combine multiple clauses to get a smaller partial assignment. For example, the DNF clauses $x_1 \wedge x_5 \wedge \neg x_6$ and $x_1 \wedge x_5 \wedge x_6$ can be combined to $x_1 \wedge x_5$. An efficient data structure is needed to support this *AddClause* operation, since many clauses may be added, and each clause can potentially be combined with more than one existing clause. We use a hash table, each entry of which contains a *trie* [47].

We give a cube enlargement heuristic procedure next, which is followed by a description of an efficient data structure that stores S_i and S_{reach}. The enlargement procedure reduces the number of enumerations, hence reducesthe amount of time, while the second procedure reduces the space requirement.

2.5.2 Cube Enlargement

There are five types of variables that appear in the SAT formula 2.7: present state variables $\mathbf{x}$, circuit inputs i, next state variables $\mathbf{x}'$, intermediate variables $\mathbf{i_s}$ introduced while converting S_{i-1} to CNF, and the intermediate variables $\mathbf{i_t}$ introduced while converting the transition relation $T(\mathbf{x}, \mathbf{i}, \mathbf{x}')$ to CNF. The SAT checker finds a satisfying assignment $\mathbf{c}$, possibly to all these variables. However, the cube $\mathbf{d}$ of line 7 in the algorithm (Fig. 2.9) is just in terms of $\mathbf{x}'$ variables. In order to reduce the number of assignments in $\mathbf{d}$, we use the following procedure. This procedure assumes that the transition relation is given in functional form, i.e., there is a transition function $f_i(\mathbf{x})$ for each next state variables x_i. This assumption is true for circuit descriptions. Let $Supp(f_i)$ denote the support set of f_i, i.e., the variables that f_i depends on. When an assignment to a next state variable x_i' can be ignored, we say that x_i' is *.

Free Variables

First, we describe the concept of free variables, i.e., the variables that are free to assume any value, despite the SAT checker assigning them specific values. In other words, we can ignore any assignment by the SAT checker to free variables. In order to detect whether the variable v is free or not, the following conservative tests are used. If v is an input variable or an intermediate variable, then it is definitely free. Moreover, for functional transition relations, we don't even need to check if an intermediate variable appears in other transition functions or not, since intermediate variables are generated from the local translation for f_i. The only real problem arises when v is a present state variable. The only constraints that are placed on the present state variables are from S_{i-1}. To see if the present satisfying assignment $\mathbf{c}$ restricts v or

not, we can just check that the assignment to v does not affect the present satisfying assignment. This can be efficiently detected as follows. While translating the DNF corresponding to S_{i-1} to CNF, we introduce one intermediate variable for each DNF cube. In essence, the truth value of each DNF cube is captured in the corresponding variable. Suppose $i_1, i_2, \ldots, i_k$ are the intermediate variables corresponding to DNF cubes $D_1, D_2, \ldots, D_k$ in S_{i-1}. The translation of the S_{i-1} constraint in Eqn. 2.7 looks like:

$$(i_1 \vee i_2 \vee \ldots \vee i_k) \wedge (i_1 \Leftrightarrow D_1) \wedge (i_2 \Leftrightarrow D_2) \wedge \ldots \wedge (i_k \Leftrightarrow D_k) \qquad (2.8)$$

Each equality $i_j \Leftrightarrow D_j$ gives rise to a set of CNF clauses, which we haven't expanded for the sake of brevity.

If the satisfying assignment c makes any of the intermediate variables true, the corresponding DNF cube is true, and we don't need to see if any other DNF cube is true, since the truth of only one DNF cube satisfies the S_{i-1} clauses. So we find the first intermediate variable i_l that is set to true. All present state variables *not mentioned in the DNF cube D_l are irrelevant* for satisfying the constraint S_{i-1}, hence, they can be assumed to be free.

Free Transition Functions

Let us denote the set of free variables in the support of a transition function f_i by $FreeSupp(f_i)$.

The main idea is that if a transition function f_i (for x'_i) depends on a variable v (which is either a present state variable, input or an intermediate variable from $\mathbf{i}_t$), and the following conditions are satisfied, then we can guarantee that x'_i can assume any value. Thus, the value of x'_i can be safely ignored from the present assignment.

1. Variable v is free.

2. After propagating the values of non-free variables in $Supp(f_i)$, f_i is not forced to a particular value. For example, suppose that $f_i = x_1 \wedge x_2$, x_1 is free, and $x_2 = 0$ in S_{i-1}. Propagating the value of x_2 forces f_i to 0. Thus, constant values of non-free variables are propagated first to detect such scenarios.

3. The function f_i does not share free support with any other transition function, i.e., $FreeSupp(f_i) \cap FreeSupp(f_j) = \phi, j \neq i$. Moreover, the variable v appears in the formula for f_i in exactly one place.

Note that there may be other conditions under which x'_i can still choose both values. However, the conditions presented above allow us to do a static analysis of the circuit.

The third condition is too restrictive in practice. Usually, transition functions do share common variables. In order to infer that a next state variable x'_i can assume both values, we can simplify the transition functions by further constant-propagating values of some free variables as well (remember that we already constant-propagate the values of non-free variables). For example, suppose that $f_1 = x_1 \vee i_2$ and $f_2 = x_1 \vee i_3$, and x_1, i_1 and i_3 are free variables. Suppose the SAT assignment is $x_1 = 0, i_1 = 0, i_2 = 1$. Since both f_1 and f_2 share the variable x_1, we can not safely say that both x'_1 and x'_2 are *. However, we can replace x_1 by 0, and propagate the effects, giving us $f_1 = i_2$ and $f_2 = i_3$. Now, both f_1 and f_2 become independent, and can be set to *. Note that since x_1 is a free variable, we could have chosen $x_1 = 1$, different from the SAT assignment. In order to determine the set of variables to assign values to, such that the transition functions become independent, we use a greedy strategy. We order the variables by the number of times they appear in all transition functions. Beginning with the variable that occurs the most number of times, we keep replacing the variables by constants (from SAT assignment) and propagating the effect, until

transition functions become independent and next state variables can be inferred to be *s. In the worst case, all transition functions become constants.

Most analysis of this procedure can be done statically just once. The only changing part is detection of free present state variables. Note that the process described above is just one alternative for cube enlargement. There can be other options. For example, we considered using efficient approximate set cover algorithms to find out the literals that cover all clauses of formula 2.7. Another option is to use BDD based symbolic simulation to infer multiple cubes. The given cube enlargement procedure produces one smaller cube. However, using BDDs for simulation of the circuit for one step and then applying constants to some of BDD variables to contain the BDD sizes can yield a set of many states at once.

2.5.3 Efficient Set Representation

The set of states are represented as a set of DNF cubes. However, it is easy to see that each new cube that is added to S_{reach} has a potential to be merged with other cubes to form shorter cubes. For example, the boolean function 1 is an exponentially more compact representation than four DNF cubes $a \wedge b, \neg a \wedge b, a \wedge \neg b, \neg a \wedge \neg b$. We describe the following procedure to add a cube to the existing set of cubes. We assume that the variables in the cubes are ordered. The set is represented by a hash table, where each hash table entry stores a subset of cubes in the *trie*, or a *prefix tree* data structure. Tries are often used to store dictionaries efficiently. Knuth's volume 3 on sorting and searching provides a good description of tries. In our case, each trie stores cubes that are made up of the same CNF variables. The hash table is indexed by the hash computed from a signature of a cube. In the following algorithm (Figure 2.11), assume that the DNF cube **d** is represented as a vector of integers, each integer identifying a particular propositional variable, negative if the literal is

negative, positive otherwise. For example, if $a, b, c, d, e, f...$ are variables, then they are identified by the integers $1, 2, 3, 4, 5, 6, ...$ So a cube $(a \wedge \neg c \wedge \neg f)$ is represented by the vector $\mathbf{d} = [1, -3, -6]$. The function *ComputeSignature* computes a bit string that is used to compute the hash value for a cube. The bit string is ordered, just as variables in the cubes are, and contains 1 for each variable present and 0 for the variables not present in the cube. The trailing $0s$ are removed to get a shorter bit string. Thus even though there may be variables numbered $7, 8, 9, ..,$ the $0s$ corresponding to them do not appear in the signature. So the signature for the cube $\mathbf{d}$ is 101001.

```
    COMPUTESIGNATURE(d, m)
    /* m is the size of the cube d, assume d is sorted */
1   j ← 1
2   for (i from 1 to d[m])
3      if (i = |d[j]|) /* variable is present in d */
4            s_d[i] ← 1
5            j ← j + 1
       else
6            s_d[i] ← 0
       endif
    endfor
7   return s_d
```

Figure 2.10: Procedure *ComputeSignature*.

Since each trie stores cubes made up of the same variables, the cubes are represented by bit strings of the same length as the number of variables in the cubes of the trie. Essentially, if a literal is positive, the bit corresponding to it is 1, and 0

otherwise. So the cube **d** is stored as 100.

The crux of the *AddCube* procedure is between lines 5–19. Given an incoming cube **d**, it tries to find all other cubes from the trie that differ from **d** in just one bit. For each such cube $\mathbf{d}'$ found (lines 10–13), the cube computed by merging **d** and $\mathbf{d}'$ is added to S by calling *AddCube* recursively. The merged cube is essentially cube **d** with the matched bit (i^{th} bit) removed. If **d** doesn't match at the ith bit, then the next bit is checked. Once the traversal over the trie is done, we check if **d** was merged with anything. If it was, then we no longer keep **d**. Line 18 just updates the hash table with potentially modified trie.

Note that the algorithm doesn't guarantee absolute minimum cubes. In fact, to do so, we may need to keep all cubes, even after they are merged, in the hopes of merging them with other future cubes. But the main focus of the algorithm is to reduce space, and not get the absolute smallest cubes. Another point to note is that since the SAT checker always finds new states that haven't been discovered so far, we assume that the trie T_d does not already contain **d**.

The complexity of this algorithm in the worst case can be $O(n^2)$. Here n is the number of state variables. Each of line 1, 3–4, 6 and 17 cost $O(n)$, while hash lookups and updates on lines 2 and 18 are essentially constant time operations. Lines 10 and 11 cost $O(m) + O(m-1) + \ldots + O(1) = O(m^2) = O(n^2)$.

2.5.4 Complexity of the Set Representation

The set of DNF cubes representing S_i or S_{reach} possess a useful property. By the negation of S_{reach} in the SAT formula (Eqn. 2.7), we guarantee that no newly generated DNF cube shares a satisfying assignment with any existing cube in sets S_i or S_{reach}. Thus the set of DNF cubes representing these sets are disjoint, in that they

```
ADDCUBE(S, d, n, m)
    /* n is the total number of variables, m is the number of variables in d */
1   s_d ← ComputeSignature(d, m)
2   T_d ← HashLookup(S, s_d) /* T_d is the trie in which d will be stored */
    /* compute the representation of d to store in T_d */
3   for (i from 1 to m)
4       b[i] ← (d[i] > 0)?1 : 0
5   match ← false
6   T_d ← TrieInsert(T_d, b)
7   curr_node ← T_d
8   for (i from 1 to m)
9       b[i] ← 1 − b[i] /* flip the i^th bit */
10      if (TrieLookup(curr_node, b[i : m]) = true)
11              T_d ← TrieDelete(T_d, b) /* match at the ith bit */
                /* insert the merged cube */
12              S ← AddCube(S, d[1 : i − 1] :: d[i + 1 : m], n, m)
13              match ← true
        endif
14      b[i] ← 1 − b[i] /* flip it back to what it was */
15      curr_node ← (b[i] = 1)?curr_node.right : curr_node.left
    endfor
16  if (match = true)
17      T_d ← TrieDelete(T_d, b)
18  S ← HashUpdate(S, s_d, T_d) /* update the trie for this cube */
19  return S
```

Figure 2.11: Procedures *AddCube*.

do not have any common assignment. For example, the DNF cube $b \wedge c \wedge d$ cannot occur if the cube $a \wedge b \wedge c$ is already present, as they share a common assignment $a = b = c = d = 1$. However, cube $\neg a \wedge b \wedge c \wedge d$ can occur. If we can detect that the set of cubes is a tautology, we can terminate the reachability, as we have reached all the states. Our cube addition algorithm is *online* in nature. We now prove that if the set of DNF cubes that do not share a common satisfying assignment is given *a priori*, then detecting if it is a tautology is polynomial. The general problem of detecting DNF tautology is coNP-complete.

Let us call the problem of tautology detection of a set of DNF cubes that do not share any pair wise common assignment an *R-TAUT* problem. The procedure for tautology detection works simply by counting the number of satisfying assignments. Suppose that there are c DNF cubes made up from a total of m variables, and that the cubes do not share common assignments pair wise. Suppose cube i has literals $l_1, l_2, \ldots, l_{c_i}$. There are a total of 2^m possible assignments to variables, and if each assignment is a satisfying assignment, then the DNF cubes are a tautology. Cube i describes a total of 2^{m-c_i} assignments agreeing with the literals in cube i. As we know that no two cubes i and j share any common assignment, the total number of assignments that satisfy both cube i and j are precisely $2^{m-c_i} + 2^{m-c_j}$. The total number of satisfying assignments for the set of DNF cubes is just

$$2^{m-c_1} + 2^{m-c_2} + \ldots + 2^{m-c_c}.$$

Clearly, the additions can be carried out in time polynomial in m and c, the size of problem input. Hence the theorem

Theorem 2 *R-TAUT is in P.*

Note that in our case, the set of DNF cubes are not given a priori. However, this procedure can be run periodically on S_{reach} to find out if all states have been reached,

in which case we stop the search. We also use this counting mechanism to report the number of reached states.

2.6 Results for SAT Based Reachability Analysis

We implemented our algorithms on top of the zChaff SAT solver. The SAT solver is modified to enumerate satisfying solutions by adding blocking clauses.

We conducted our experiments on a 1.53GHz dual AMD Athlon processor machine with 3GB of memory running Linux. The memory cutoff was set to 1.5GB of resident program size, and the time cut off was set to 1000 seconds. The results are summarized in table 2.5. For each circuit, we report the number of latches, the number of reachability steps that we could complete, the number of cubes stored in the representation for the reachable states, the number of cubes that were enumerated as blocking clauses (or how many times line 7 in algorithm of Figure 2.9 was called), the ratio of the number cubes v/s the number of blocking clauses added in percentage, and the total running time (user time+system time) in seconds. Note that the number of cubes in the final set representation is much smaller than the total number of enumerated cubes, as evidenced by the %age size column, asserting that the space saving data structure for storing cubes is effective. We compare our results with primarily that of [57]. We would like to emphasize that in [57], only the depth was computed, and the actual set of reachable states was not computed.

The circuits that we report come from mainly three sources, ISCAS'89 benchmarks, IU set of circuits from Synopsys, and some circuits that were translated from Verilog code available from various sources. The IU set of circuits are various abstractions of parts of a picoJava microprocessor implementation.

For a relatively small timeout value, we have been able to do reachability for many

Circuit	# latches	# steps	Space Requirement			Time (sec)	Comparison with [57]	
			# cubes	# blocking clauses	%age space		Max. Depth	Time (sec)
decss	86	85*	655	131304	0.50	1000.00		
iu30	30	4*	3343	72037	4.64	1000.00		
iu35	35	3*	1479	94424	1.57	1000.00		
iu40	40	2*	20	33168	0.06	1000.00		
iu45	45	1*	2294	165192	1.39	1000.00		
s208.1	8	255	8	255	3.14	0.56		
s298	14	18	33	217	15.21	0.33	18	19.3
s344	15	6	558	2624	21.27	15.30		
s349	15	6	546	2624	20.81	14.82		
s382	21	150	337	8864	3.80	7.71		
s386	6	7	6	12	50.00	0.21	7	0.18
s400	21	150	336	8864	3.79	7.81		
s420.1	16	65535	16	65535	0.02	213.97		
s444	21	150	341	8864	3.85	8.00		
s499	22	21	21	21	100.00	1.74	21	1.07
s510	6	46	10	46	21.74	0.47	46	144.81
s526	21	150	381	8867	4.30	9.35		
s526n	21	150	372	8867	4.20	9.21		
s635	32	125528*	66	125528	0.05	1000.00		
s641	19	6	321	1543	20.80	2.24	6	97.03
s713	19	6	363	1543	23.53	2.53	6	126.94
s820	5	10	11	24	45.83	0.48	10	2.51
s832	5	10	11	24	45.83	0.47		
s838.1	32	155441*	26	155441	0.02	1000.00		
s953	29	10	189	503	37.57	2.01	10	102.23
s967	29	10	177	548	32.30	3.12		
s1196	18	2	802	2615	30.67	6.79	2	232.84
s1238	18	2	849	2615	32.47	7.26		
s1269	37	1*	2136	4339	49.23	1000.00	7*	5000
s1423	74	3*	2652	55568	4.77	1000.00	26*	5000
s1488	6	21	19	47	40.43	0.87	21	96.87
s1494	6	21	19	47	40.43	0.87		
s1512	57	4*	2035	178175	1.14	1000.00		
s9234	228	8*	507	6651	7.62	1000.00		
s13207	669	2*	76	1824	4.17	1000.00		
s15850	597	5*	362	2558	14.15	1000.00		
s38584	1452	2*	58	452	12.83	1000.00		

Table 2.5: Experimental results on a set of circuits from various sources including ISCAS'89 and Synopsys. The comparison is against [57]. Note: (*)-reachability was not complete. Empty boxes denote results N/A.

circuits. Our technique outperformed the one in [57] by a large magnitude on all but one small completed benchmarks. The authors of [57] used a faster machine (2GHz v/s 1.53GHz) as well. The effectiveness of the cube merging procedure is evident from "%age space" column. The savings are dramatic for circuits that have counter-like structures in them (iu**, s208.1, s420.1, s838.1, s635), and also for some circuits that are not known to have counters (s1512, s9234, s13207, s1423, s526, s526n). For other circuits, it can be inferred that the SAT checker and cube enlargement procedures generate many disjoint cubes that can not be merged with the existing set of cubes. This may be dependent on circuit structure.

Lahiri *et al.* [50] used our tool to enumerate symbolic solutions to certain predicate abstraction formulas. The characteristic of these formulas was that the number of variables to be quantified was much larger (an order of magnitude) than the number of variables representing the set of states. For image computation, the number of variables to be quantified may not necessarily be much larger than the number of state variables.

2.7 Related Work

Burch *et al.* [12] and Touati *et al.* [70] first recognized the importance of early quantification for image computation. Geist and Beer [33] proposed a simple heuristic algorithm, in which they ordered conjuncts in the increasing order of the number of support variables. Touati *et al.* were the first to formulate the early quantification problem as an evaluation of a parse tree and proved the NP-completeness of the problem. They also offered a greedy strategy for evaluation of the parse tree by evaluating the node with the smallest support set next. However, they do not compare their technique against other techniques, so the effectiveness of their algorithms was not

clear. All successful techniques so far in the literature consider only linear conjunction schedules and use the same conjunction schedule for all the image computations during symbolic analysis. These techniques begin by first ordering the conjuncts and then clustering them and finally ordering the clusters again using the same heuristics. Ranjan *et al.* [64] proposed the first successful heuristics for this problem and Yang [73] refined their technique. The ordering procedures of both papers linearly orders the BDDs based on a heuristic score. The individual BDDs are then formed into clusters by conjoining them according to the order until BDD size grows beyond certain threshold. Finally, these clusters are ordered using the same algorithm. A recent paper by Moon and Somenzi [60] presents an ordering algorithm (henceforth referred to as FMCAD00) based on computing the *Bordered Block Triangular* form of the dependence matrix to minimize the *average active lifetime* of variables. Their clustering algorithm is based on the sharing of support variables (affinity). We extended their notion of lifetimes and used combinatorial algorithms to improve the performance [16].

The first completely SAT based reachability algorithm was reported by McMillan in [53]. The main difference between our SAT based reachability algorithm is that we represent the set of states in DNF, while he represented the set of states in CNF. A SAT based enumeration algorithm is used to compute a CNF formula equivalent to a given formula characterizing preimages. However, we use intermediate variables to convert the DNF representation to CNF while running SAT. He used *zero suppressed* BDDs (zDDs) to store the CNF clauses, and used a SAT conflict analysis based heuristic to enlarge the cubes. We did not compare the results reported in [53] as the set of benchmarks in [53] was not publicly available.

In [44], the authors used a procedure similar to our SAT based reachability to compute preimages. They also use intermediate variables to convert DNF cubes to

CNF formulas. However, they use the offline version of the Espresso [65] algorithm to reduce the number of cubes. Our cube storage procedure is on-line, in the sense that it processes the cubes as they are generated. Moreover, they do not have any algorithm to enlarge the cubes. They also reported the results only on two different circuits and for safety property checking only, which can be much easier than to do than reachability when the property is false. Our attempts to contact them to get more information about the properties they checked failed.

In [68], the authors used ATPG instead of SAT to compute preimages. They used BDDS to store the resultant sets of states. ATPG allows reasoning directly on the circuits, hence they do not have any intermediate variables. They report results on only two circuits. These are known to be difficult circuits, however.

In [57], the only aim is to compute the sequential diameter, also called the *diameter* of the circuit. They do not compute the reachable set of states at all. Their procedure is based on the Chaff SAT checker as ours is. Their procedures shares many similarities with bounded model checking (BMC) [5]. They build a SAT formula describing symbolic simulations of increasing length. In our SAT based reachability approach, we explicitly compute the set of reachable states, and the SAT checker does not have to compute more than one step of symbolic simulation at a time. We believe that this is a significant advantage that our method has over [57] and BMC. Using BMC for depth equal to circuit diameter is sufficient for $\mathbf{G}p$ kind of LTL properties. In [48], this notion is generalized to that of *completeness threshold* (CT). The authors describe a sorting network built on top of SAT formula for computing diameters.

In [38, 39], a mixed BDD and SAT based approach to image computation is described. They use SAT procedure to derive a top level disjunctive decomposition of image computation and use BDD based image computation for each leaf subproblem.

2.8 Summary

We have proposed simple yet effective quantification scheduling algorithms for the image computation problem. We view the problem of quantification scheduling for symbolic image computation as a quantified Boolean formula evaluation problem. We have also proposed heuristic algorithms based on scoring of quantification variables to reduce the size of the intermediate BDDs. We have demonstrated that our simple yet flexible approach yields better experimental results for many reachability analysis and model checking problems.

We can view the problem of building an optimal parse tree as a combinatorial optimization problem and apply techniques like simulated annealing to get better quantification schedules. A middle ground between dynamic and static techniques seems promising. For example, we believe that beginning with some static schedule, the schedule can be tuned for a particular image computation with a little effort. We also want to investigate techniques of approximating sizes of BDDs based on the size of support sets, which will definitely improve all image computation heuristics. The techniques developed for quantification scheduling can be applied to other related problems, like splitting orders in SAT checkers [7] and hierarchical model checking [58].

Moving on to SAT, we presented a completely SAT based image computation algorithm. The effectiveness of this algorithm is demonstrated for reachability analysis on many large circuits. This algorithm can be used for computing pre images equally well, hence it can be used in a general SAT based symbolic model checking algorithm. The novel features of our algorithm are an efficient data structure for storing sets of states as DNF cubes and a cube enlargement procedure based on static circuit analysis.

Chapter 3

SAT Based Reparameterization Algorithm for Symbolic Simulation

3.1 Introduction

Symbolic simulation is a widely applied technique for analysis of complex transition systems and synchronous circuits in particular. In symbolic simulation, the transition relation is unwound m times into an equation that represents the set of states that is reachable in exactly m steps. The simulator keeps separate equations for each state variable. They are parameterized in the initial state and the inputs of the circuit. Thus, the set of states is stored in a *parametric representation*.

An efficient way to store and manipulate this parametric representation of the set of states is crucial for the performance of the algorithm. Such a representation describes a set of states as a vector $(f_1, f_2, \ldots, f_n)$ of functions in parameters $P = \{p_1, p_2, \ldots, p_m\}$. Each parametric function gives the value of one state variable. For example, the set of states $S = \{10, 01\}$ is represented parametrically as $(p_1, \neg p_1)$. In this case, there is only one parameter p_1.

Most implementations use BDDs to represent these functions [1, 30, 34, 35, 43, 74]. These BDDs may grow exponentially in the number of simulation steps, as the number of variables grows. In order to address this problem, symbolic simulators compute a new, equivalent parametric representation. The new representation can be significantly smaller since it usually requires much fewer variables. This step is done as soon as one of the BDDs becomes too large. The process of converting one parametric representation to another is called *reparameterization*. In [30] and [43], the reparameterization algorithm first converts the parametric representation into characteristic function form and then parameterizes this form. In [34], an algorithm is given for computing set union in parametric form. Algorithms for reparameterization and quantification are given that are based on this set union algorithm. However, the reparameterization is done using BDDs, hence as the number of simulation steps grows, the algorithm quickly becomes very expensive. This is due to the fact that each simulation step introduces more input variables, which need to be quantified during reparameterization.

Novel Contributions We describe a SAT-based algorithm to perform the reparameterization step for symbolic simulation. The algorithm performs better than BDD-based reparameterization especially in the presence of many input variables. The algorithm takes arbitrary Boolean equations as input. Therefore, it does not require BDDs for the symbolic simulation. Thus, symbolic simulation can benefit from non-canonical forms that grow at most linearly with the number of simulation steps.

In essence, the SAT-based reparameterization algorithm computes a new parametric function for each state variable one at a time. In each computation, a large number of input variables are quantified by a single call to a SAT-based enumera-

tion procedure, e.g. [18, 53], described in Chapter 2. The advantage of this approach is twofold: First, all input variables are quantified at the same time, and second, the performance of SAT-based enumeration procedure is largely unaffected by the number of input variables that are quantified.

We demonstrate the efficiency of this new technique using large industrial circuits with thousands of latches. We compare it to both SAT-based Bounded Model Checking and BDD-based symbolic simulation. Our new algorithm can go much deeper than a standard Bounded Model Checker can. Moreover, the overall memory consumption and the run times are, on average, 3 times less than the values measured using a Bounded Model Checker. The BDD-based symbolic simulator could not even verify most of the circuits that we used.

3.2 Parametric Representation

Characteristic functions and parametric representations are two well known methods of representing a set of Boolean vectors. A set of Boolean vectors over the state variables represents a set of states. Consider a set S of vectors over the variables $V = \{v_1, v_2, \ldots, v_n\}$. As described above, $\bar{v} = (v_1, v_2, \ldots, v_n)$ denotes a particular vector or a particular assignments to the variables in V. If the characteristic function $\xi(\bar{v})$ represents the set S of vectors, then

$$S = \{\bar{v} \in \mathcal{S}_n \mid \xi(\bar{v}) = 1\}. \tag{3.1}$$

Example The following example will be used throughout this chapter. Let v_1 and v_2 be two Boolean state variables. Consider the set of states $\{01, 10, 11\}$. A characteristic function for this set of states is $\xi(\bar{v}) = v_1 \vee v_2$.

On the other hand, if S is represented parametrically with a vector of n functions

$\bar{f}(\bar{p}) = (f_1(\bar{p}), f_2(\bar{p}), \ldots, f_n(\bar{p}))$ over m parameters $\bar{p} = (p_1, p_2, \ldots, p_m)$, then

$$S = \{\bar{v} \in \mathcal{S}_n \mid \exists \bar{p} \in \mathcal{P}_m[v_1 = f_1(\bar{p}) \wedge v_2 = f_2(\bar{p}) \wedge \ldots \wedge v_n = f_n(\bar{p})]\}. \quad (3.2)$$

Informally, the set of vectors in S is given by the range of the vector of functions $(f_1(\bar{p}), f_2(\bar{p}), \ldots, f_n(\bar{p}))$, where $\bar{p}$ ranges over all possible Boolean vectors in $\mathcal{P}_m$. For the running example, one possible parametric representation with three parameters $P = \{p_1, p_2, p_3\}$ is

$$(f_1(\bar{p}) = p_1 \wedge p_2, f_2(\bar{p}) = \neg(p_1 \wedge p_2) \vee p_3).$$

Note that, in general, $m \neq n$. For the particular case of symbolic simulation that we will discuss later, the number of parameters will be equal to the number of input variables to the circuit times the number of simulation steps, which can be much larger than n.

A parametric representation can be easily converted to a characteristic function by using the following equation:

$$\xi(\bar{v}) = \exists \bar{p}[(v_1 \leftrightarrow f_1(\bar{p})) \wedge (v_2 \leftrightarrow f_2(\bar{p})) \wedge \ldots \wedge (v_n \leftrightarrow f_n(\bar{p}))]. \quad (3.3)$$

In other words, $\xi(\bar{v})$ is true if the there exists an assignment $\bar{p}$ to the parameters such that the parametric function $f_1(\bar{p})$ evaluates to v_1, $f_2(\bar{p})$ evaluates v_2, and so on. This is what is desired, since ξ is supposed to be true exactly for the vectors in the set. In the case of symbolic simulation, $\bar{p}$ consists of the initial state and the inputs on the path to the state $\xi(\bar{v})$.

Note that the conversion to characteristic function involves Boolean quantification over the parameters. If the functions are represented by BDDs, then this quantification becomes harder as the number of parameters m and the number of state variables n increase. As we have seen in chapter 2, a similar quantification problem

occurs in BDD-based image computation when a transition relation is represented in conjunctively decomposed form. In that case, the variables to be quantified are the present state and input variables of the circuit, while the next state variables are not quantified.

Before proceeding further, we describe the notations and conventions we will use in this chapter.

Notations and Conventions

Sets will be denoted by capital letters, as in S for the set of states, V for the set of state variables, I^k for the set of input variables, and P for the set of parametric variables. We use a superscript of k for input variables to denote input variables accumulated over k steps of symbolic simulation. An ordered tuple of lower case letters denotes a vector of variables. For example, the state variable vector with n state variables is $(v_1, v_2, \ldots, v_n)$. A vector is denoted by using a bar over the symbol. For example, a state vector will be denoted by $\bar{v}$, an input vector of variables from I^k is denoted by $\bar{\iota}$. Similarly, a parameter vector is denoted by $\bar{p} = (p_1, p_2, \ldots, p_m)$. The set of all possible 2^n vectors of n state variables is $\mathcal{S}_n$, the set of all possible 2^m assignments to m parameters is $\mathcal{P}_m$, and the set of all possible input vectors is $\mathcal{W}^k$. Other uppercase calligraphic letters denote subsets of these sets. When the number of components in a vector is clear, we will often drop the subscripts, and just use $\mathcal{S}, \mathcal{P}$, and so on. Functions will be denoted by lower case symbols, e.g., $f(\bar{\iota})$. In the parenthesis after a function symbol, the list of variables on which the function depends (the support set) is given, e.g., $h_i^1(p_1, p_2, \ldots, p_i)$. A vector of functions will be denoted by a bar over the top of the function symbol. For example, a vector of parametric functions is $\bar{h}(\bar{p}) = (\bar{h}_1(\bar{p}), \bar{h}_2(\bar{p}), \ldots, \bar{h}_n(\bar{p}))$. The symbol α will denote the constants 0 or 1. We sometimes use the symbol $t(j)$ to denote the state vector

at step j of the simulation in the trace $t(0), \ldots, t(k)$ of length k.

We summarize this notation in the following Table 3.1.

$$n : \text{number of state variables}$$
$$m : \text{number of parameters}$$
$$l, k : \text{number of simulation steps}$$

Sets of Variables	**Vectors of Variables**	**Sets of Vectors**
$V = \{v_1, v_2, \ldots, v_n\}$: state variables	$\bar{v} = (v_1, v_2, \ldots, v_n)$: state variable vector	$\mathcal{S}_n$ or $\mathcal{S}$: set of all state vectors $\mathcal{X}_n, \mathcal{Y}_n$ or $\mathcal{X}, \mathcal{Y}$: subsets of S_n
$P = \{p_1, p_2, \ldots, p_m\}$: parameters	$\bar{p} = (p_1, p_2, \ldots, p_m)$: parameter vector	$\mathcal{P}_m$ or $\mathcal{P}$: set of all parameter vectors
I^k : all inputs from step 1 to k	$\bar{\imath}^k$ or $\bar{\imath}$: input vector	$\mathcal{W}^k$: all input vectors $\mathcal{J}^k, \mathcal{K}^k$: subsets of $\mathcal{W}^k$

Functions	**Vectors of Functions**
$f_i(\bar{\imath})$: simulated expression for state variable v_i	$\bar{f}(\bar{\imath}) = (f_1(\bar{\imath}), f_2(\bar{\imath}), \ldots, f_n(\bar{\imath}))$: vector of simulated expressions for all state variables
$h_i(\bar{p})$: parametric function for v_i	$\bar{h}(\bar{p}) = (h_1(\bar{p}), h_2(\bar{p}), \ldots, h_n(\bar{p}))$: vector of parametric functions

Table 3.1: Notations and Conventions.

Parametric Representation in Symbolic Simulation

Consider a circuit C with p inputs and n state variables. Suppose the circuit is symbolically simulated for k steps, by building Boolean expressions that represent

the values of each of the state bits. After the k-step simulation, suppose each state bit v_i is given by a Boolean expression denoted by the function $f_i(\bar{\imath})$. The variables I^k appearing in each function $f_i(\bar{\imath})$ are the $p \cdot k$ inputs plus the n initial values of the state variables. Thus, $|I^k| = m = p \cdot k + n$. We will denote the set of input vectors over I^k variables by $\mathcal{W}^k$ and a particular input vector by $\bar{\imath}$. Traditional symbolic simulators can simulate a large number of steps, making $p \cdot k \gg n$. The set of reachable states in k steps, as a set of state vectors in V variables, is given by

$$S = \{\bar{v} \in \mathcal{S}_n \mid \exists \bar{\imath} \in \mathcal{W}^k [v_1 = f_1(\bar{\imath}) \wedge v_2 = f_2(\bar{\imath}) \wedge \ldots \wedge v_n = f_n(\bar{\imath})]\}.$$

Thus symbolic simulation builds a parametric representation of the set of states reachable in exactly k steps, where the parameters are input variables I^k.

Usually, the number of parameters $|I^k|$ is very large. The number of possible valuations of these variables is $2^{|I^k|}$, while the number of possible valuations of the state variables is 2^n. Therefore, many vectors in $\mathcal{W}^k$ variables will map to the same state vector. Hence, it should be possible to reduce the number of parameters. We aim at finding new functions $h_1(\bar{p}), h_2(\bar{p}), \ldots, h_n(\bar{p})$ in new parameters P, where $|P| \ll |I^k|$. This is why reparameterization is useful. Obviously, a set of vectors in n variables can be represented by parametric functions of n variables. Hence, $|P| \leq n$. This process of converting from one parametric representation to another is called *reparameterization* [30, 34].

For the example above, another parametric representation in just two parameters $P = \{p_1, p_2\}$ is $(h_1(\bar{p}) = p_1, h_2(\bar{p}) = \neg p_1 \vee p_2)$.

There has been some work on reparameterization using BDDs. The most complete description can be found in [34, 43]. The BDD-based method quantifies the input variables one at a time from the parametric representation $\bar{f}(\bar{\imath})$. Each quantification involves a parametric union of the two sets, each of which could require a number of

BDD operations, linear in the number of state bits. The BDD-based algorithm has $|I^k|$ variable eliminations in the outer loop, and the inner loop iterates over all state bits. Thus, to eliminate all I^k variables, $|I^k| \cdot n$ BDD operations are needed [34, 43].

We present a SAT-based reparameterization algorithm. Our SAT-based algorithm does this in one pass over the state bits. The outer loop iterates over the state bits, and the inner computation quantifies all I^k variables in one run of the SAT checker. The details of the algorithm are described in the next section.

3.3 Reparameterization using SAT

We first show how to compute the set of states in an efficient parametric form when the transition relation for the state transition system is given in functional form, i.e., one next state function for each state variable. Next, we will generalize the algorithm to compute efficient parametric forms of the set of states when given a general transition relation $R(v, v')$. This extension is useful in many ways. We require this ability to handle many circuits described this way. Next, this extension is required to simulate counterexamples as will be required in the abstraction-refinement framework.

3.3.1 Background

The algorithm computes functions $h_1(\bar{p}), h_2(\bar{p}), \ldots, h_n(\bar{p})$ in parameters P, where $|P| \leq n$. Thus, the number of parameters is at most equal to the number of state variables. Moreover, the functions h_i will have a specific structure, in that the function h_i will only depend on the variables $\{p_1, p_2, \ldots, p_i\}$. This will be explicitly denoted by $h_i(p_1, \ldots, p_i)$. We will derive these functions in the order $h_1, h_2, \ldots, h_n$.

Intuitively, each new parameter p_i allows for the free choice of the ith state bit v_i. Let $h_i^1(p_1, \ldots, p_{i-1})$ denote the Boolean condition under which the state bit v_i is forced to take value 1, and let $h_i^0(p_1, \ldots, p_{i-1})$ denote the Boolean condition under which the state bit v_i is forced to take value 0, and $h_i^c(p_1, \ldots, p_{i-1})$ denote the Boolean condition under which v_i is free to choose a value (is not forced to either 0 or 1).

For the set $\{01, 10, 11\}$ in the running example, suppose we let the first bit be represented by free parameter p_1. If the first bit is 0, then the second bit is forced to be 1 in the set. Thus, the Boolean condition under which v_2 is forced to 1 is $h_2^1(p_1) = \neg p_1$. Moreover, if the first bit is 1, then the second bit is free to be either 0 or 1. Thus, $h_2^c(p_1) = p_1$. Note that $h_2^0(p_1) = 0$, since the second bit is not forced to 0 in any condition.

The following decomposition of h_i was introduced in [34, 35]:

$$h_i(p_1, \ldots, p_i) \quad = \quad h_i^1(p_1, \ldots, p_{i-1}) \vee (p_i \wedge h_i^c(p_1, \ldots, p_{i-1})) \,. \tag{3.4}$$

Intuitively, Equation 3.4 is interpreted as follows. The value of bit v_i is 1 precisely under the condition h_i^1, hence the first term in the equation. If the parameters p_1 to p_{i-1} do not force the bit v_i to be 1, then the bit is given by the free parameter p_i under the free choice condition h_i^c.

The three conditions h_i^0, h_i^1 and h_i^c are mutually exclusive and complete, thus

$$h_i^c \quad = \quad \neg(h_i^1 \vee h_i^0) = \neg h_i^1 \wedge \neg h_i^0. \tag{3.5}$$

Continuing our example, we get $h_2(p_1, p_2) = \neg p_1 \vee (p_2 \wedge p_1)$, which is equivalent to the smaller parametric representation $\neg p_1 \vee p_2$ we presented in the previous section. It should be evident that h_i^0, h_i^1, and h_i^c depend only on the parameters p_1 to p_{i-1}. Assigning some specific value to a bit restricts the set of choices for the following bits. In our example, choosing $v_1 = 0$ restricts the value of the bit v_2 to 1. In this

special form of a parametric representation, the parametric function h_i is restricted only by the choices made for the earlier bits. Thus, the critical part of computing h_i is computing the three conditions h_i^1, h_i^0 and h_i^c, which we describe now.

3.3.2 Computing h_i^1 and h_i^c

Let us recall the meaning of h_i^1: It denotes the Boolean condition in variables $\{p_1, \ldots, p_{i-1}\}$ under which the ith bit v_i is forced to take the value 1. In the given representation $\bar{f}(\bar{\iota})$, bit v_i is constrained by other bits in what values it can take. Initially, these constraints are given by the common variables I^k. We want to re-express these constraints in P variables. Let $\bar{p} = (p_1, p_2, \ldots, p_{i-1})$ be a specific assignment which makes the Boolean condition $h_i^1(p_1, \ldots, p_{i-1})$ true. Then all input vectors $\bar{\iota} \in \mathcal{W}^k$, for which the functions $f_1, \ldots, f_{i-1}$ evaluate to the same values as $h_1, \ldots, h_{i-1}$, are said to be confirming to the assignment $(p_1, p_2, \ldots, p_{i-1})$. In essence, the evaluation of the new parametric functions and the old parametric functions is the same for these input vectors. The *restriction function* $\rho_i(p_1, \ldots, p_{i-1}, \bar{\iota})$ is used to find this set of confirming inputs. The function ρ_i restricts the set of input vectors $\mathcal{W}^k$ to only those that conform with the given assignment to the parameters. Formally, it can be written as

$$\rho_i(p_1, \ldots, p_{i-1}, \bar{\iota}) \quad = \quad \bigwedge_{j=1}^{i-1} h_j(p_1, \ldots, p_j) = f_j(\bar{\iota}). \tag{3.6}$$

Note that $\rho_1 = 1$. Now the condition h_i^1 can be easily expressed as follows: We want a Boolean condition in $\{p_1, \ldots, p_{i-1}\}$ variables under which v_i is forced to take the value 1. So if an assignment $(\bar{p}_1, \bar{p}_2, \ldots, \bar{p}_{i-1})$ makes h_i^1 true, then that means that for all input vectors $\bar{\iota}$ that conform with this assignment, the function $f_i(\bar{\iota})$ evaluates to 1. Hence,

$$h_i^1(p_1, \ldots, p_{i-1}) = \forall \bar{\iota} \in \mathcal{W}^k \left[(\rho_i(p_1, \ldots, p_{i-1}, \bar{\iota}) \Rightarrow f_i(\bar{\iota}) = 1) \right]. \tag{3.7}$$

Analogously, h_i^0 can be expressed as

$$h_i^0(p_1, \ldots, p_{i-1}) = \forall \bar{\iota} \in \mathcal{W}^k \left[(\rho_i(p_1, \ldots, p_{i-1}, \bar{\iota}) \Rightarrow f_i(\bar{\iota}) = 0) \right]. \tag{3.8}$$

Equation 3.5 can be used to compute h_i^c, given both h_i^1 and h_i^0. Thus h_i can be easily computed. Note that $h_1 = p_1$, unless the bit v_1 is always 1 or 0, in which case $h_1 = 1$ or $h_1 = 0$. This follows automatically from $\rho_1 = 1$.

Thus, Equations 3.4 to 3.8 give us the following high level reparameterization algorithm, that we call OrderedReparam.

// Input: Parametric Representation $\bar{f}(\bar{\iota}) = (f_1(\bar{\iota}), f_2(\bar{\iota}), \ldots, f_n(\bar{\iota}))$.

// Output: Parametric Representation $\bar{h}(\bar{p}) = (h_1(\bar{p}), h_2(\bar{p}), \ldots, h_n(\bar{p}))$.

OrderedReparam($\bar{f}(\bar{\iota}) = (f_1(\bar{\iota}), f_2(\bar{\iota}), \ldots, f_n(\bar{\iota}))$

1 $\rho \leftarrow 1$
2 **for** $i = 1$ **to** n
3 $\quad h_i^1 \leftarrow \forall \bar{\iota}.(\rho_i \Rightarrow f_i = 1)$
4 $\quad h_i^0 \leftarrow \forall \bar{\iota}.(\rho_i \Rightarrow f_i = 0)$
5 $\quad h_i^c \leftarrow \neg(h_i^1 \vee h_i^0)$
6 $\quad h_i \leftarrow h_i^1 \vee (p_i \wedge h_i^c)$
7 $\quad \rho \leftarrow \rho \wedge (h_i = f_i)$
8 **endfor**
9 **return** $(h_1(\bar{p}), h_2(\bar{p}), \ldots, h_n(\bar{p}))$

Figure 3.1: High Level Description of the Reparameterization Algorithm

The following theorem states that the algorithm is correct. It states that the set of state vectors $\mathcal{Y}$ given by the new parametric representation is exactly the same as that given by the original set of state vectors $\mathcal{X}$.

Theorem 3 *Suppose beginning with the parametric representation* $\mathcal{X} = \{\bar{v} \in \mathcal{S} \mid \exists \bar{\iota} \in \mathcal{W}^k . \bar{v} = \bar{f}(\bar{\iota})\}$, *we obtain* $\mathcal{Y} = \{\bar{v} \in \mathcal{S} \mid \exists \bar{p} \in \mathcal{P} . \bar{v} = \bar{h}(\bar{p})\}$ *by following the algorithm* OrderedReparam. *Then* $\mathcal{X} = \mathcal{Y}$.

We prove this theorem in Appendix B.

Computing h_i^1 and h_i^0 from equations 3.7 and 3.8 involves universally quantifying a large number of I^k variables. This is especially expensive with a BDD-based representation. Moreover, representing parametric functions with BDDs becomes very expensive as the number of simulation steps becomes larger. BDDs can blow up due to variable ordering problems, and the size of BDDs can become exponential in $|I^k|$. However, if the parametric functions are represented by Boolean expressions, the size of each expression is bounded by the size of the circuit being simulated times the number of simulation steps. Therefore, symbolic simulators that use non-canonical Boolean expressions can go much deeper. Thus, we seek to compute h_i when the functions are given as Boolean expressions.

In Chapter 2, we reported an efficient procedure to quantify existentially a large number of variables from a Boolean formula. To summarize, the procedure essentially uses powerful SAT checkers like Chaff to enumerate cubes (partial assignments) given in terms of the variables that are not to be quantified and stores these cubes in an efficient data structure. We used the procedure to compute successive images of a set of states to get the set of reachable states. The procedure assumes that the formula is given in conjunctive normal form (CNF). The procedure quantifies a subset of the variables and generates a disjunctive normal form (DNF) clausal representation in terms of the remaining variables. It is worthwhile to note that the complexity of the procedure is mostly related to the number of variables **not** quantified and not to the number of variables to be quantified. If the formula is not given in CNF, intermediate variables can be used to convert it to CNF. In essence, the variables to be quantified

are treated in the same way as the intermediate variables.

We intend to use the same procedure to compute h_i^α (where α is either 1 or 0). However, note that we need to universally quantify I^k variables, while the procedure does existential quantification. So we re-express h_i^α as

$$h_i^\alpha(p_1, \ldots, p_{i-1}) = \forall \bar{\iota}. \rho_i(p_1, \ldots, p_{i-1}, \bar{\iota}) \rightarrow f_i(\bar{\iota}) = \alpha \tag{3.9}$$

$$= \neg \exists \bar{\iota}. \neg \left(\rho_i(p_1, \ldots, p_{i-1}, \bar{\iota}) \rightarrow f_i(\bar{\iota}) = \alpha \right) \tag{3.10}$$

$$= \neg \exists \bar{\iota}. \rho_i(p_1, \ldots, p_{i-1}, \bar{\iota}) \wedge f_i(\bar{\iota}) \neq \alpha \tag{3.11}$$

Thus, the existential quantification can be carried out by our SAT-based procedure to compute $\neg h_i^\alpha$. The formula $\rho_i(p_1, \ldots, p_{i-1}, \bar{\iota}) \wedge f_i(\bar{\iota}) \neq \alpha$ is given to the SAT checker in CNF, which is done by introducing intermediate variables. The large number of I^k variables poses no problem, as they are treated just like intermediate variables by our SAT-based enumeration procedure. The procedure computes $\neg h_i^\alpha$ in disjunctive normal form (DNF) over $\{p_1, \ldots, p_{i-1}\}$ variables.

After computing h_i^1 and h_i^0 (thus in CNF), h_i^c is given by $\neg h_i^1 \wedge \neg h_i^0$. This can be converted to CNF, if required for the SAT checker, by again introducing intermediate variables. This allows us to derive h_i using Equation 3.4. It appears that for computing each h_i, two SAT-based enumerations are required, hence a total of $2n$ SAT-based enumerations. In the next section, we show that there are a number of optimizations. First, we show that a single SAT-based enumeration can be used to compute both $\neg h_i^1$ and $\neg h_i^0$. Moreover, we show that successive SAT runs are similar to earlier runs and how to use this similarity to improve the performance of the SAT checker.

3.3.3 Computing h_i^0 and h_i^1 in a single SAT run

While enumerating cubes in variables $\{p_1, \ldots, p_{i-1}\}$ for computing h_i^1 and h_i^0, we note that the SAT formulas are very similar to each other. In fact, the only difference is whether $f_i(\bar{\iota})$ equals 0 or 1. In order to merge these two computations, we ask the SAT-based enumeration procedure to enumerate cubes in $\{p_1, \ldots, p_{i-1}\}$ variables for the following formula:

$$\rho_i(p_1, \ldots, p_{i-1}, \bar{\iota}) \tag{3.12}$$

For each solution enumerated (in p_1 to p_{i-1} and I^k), we check the value of $f_i(\bar{\iota})$. If $f_i(\bar{\iota})$ evaluates to 0, then we know that the cube found by the SAT checker cannot belong to h_i^1. This is because we found at least one consistent assignment to I^k variables that leads to the value 0 for $f_i(\bar{\iota})$, hence bit i is not forced to 1 for all consistent assignments to I^k. Thus, the cube in $\{p_1, \ldots, p_{i-1}\}$ is added to $\neg h_i^1$. Similarly, if $f_i(\bar{\iota})$ evaluates to 1, then the cube is added to $\neg h_i^0$. Thus, both $\neg h_i^0$ and $\neg h_i^1$ are computed in a single SAT run, and then h_i^c is computed as given in Equation 3.5.

We check the value of $f_i(\bar{\iota})$ by just evaluting it under the assignment to the I^k variables computed by the SAT checker. Note that we have to do this evaluation a large number of times, hence it should be made as fast as possible. Since this is just a function evaluation, techniques such as compiled simulation can be used to do this much faster than what we do at present. Another option is to use the SAT checker itself to do this evaluation, rather than using a separate function evaluator. This can be done as follows: Instead of asking SAT to enumerate cubes in p_1 to p_{i-1} to the formula $\rho_i(p_1, \ldots, p_{i-1}, \bar{\iota})$, we ask it to enumerate on

$$t_i(p_1, \ldots, p_{i-1}, \bar{\iota}) = \rho_i(p_1, \ldots, p_{i-1}, \bar{\iota}) \wedge (f_i(\bar{\iota}) = \beta_i). \tag{3.13}$$

Here, β_i is a new intermediate variable. The last set of clauses corresponding to $f_i(\bar{\iota}) = \beta_i$ does not place any constraints on the solution space. However, since the

SAT checker assigns values to all variables, the value it assigns to β_i is the evaluation of the function $f_i(\bar{\iota})$. It appears that we are unnecessarily adding CNF clauses to the SAT instance. However, as we will see in the next subsection, these additional clauses can be used when doing SAT-based enumeration for computing h_{i+1}^{α}.

3.3.4 Incremental SAT

The optimized SAT formula for computing $h_{i+1}^{\alpha}, \alpha \in \{0,1\}$ (Equation 3.12) is very similar to the formula given to the SAT checker for computing h_i. Since $\rho_{i+1} = \bigwedge_{j=1}^{i}(h_j = f_j)$, the following recurrence is evident:

$$\begin{aligned}\rho_{i+1}(p_1,\ldots,p_i,\bar{\iota}) &= \rho_i(p_1,\ldots,p_{i-1},\bar{\iota}) \wedge \\ &\quad (h_i(p_1,\ldots,p_i) = f_i(\bar{\iota}))\end{aligned} \tag{3.14}$$

Thus, an incremental SAT checker can be used while enumerating satisfying assignments for ρ_{i+1}, provided we add the clauses corresponding to $h_i(p_1,\ldots,p_i) = f_i(\bar{\iota})$ to the sat instance ρ_i, and delete the clauses that were added as blocking clauses and the conflict clauses inferred from the blocking clauses. An incremental SAT checker keeps all the conflict clauses learned while enumerating solutions to ρ_i. This is correct because of the recurrence above.

We have implemented an incremental SAT checker on top of zChaff along with the cube enumeration. This SAT checker allows us to remove the blocking clauses and the conflict clauses derived from these blocking clauses from the previous SAT run. The advantage of incremental SAT checking is that all the learning done while computing ρ_i comes for free when checking ρ_{i+1}. Only the clauses corresponding to $h_i = f_i$ need to be added.

The incremental SAT checker can be used in the following manner when the SAT checker is also used to evaluate $f_i(\bar{\iota})$ (Equation 3.13), as described in the previous

section. In t_i, the clauses corresponding to $f_i(\bar{\iota}) = \beta_i$ are already present. Then, the formula for t_{i+1} is

$$t_{i+1}(p_1, \ldots, p_i, \bar{\iota}) = \rho_{i+1}(p_1, \ldots, p_i, \bar{\iota}) \wedge (f_{i+1}(\bar{\iota}) = \beta_{i+1}). \tag{3.15}$$

Here, β_{i+1} is a new intermediate variable. Since $f_i = \beta_i$ is already present in t_i, t_{i+1} can be expressed as

$$t_{i+1}(p_1, \ldots, p_i, \bar{\iota}) = t_i(p_1, \ldots, p_{i-1}, \bar{\iota}) \wedge (\beta_i = h_i(p_1, \ldots, p_i)) \wedge (f_{i+1}(\bar{\iota}) = \beta_{i+1}). \tag{3.16}$$

Thus, the clauses corresponding to the last two conjuncts are added to the incremental sat solver when going from t_i to t_{i+1}.

3.3.5 Extensions to Handle General Transition Relations

So far, we have restricted ourselves to functional transition relations. Next, we generalize the reparameterization algorithm to work with any transition relation. Transition relations allow us to easily specify non-deterministic behaviour and are most useful when behavioural circuits are translated to languagues like SMV.

We essentially redefine the functions ρ_i, h_i^0, h_i^1, which will then allow us to compute parametric form of the set of states reachable in k steps of the simulation under any general transition relation $R(v, v')$.

Let t denote a trace of length k, $t(0), \ldots, t(k)$, where each $t(i)$ is a vector of n state variables. Individual bits of $t(i)$ will be denoted by subscripts, as in $t(i)_j$. Let $\tau(t)$ denote a predicate that holds if and only if t is a valid trace of length k in the model M, or formally:

$$\tau(t) \quad :\Longleftrightarrow \quad I(t(0)) \wedge \bigwedge_{j=0}^{k-1} R(t(j), t(j+1)) \tag{3.17}$$

Thus, τ is a BMC instance without a property. We aim at obtaining a small, symbolic representation for the set of all states $\bar{v}$ such that there exists a trace of length k in M that ends in the state $\bar{v}$. We denote the set by $\mathcal{X}$, as we did earlier.

$$\mathcal{X} \quad := \quad \{\bar{v} \in \mathcal{S} \,|\, \exists t \in \mathcal{S}^{k+1} : \tau(t) \wedge v = t(k)\} \tag{3.18}$$

Here, $\mathcal{S}^{k+1}$ denotes all traces of length k.

We compute the parametric form $\bar{h}(\bar{p}) = (h_1(\bar{p}), h_2(\bar{p}), \ldots, h_n(\bar{p})$, which denotes the set:

$$\mathcal{Y} \quad := \quad \{\bar{v} \in S \,|\, \exists \bar{p} \in \mathcal{P}.\bar{h}(\bar{p}) = \bar{v}\} \tag{3.19}$$

as earlier.

Next, we redefine ρ_i, h_i^0 and h_i^1.

Choosing specific values for the parameters p_1 to p_{i-1} restricts the value the function h_i can have, as the values for the previous bits v_1 to v_{i-1} may force v_i to be either 0 or 1. We formalize this as follows: the predicate ρ_i takes as arguments the parameters p_1 to p_{i-1} and a trace t. The predicate ρ_i is true if and only if the following two conditions hold:

1. The trace is a valid trace in M, i.e., $\tau(t)$ holds.
2. The first $i-1$ state bits of the last state in the trace match the values given by the functions $h_1(p_1), h_2(p_1, p_2), \ldots, h_{i-1}(p_1, \ldots, p_{i-1})$.

Formally, ρ_i is defined as:

$$\rho_i(p_1, \ldots p_{i-1}, t) \quad := \quad \tau(t) \wedge \bigwedge_{j=1}^{i-1} h_j(p_1, \ldots, p_j) = t(k)_j. \tag{3.20}$$

Here, $t(k)_j$ denotes the jth state bit of state $t(k)$. Intuitively, $\rho_i(p_1, p_2, \ldots, p_{i-1}, t)$ indicates that a trace t is valid and it conforms to the parameters $p_1, p_2, \ldots, p_{i-1}$.

Note that $\rho_1(t) = \tau(t)$, thus, ρ_1 is 1 for any valid trace and that $\rho_i(p_1, \ldots, p_{i-1}, t) = 0$ for any invalid trace t.

Now the condition h_i^1 can be easily expressed as follows: We want a Boolean condition in $\{p_1, \ldots, p_{i-1}\}$ variables under which v_i is forced to take the value 1. Thus, if an assignment $(p_1, p_2, \ldots, p_{i-1})$ makes $h_i^1(p_1, \ldots, p_{i-1})$ true, then that implies that all traces t that conform with this assignment end in a state $t(k)$ where $t(k)_i$ is 1.

$$h_i^1(p_1, \ldots, p_{i-1}) = \forall t \in \mathcal{S}^{k+1}. \left(\rho_i(p_1, \ldots, p_{i-1}, t) \Rightarrow t(k)_i = 1\right) \tag{3.21}$$

Analogously, h_i^0 can be expressed as

$$h_i^0(p_1, \ldots, p_{i-1}) = \forall t \in \mathcal{S}^{k+1}. \left(\rho_i(p_1, \ldots, p_{i-1}, t) \Rightarrow t(k)_i = 0\right). \tag{3.22}$$

Note that $h_1(p_1) = p_1$, unless the bit v_1 is always 1 or 0, in which case $h_1 = 1$ or $h_1 = 0$. This follows automatically from $\rho_1 = \tau(t)$. The Equations 3.4 and 3.20 to 3.22 give us an algorithm for computing a symbolic representation of the set of states reachable in exactly k steps.

The following theorem states that the algorithm is correct, i.e., the set of state vectors $\mathcal{Y}$ given by the parametric representation is exactly the same as that given by the original set of state vectors $\mathcal{X}$.

Theorem 4 *Suppose beginning with the set of states* $\mathcal{X} = \{\bar{v} \in \mathcal{S} \mid \exists t \in \mathcal{S}^{k+1}.\bar{v} = t(k) \wedge \tau(t)\}$ *given by a BMC instance, we obtain the set of states* $\mathcal{Y} = \{\bar{v} \in \mathcal{S} \mid \exists \bar{p} \in \mathcal{P}.\bar{v} = \bar{h}(\bar{p})\}$ *in parametric form according to equations 3.4 and 3.20 to 3.22. Then* $\mathcal{X} = \mathcal{Y}$.

The proof is this theorem is similar to the proof of the first theorem, and it is presented in Appendix C.

3.4 Checking Safety Properties

So far, we have described how to do SAT-based symbolic simulation when the initial state constraint is given in parametric form. Most circuits are in functional form, however, the initial state constraint is frequently given as a predicate on the initial state variables.

Moreover, for verification, invariant statements are often used to restrict the state space for verification. Such invariants are often called *verification conditions* [43].

Safety properties are usually given as predicates. We now describe how to handle the initial state and the safety property predicates and how to generate counterexamples.

3.4.1 Safety Property Checking

Symbolic simulation with reparameterization works as follows: Beginning with the initial states, the circuit is simulated up to a certain depth, say k, when the functions become too large. At this point, reparameterization is applied, and a smaller parametric representation $\bar{h}^k(\bar{p}^k) = (h_1^k(\bar{p}^k), h_2^k(\bar{p}^k), \ldots, h_n^k(\bar{p}^k))$ is computed representing the set of states reached in exactly k steps. The superscript here just emphasizes the fact that this parametric representation is for step k. After step k, symbolic simulation continues using $\bar{h}^k(\bar{p}^k)$ as the set of initial states in parametric form, like starting over again. This is continued until a bug is found or the time limit is exceeded. Next, we describe the method used for finding violations of safety properties.

Let us assume that $S_0(\bar{v})$ is the initial state predicate and $Bad(\bar{v})$ is the predicate describing the set of states that violate the safety property of interest. For the initial states, we generate a parametric representation from the predicate $S_0(\bar{v})$ using the

algorithm by Jones *et al.* [43]. The initial state predicates are usually small, hence this is not very expensive. If $(h_1(\bar{p}), h_2(\bar{p}), \ldots, h_n(\bar{p}))$ is the parametric representation at some step of the simulation, then the SAT checker is asked to provide an assignment to the parameters such that the state vector satisfies the $Bad(\bar{v})$ predicate. Formally, the SAT checker is asked to find a satisfying assignment for

$$v_1 = h_1(\bar{p}) \wedge v_2 = h_2(\bar{p}) \wedge \ldots \wedge v_n = h_n(\bar{p}) \wedge Bad(\bar{v}) \tag{3.23}$$

If the SAT checker generates a satisfying assignment, then we know that the property fails, and a counterexample needs to be generated.

3.4.2 Counterexample Generation

For our symbolic simulator, the counterexample generation is nontrivial, since we do not keep the whole simulation. Periodically, we reparameterize the representation and hence lose the information about input variables up to that point. In order to generate counterexamples, we need to store all intermediate parametric representations and the simulated functions f_is that these representations are derived from. This storage can be done on a disk, offline. We pick up one state that violates the safety property and ask the SAT checker to provide an assignment to the input variables that lead from the most recent parameterized representation to the bug. Since the simulated functions are stored on the disk, they can be directly used in the SAT checker, rather than unrolling the circuit again. Once we get a state at the step when the last reparameterization was done, we choose one state from that step and repeat the whole process again. This is somewhat similar to the strategy that standard BDD-based model checkers use. They begin with one bad state, and then keep on intersecting pre-images with the frontier state sets, until they get to an initial state.

In our case, instead of computing pre-images, we just find one state in the pre-image.

3.5 Experimental Results

The SAT based reparameterization algorithm is evaluated against plain bounded model checking without reparameterization. The experiments were run on a 1.3 GHz AMD Athlon processor machine with 1 GB of main memory running RedHat Linux 7.1. We set a memory limit of 0.7GB, and time limit of 6 hours. We invoke the reparameterization algorithm when the memory consumption of the SAT checker exceeds 300 MB.

We report experimental results (table 3.2) on large industrial circuits. These circuits are taken from various processor designs. They fall under three different classes. The M series circuits are MIPS like processor designs, and the D series circuits are various abstractions of the M series circuits. The IU circuits are models of picoJava microprocessor from Synopsys. The D series and the IU circuits were used in [19], where SAT-based abstraction-refinement was done for verification of safety properties. All D series circuits have a counterexample, while all the properties hold on the M and IU circuits. IUp1, IUp2 and IUp3 are the same circuits, but checked with different properties. The circuits range from small to very large. It should also be noted that M-series circuits and the circuit D19 make extensive use of TRANS and INVAR constraints, therefore, they were not handled by our earlier symbolic simulator in [17] that can only work with functional transition relations.

We compare our algorithm against a BMC algorithm implemented in the NuSMV model checker with the zChaff SAT checker and the abstraction refinement results in [19]. We implemented incremental SAT for BMC in NuSMV, because we need incremental SAT between various simulation steps and also between different state

bits. BMC keeps on unwinding the transition relation, while we periodically reduce the size of representation with reparameterization. Therefore, comparing against BMC is fair. Our algorithm is not yet complete for safety properties, in that it cannot prove properties true without resorting to abstraction-refinement. However, as we will describe later, we can combine abstraction-refinement with our symbolic simulator to make the property checking complete.

ckt	# regs	# PIs	bug len.	Bug time		BMC max		sym max		
				BMC	sym	len	time	len.	time	# rest.
D2$^+$	94	11	15	18	32	64	8084^M	4336	21600^T	163
D5$^+$	343	7	32	15	17	45	3594^M	2793	21600^T	338
D24	223	47	10	5	7	913	13293^M	10298	21600^T	152
D6	161	16	20	289	145	48	6094^M	1521	21600^T	93
D19	285	49	32	6834	1698	23	13721^M	399	21600^T	144
D20	532	30	14	2349	574	36	3984^M	1856	21600^T	185
M3	334	155	true	-	-	68	7039^M	781	21600^T	22
M4	744	95	true	-	-	26	12695^M	302	21600^T	38
M5	316	104	true	-	-	41	7492^M	518	21600^T	45
IUp1	4494	361	true	-	-	39	2870^M	1278	21600^T	902
IUp2	4494	361	true	-	-	39	3192^M	1103	21600^T	1242
IUp3	4494	361	true	-	-	39	2994^M	1284	21600^T	856

Table 3.2: Experimental Results on Large Industrial Benchmarks comparing plain BMC against SAT-based reparameterization.

In the table, the column marked #PIs is denotes the number of primary inputs. The column “bug len.” gives the length of the shortest counterexample, if any. The columns under ”Bug time” are times for finding a bug. The columns in the ”BMC max” group denote the largest BMC simulation completed in the time and

memory limits, while columns in the "sym max" group denote the largest simulation completed with our tool. The times reported are in seconds. The circuits that do not have any bug have "-" in the "Bug time" columns. Entries with ^{M} ran out of memory, while the entries with ^{T} ran out of time. The column "# rest." denotes the number of times reparameterization was done.

We would like to point out that in [19], a spurious counterexample of length 72 was found, which could not even be simulated with SAT on a machine with 3 GB of memory[1]. However, we could simulate it for 72 steps in 987 seconds on the smaller machine with our algorithm.

It is evident from the results that our algorithm is more powerful than the plain BMC algorithm. We are able to go much deeper and can do it in shorter amount of time. In fact, we were even able to do better than the results obtained with abstraction. It should be noted that multiple refinement steps are required in abstraction-refinement, and in each step, a spurious counterexample is simulated using SAT. Therefore, abstraction-refinement can be slower in many cases.

The BDD-based reachability program of [35] does property checking and can also do fixed-points. However, it was able to find bugs for circuits D2 and D5 only. For the rest of the circuits, it either exceeded the time or memory limit. The BDD based algorithm computes set unions at every step, while we do not. Therefore, the comparison with our simulator is not completely fair to the BDD based approach.

3.6 Fixed-Points with Reparameterization

The symbolic simulation computes the set of states reachable in exactly k steps. In order to find fixed-points, we need to compute the set of states reachable in k

[1]It was only possible to simulate it on a machine with 8GB of memory.

steps or less and we also need a method to compare two representations. We first present a simple method for computing set unions in our framework. This, while theoretically possible, is practically prohibitive, hence we next describe a method based on introducing self loops in the transition relation.

3.6.1 Set Union with an Auxiliary Variable

Suppose two sets of states S_1 and S_2 are given using the parametric representations $\bar{h}(\bar{p}) = (h_1(\bar{p}), \ldots, h_n(\bar{p}))$ and $\bar{g}(\bar{q}) = (g_1(\bar{q}), \ldots, g_n(\bar{q}))$, respectively. Note that the two sets of parameters P and Q need not be disjoint. We define $\uplus$ as an operator for two parametric representations as follows:

$$\bar{h}(\bar{p}) \uplus \bar{g}(\bar{q}) = (z?h_1(\bar{p}) : g_1(\bar{q}), z?h_2(\bar{p}) : g_2(\bar{q}), \ldots, z?h_n(\bar{p}) : g_n(\bar{q})).$$

Here, the expression $z?h_i(\bar{p}) : g_i(\bar{q})$ is just a short form for $(z \wedge h_i(\bar{p})) \vee (\neg z \wedge g_i(\bar{q}))$ and z is a new parameter. The claim below that $\bar{h}(\bar{p}) \uplus \bar{g}(\bar{q})$ represents $S_1 \cup S_2$ is easy to prove.

Theorem 5 *If S_1 and S_2 are given by parametric representations $\bar{h}(\bar{p})$ and $\bar{g}(\bar{q})$, then $S_1 \cup S_2$ is given by the parametric representation $\bar{h}(\bar{p}) \uplus \bar{g}(\bar{q})$.*

This set union operation can be generalized to take the union of n different parametric representations by using $\lceil log_2 n \rceil$ new parameters.

The number of parameters after set union of two sets is $|P \cup Q| + 1$. This representation can be reparameterized by our SAT-based algorithm to get a parametric form in n parameters. Since our algorithm generates canonical forms, the fixed-point could be detected by comparing the last two representations. Thus, fixed-point detection would require a reparameterization run after each step of simulation. This would nul-

lify the performance gained by the new algorithm, which benefits from performing the reparameterization only when the equations become too big.

Hence, the fixed-point detection algorithm, while a theoretical possibility, should not be used for performance reasons. The user of Bounded Model Checking has the same problem: the Bounded Model Checker only guarantees the absence of bugs up to the bound. As described in the introduction, there are several techniques to detect that the property holds. Thus, we propose to use SAT-based symbolic simulation as a replacement for BMC within these frameworks. The symbolic simulator is used to disprove the property only.

3.6.2 Fixed-Points by Using *Stall* Signal

The following method can be used to compute the union of the set of states without invoking reparameterization after every step. The idea is to modify the transition relation such that it also allows self-loops back to each state. Thus, if the original transition relation is $R(v, v')$, we change it to $R(v, v') \vee (v = v')$. For functional circuit descriptions, this can be achieved by driving each latch input from a multiplexer controlled by a new free input called *stall*. The multiplexer selects either the original latch input or the present latch state. This is a well known approach for nondeterministically "stalling" the state machine.[2] When simulating using this modified transition relation for k steps, we get the set of states reachable in k steps or less.

In order to detect whether we have reached a fixed-point or not, we need to compare two state set descriptions for equality. Since our reparameterization algorithm produces canonical representations (provided the order of the state vari-

[2]The authors thank Armin Biere for suggesting this.

ables is the same), we only need to compare the two parametric representations on a function by function basis. Note that we do not need to invoke reparameterization after each step of the simulation. We just need to compare the last two parametric representations for equality. Suppose $H^k(P) = (h_1^k(P), \ldots, h_n^k(P))$ and $H^{k+\delta}(P) = (h_1^{k+\delta}(P), \ldots, h_n^{k+\delta}(P))$ are the last two parametric representations. Note that δ can be and is usually greater than 1. In order to compare these two representations, we need to compare each function $h_i^k(P)$ with $h_i^{k+\delta}(P)$. Since we represent these functions by Boolean expressions and not by some canonical data structure such as a BDD, a method for checking equality is required. The simplest method is to check $h_i^k(P) \oplus h_i^{k+\delta}(P)$ for satisfiability. If the formula is satisfiable for any i, then the two representations are not equal, and the fixed point is not yet reached. We can also use state of the art combinational equivalence checkers to accomplish this task.

For the circuits we experimented with, the diameter is far too large to actually reach the fixed-point. Within the time bound of 6 hours, we were able to simulate the circuit D24 for 8744 steps without reaching a fixed-point, the circuit M4 was simulated for 238 steps without reaching the fixed-point and the circuit IUp1 was simulated for 936 steps without reaching the fixed-point. Even though the the algorithm was not able to reach fixed-point for the circuits, the extension of adding self loops to compute the unions of the sets of states at least theoretically allows one to use the reparameterization based algorithm for general property checking. To the best of our knowledge, there is no other algorithm available that is able to reach these depths in a fixed-point iteration on such large circuits.

3.7 Summary

We presented a SAT-based reparameterization algorithm which greatly improves the capacity of BMC engines. The method uses an unwinding of the transition relation and thus is comparable to BMC. However, the reparameterization step, which is done when the equation becomes too big, makes it possible to go much deeper into the transition system than what BMC without reparameterization can do. The reparameterization algorithm captures a small, symbolic representation of the states that are reachable with exactly k steps. This can be also viewed as an efficient re-encoding of the set of states reachable in k steps. Using this representation as new initial state predicate, the algorithm starts over. The algorithm is also extended so as not to rely on the functional representation for the transition relation, but uses an arbitrary total transition relation.

The reparameterization algorithm is most effective for symbolic simulation. However, it is not very practical (yet) for fixed points, and hence for proving the properties correct. This is true for BMC as well, and the presented algorithm can be used as a replacement for BMC within most methods that make BMC complete, such as counterexample guided abstraction refinement.

Chapter 4

SAT Based Reparameterization in an Abstraction-Refinement Framework

4.1 Introduction

Abstraction reduces the size of the design by focusing only on relevant portions of the design. A conservative abstraction is one which preserves all behaviors of a concrete system. Conservative abstractions benefit from a *preservation* theorem which states that the correctness of any universal (e.g. ACTL*) formulas on an abstract system automatically implies the correctness of the formula on the concrete system. However, a counterexample on an abstract system may not correspond to any real path, in which case it is called a *spurious* counterexample. To get rid of a spurious counterexample, the abstraction needs to be made more precise via refinement. It is obviously desirable to automate this procedure. There are multiple approaches for automated abstraction-refinement, the most relevant of which are summarized below:

1. In the counterexample guided abstraction refinement framework (CEGAR) [19, 23, 25], model checking is performed on a safe abstraction of the model. Thus, if the property holds on the abstract model, it also holds on the concrete model. If this is not so, an abstract counterexample is obtained from the model checker. This abstract counterexample is then used to constrain the states in a Bounded Model Checking SAT instance. If the constrained BMC SAT instance is satisfiable, the abstract counterexample can be simulated on the concrete model and a bug is found. If not, the abstraction is refined using various heuristics.

2. In [55], this framework is changed as follows: An abstract counterexample is no longer obtained. The only information of interest is the *length* m of the abstract counterexample. This length m is then used as the bound for a normal, unconstrained BMC instance. If the BMC instance is satisfiable, a bug is found. If this is not the case, information from the SAT solver is used to generate the next abstract model.

3. In [54], a new framework is introduced: The algorithm initially performs Bounded Model Checking for some m steps in order to refute the property. If this fails, the proof of unsatisfiability extracted from the SAT solver is used to simplify a fixed-point computation. The purpose of the fixed-point computation is to detect the case when the property actually holds. This may fail, and if so, the algorithm is repeated with an increased value of m.

All these, and other approaches solely rely on Bounded Model Checking to refute the property. For large systems, bounded model checking becomes a bottleneck for validating counterexamples. Our reparameterization can thus be used improve the capacity of counterexample validation. The reparameterization algorithm is used in

the abstraction-refinement framework of [19].

Next, in this section, we briefly describe the SAT based abstraction-refinement framework of [19]. Our abstraction function is based on hiding irrelevant parts of the circuit by making a set of variables *invisible*. This simple abstraction function yields an efficient way to generate minimal abstractions, a source of difficulty in previous approaches. We describe two techniques to produce abstract systems by removing invisible variables. The first is simply to make the invisible variables into input variables. This is shown to be a minimal abstraction. However, this leaves a large number of input variables in the abstract system and, consequently, BDD based model checking even on this abstract system becomes very difficult [72]. We propose an efficient method to pre-quantify these variables on the fly during image computation. The resulting abstract systems are usually small enough to be handled by standard BDD based model checkers. We use an enhanced version [15, 16] of NuSMV [20] for this. If a counterexample is produced for the abstract system, we try to simulate it on the concrete system symbolically using a fast SAT checker (Chaff [61, 76] in our case).

The refinement is done by identifying a small set of invisible variables to be made visible. We call these variables the *refinement variables*. Identification of refinement variables is the main focus of this work. Our techniques for identifying important variables are based on analysis of effective *boolean constraint propagation (BCP)* and *conflicts* [61] during the SAT checking run of the counterexample simulation.

The efficiency of SAT procedures has made it possible to handle circuits with a few thousand of variables, much larger than any BDD based model checker is able to do at present. Our approach is similar to BMC, except that the propositional formula for simulation is constrained by assignments to visible variables. This formula is *unsatisfiable* for a spurious counterexample. We proposed heuristic scores based on

backtracking and conflict clause information, similar to VSIDS heuristics in Chaff, and conflict dependency analysis algorithm to extract the reason for unsatisfiability. Our techniques are able to identify those variables that are critical for unsatisfiability of the formula and are, therefore, prime candidates for refinement. The main strength of our abstraction-refinement framework is that we use the SAT procedure itself for refinement. We do not need to invoke multiple SAT instances or solve separation problems as in [25].

4.2 SAT Based Abstraction-Refinement

4.2.1 Abstraction in Model Checking

We give a brief summary of the use of abstraction in model checking and introduce notation that we will use in the remainder of the section (refer to [24] for a full treatment). A transition system is modeled by a tuple $M = (S, I, R, \mathcal{L}, L)$ where S is the set of states, $I \subseteq S$ is the set of initial states, R is the set of transitions, $\mathcal{L}$ is the set of atomic propositions that label each state in S with the labeling function $L : S \rightarrow 2^{L}$. The set I is also used as a predicate $I(s)$, meaning the state s is in I. Similarly, the transition relation R is also used as a predicate $R(s_1, s_2)$, meaning there exists a transition between states s_1 and s_2. Each program variable v_i ranges over its non-empty domain D_{v_i}. The state space of a program with a set of variables $V = \{v_1, v_2, \ldots, v_n\}$ is defined by the Cartesian product $D_{v_1} \times D_{v_2} \times \ldots \times D_{v_n}$.

In existential abstraction [24] a surjection $h : S \rightarrow \hat{S}$ maps a concrete state $s_i \in S$ to an abstract state $\hat{s}_i = h(s_i) \in \hat{S}$. We denote the set of concrete states that map to an abstract state $\hat{s}_i$ by $h^{-1}(\hat{s}_i)$.

Definition 5 *The* ***minimal existential abstraction*** $\hat{M} = (\hat{S}, \hat{I}, \hat{R}, \hat{\mathcal{L}}, \hat{L})$ *corre-*

sponding to a transition system $M = (S, I, R, \mathcal{L}, L)$ *and an abstraction function* h *is defined by:*

1. $\hat{S} = \{\hat{s} | \exists s. s \in S \wedge h(s) = \hat{s}\}$.

2. $\hat{I} = \{\hat{s} | \exists s. I(s) \wedge h(s) = \hat{s}\}$.

3. $\hat{R} = \{(\hat{s}_1, \hat{s}_2) | \exists s_1. \exists s_2. R(s_1, s_2) \wedge h(s_1) = \hat{s}_1 \wedge h(s_2) = \hat{s}_2\}$.

4. $\hat{\mathcal{L}} = \mathcal{L}$.

5. $\hat{L}(\hat{s}) = \bigcup_{h(s)=\hat{s}} L(s)$.

Condition 3 can be stated equivalently as

$$\exists s_1, s_2 (R(s_1, s_2) \wedge h(s_1) = \hat{s}_1 \wedge h(s_2) = \hat{s}_2) \Leftrightarrow \hat{R}(\hat{s}_1, \hat{s}_2) \tag{4.1}$$

An atomic formula f *respects* h if for all $s \in S$, $h(s) \models f \Rightarrow s \models f$. In other words, if an abstract state $\hat{s}$ satisfies the atomic formula f, then *all* the concrete states that correspond to $\hat{s}$ also satisfy f. Labeling $\hat{L}(\hat{s})$ is *consistent*, if for all $s \in h^{-1}(\hat{s})$ it holds that $s \models \bigwedge_{f \in \hat{L}(\hat{s})} f$. In other words, all atomic formulas that make up the labeling $\hat{L}(\hat{s})$ respect h. The following theorem due to David Long and Yuan Lu *et al.* [23, 51, 52] is stated without proof. The detailed proof of this theorem is in Yuan Lu's thesis [52].

Theorem 6 *Let* h *be an abstraction function and* ϕ *an* $ACTL^*$ *specification where the atomic sub-formulas respect* h*. Then the following holds: (i) For all* $\hat{s} \in \hat{S}$, $\hat{L}(\hat{s})$ *is consistent, and (ii)* $\hat{M} \models \phi \Rightarrow M \models \phi$.

This theorem is the core of all abstraction refinement frameworks. However, the converse may not hold, i.e., even if $\hat{M} \not\models \phi$, the concrete model M may still satisfy ϕ. In this case, the counterexample on $\hat{M}$ is said to be spurious, and we need to

refine the abstraction function. Note that the theorem holds even if only the right implication holds in Equation 4.1. In other words, even if we add more transitions to the minimal transition relation $\hat{R}$, the validity of an ACTL* formula on $\hat{M}$ implies its validity on M.

Example 4 **[Counter]** *Consider the state machine of Figure 4.1(A). It describes a counter that repeatedly counts from 0 to 7. In Figure 4.1(B), we produce an abstraction of the state machine where each pair of adjacent states is mapped to the same abstract state, starting at 0. The abstraction function is thus* $h(s) = s$ ***div*** 2*. Here,* ***div*** *denotes integer division. Clearly, the ACTL* property* $\mathbf{AG}\,\mathbf{AF}(counter == 5 \Rightarrow \mathbf{AX}(counter > 5))$ *holds true on the original state machine, but does not hold on the abstraction, as the counter could get stuck on value 5. On the other hand, the property* $\mathbf{AG}(counter < 8)$ *holds on both the original machine and the abstraction. If* h *is refined such that it no longer maps the states* 4 *and* 5 *to the same state (Figure 4.1(C)), we prove the property on the abstract state machine, and hence on the original machine.*

Definition 6 *An abstraction function* h' *is a* ***refinement*** *for the abstraction function* h *and the transition system* $M = (S, I, R, \mathcal{L}, L)$ *if for all* $s_1, s_2 \in S, h'(s_1) = h'(s_2)$ *implies* $h(s_1) = h(s_2)$*. Moreover,* h' *is a* ***proper refinement*** *of* h *if there exist* $s_1, s_2 \in S$ *such that* $h(s_1) = h(s_2)$ *and* $h'(s_1) \neq h'(s_2)$*.*

Obviously, the function h itself is a refinement of h', but is not very useful. Refinement h' is useful if it includes more details than h, or in other words, separates at least one abstract state into more than one abstract state. In the abstraction refinement procedure that follows, a proper refinement guarantees an eventual termination, due to the fact that the identity function generate the original transition system itself, and hence, can not be refined further.

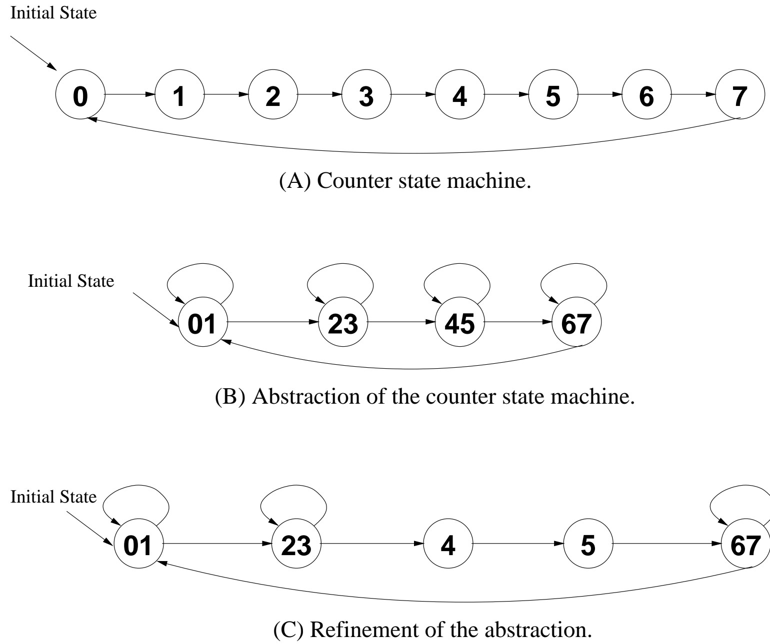

Figure 4.1: A counter state machine to illustrate abstraction and refinement.

In general, ACTL* formulas can have *tree-like* counterexamples [26]. In this chapter, we focus only on safety properties, which have finite path counterexamples. It is possible to generalize our approach to full ACTL* as done in [26]. The following iterative abstraction refinement procedure for a system M and a safety formula ϕ follows immediately.

1. Generate an initial abstraction function h.

2. Model check $\hat{M}$. If $\hat{M} \models \phi$, return `TRUE`.

3. If $\hat{M} \not\models \phi$, check the generated counterexample $\widehat{T}$ on M. If the counterexample is real, return `FALSE`.

4. Refine h to get a proper refinement h', and goto step 2.

Since each refinement step partitions at least one abstract state (as h' is a proper refinement of h), the above procedure is complete for finite state systems for ACTL*

formulas that have path counterexamples. Thus the number of iterations is bounded by the number of concrete states. However, as we will show in the next two sections, the number of refinement steps can be at most equal to the number of program variables.

We would like to emphasize that we model check abstract system in step 2 using BDD based symbolic model checking, while steps 3 and 4 are carried out with the help of SAT checkers.

4.2.2 Generation of Abstract State Machine

We consider a special type of abstraction for our methodology, wherein, we hide a set of variables that we call *invisible* variables, denoted by $\mathcal{I}$. The set of variables that we retain in our abstract machine are called *visible* variables, denoted by $\mathcal{V}$. The visible variables are considered to be important for the property and hence are retained in the abstraction, while the invisible variables are considered irrelevant for the property. The initial abstraction and the refinement in steps 1 and 4 respectively correspond to different partitions of V. Typically, we would want the number of visible variables to be much less than the number of invisible variables, i.e., $|\mathcal{V}| \ll |\mathcal{I}|$. Formally, the value of a variable $v \in V$ in state $s \in S$ is denoted by $s(v)$. Given a set of variables $U = \{u_1, u_2, \ldots, u_p\}, U \subseteq V$, let s^U denote the portion of s that corresponds to the variables in U, i.e., $s^U = (s(u_1)s(u_2)\ldots s(u_p))$. Let $\mathcal{V} = \{v_1, v_2, \ldots, v_k\}$. This partitioning of variables defines our abstraction function $h : S \rightarrow \hat{S}$. The set of abstract states is $\hat{S} = D_{v_1} \times D_{v_2} \ldots \times D_{v_k}$ and $h(s) = s^{\mathcal{V}}$.

Example 5 [Counter, contd.] *If we encode the counter state machine of Figure 4.1 with three boolean variables, v_1, v_2 and v_3, with v_1 denoting the most significant bit of the counter and v_3 the least significant bit, we get the transition relation shown*

in Figure 4.2(A). The set of states is $S = \{0,1\} \times \{0,1\} \times \{0,1\}$. *If we define the set of visible variables to be* $\mathcal{V} = \{v_1, v_2\}$ *and the set of invisible variables to be* $\mathcal{I} = \{v_3\}$, *then the set of abstract states is* $\hat{S} = \{0,1\} \times \{0,1\}$, *and the abstraction is* $h(s) = (s(v_1)s(v_2))$.

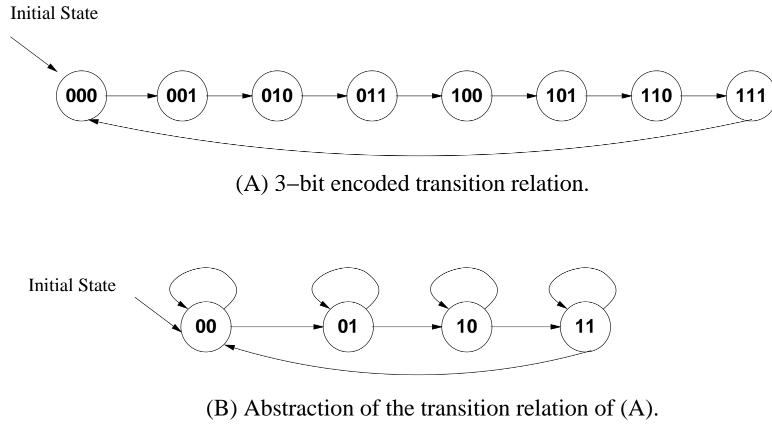

Figure 4.2: The counter state machine of Figure 4.1 encoded with 3 bits.

In our approach, the initial abstraction is to take the set of variables mentioned in the property as visible variables. Another option is to make the variables in the cone of influence (COI) of the property visible. However, the COI of a property may be too large and we may end with a large number of visible variables. The idea is to begin with a small set of visible variables and then let the refinement procedure come up with a small set of invisible variables to make visible.

We also assume that the transition relation is described not as a single predicate, but as a conjunction of bit relations R_j of each individual variable v_j. More formally, we consider a sequential circuit with registers $V = \{v_1, v_2, \ldots, v_m\}$ and inputs $I = \{i_1, i_2, \ldots, i_q\}$. Let $s = (v_1, v_2, \ldots, v_m)$, $i = (i_1, i_2, \ldots, i_q)$ and $s' = (v'_1, v'_2, \ldots, v'_m)$. Let $f_{v_j}(s, i)$ be the next state function for the state variable v_j. The primed variables denote the next state versions of unprimed variables as usual. Then, the bit relation

for v_j becomes $R_j(s, i, v'_j) = (v'_j \leftrightarrow f_{v_j}(s, i))$. The transition relation for the system is then

$$R(s, s') = \exists i \bigwedge_{j=1}^{m} R_j(s, i, v'_j) \tag{4.2}$$

Example 6 [Counter, contd.] *For our 3-bit encoded counter we do not have any input variables, just the three registers v_1, v_2 and v_3. The next state functions for individual bits are given by*

$$\begin{aligned} f_{v_1}(v_1, v_2, v_3) &= (v_2 \wedge v_3) \oplus v_1 \\ f_{v_2}(v_1, v_2, v_3) &= v_3 \oplus v_2 \\ f_{v_3}(v_1, v_2, v_3) &= \neg v_3 \end{aligned}$$

Thus, the individual bit-relations are

$$\begin{aligned} v'_1 &\Leftrightarrow (v_2 \wedge v_3) \oplus v_1 \\ v'_2 &\Leftrightarrow v_3 \oplus v_2 \\ v'_3 &\Leftrightarrow \neg v_3 \end{aligned}$$

The transition relation for the whole system (Figure 4.2(A)) is given by the conjunction of these three bit-relations.

Two methods for hiding invisible variables are described in our paper [19]. One is called input abstraction, where the logic corresponding to the invisible latches is removed. This corresponds to existentially quantifying out the invisible present state variables $s^{\mathcal{I}}$ from $R(s, s')$. In other words, we have made all the invisible variables as primary inputs. If the state variables s are explicitly broken down into visible and invisible sets, $s^{\mathcal{I}}$ and $s^{\mathcal{V}}$, the abstract transition relation is given by the following equation.

$$\hat{R}(\hat{s}, \hat{s}') = \exists s^{\mathcal{I}} \exists i \bigwedge_{v_j \in \mathcal{V}} R_j(s^{\mathcal{V}}, s^{\mathcal{I}}, i, v'_j) \tag{4.3}$$

Example 7 [Counter, contd.] *We have chosen to hide the variable v_3. Thus, the abstract transition relation for our counter is given by $\hat{R}(\hat{s}, \hat{s}') = \exists v_3(f_{v_1} \wedge f_{v_2})$. This can be simplified to $[(v'_2 \Leftrightarrow v_2) \wedge (v'_1 \Leftrightarrow v_1)] \vee [(v'_2 \Leftrightarrow \neg v_2) \wedge (v'_1 \Leftrightarrow v_1 \oplus v_2)]$. The abstract transition relation is shown in Figure 4.2(B). Intuitively, all the self loops in the abstract transition relation are given by the first disjunct, and the other transitions are given by the second disjunct.*

Since the number of invisible variables could be large, this requires a large number of input variables to quantify. In the model checking of abstract transition system, these potentially large number of inputs have to be quantified for every image computation step. On the other hand, if some of the invisible variables and original input variables are pre-quantified, the abstract model has fewer input variables. The transition system after pre-quantification of a subset of input and invisible variables, which we denote by $\tilde{R}(\hat{s}, \hat{s}')$, is an approximation to $\hat{R}(\hat{s}, \hat{s}')$, and is given by:

$$\tilde{R}(\hat{s}, \hat{s}') = \exists s^{W} \bigwedge_{v_j \in \mathcal{V}} \exists s^{Q} R_j(s^{\mathcal{V}}, s^{\mathcal{I}}, i, v'_j) \tag{4.4}$$

Here, $Q \subseteq \mathcal{I} \cup I$ denotes the set of variables to be pre-quantified and $W = (\mathcal{I} \cup I) \setminus Q$ denotes the set of variable that are not pre-quantified. Since the BDDs for state sets do not contain input variables in the support, this is a safe step to do. This does not violate the soundness of the approximation, i.e., for each concrete transition in R, there will be a corresponding transition in $\hat{R}$, as stated below.

Theorem 7 $\exists s_1, s_2(R(s_1, s_2) \wedge h(s_1) = \hat{s}_1 \wedge h(s_2) = \hat{s}_2) \Rightarrow \tilde{R}(\hat{s}_1, \hat{s}_2)$.

Proof: Follows from the basic rule of distributing existential quantification over conjuction, i.e., $\exists x \exists y(f_1 \wedge f_2) \Rightarrow \exists x(\exists y f_1 \wedge \exists y f_2)$. Here, out of the two variables x and y, we have distributed y over the conjunction. Now, if this rule is applied to Equation 4.3 to distribute the subset Q of invisible variables and input variables, we arrive at Equation 4.4. Equation 4.3 is true, because the precondition of the theorem says that there is a concrete transition from s_1 to s_2, with $h(s_1) = \hat{s}_1$ and $h(s_2) = \hat{s}_2$, implying that there is an abstract transition from $\hat{s}_1$ to $\hat{s}_2$.

The other direction of this implication does not hold because of the approximations introduced.

Example 8 [Counter, contd.] *For our running example, let us pre-quantify the sole invisible variable. Thus* $W = \{\}$, *and* $Q = \{v_3\}$. *The approximate transition relation then becomes* $\tilde{R}(\hat{s}_1, \hat{s}_2) = \exists v_3 f_{v_1} \wedge \exists v_3 f_{v_2}$. *This can be simplified to* $(v_1' \Leftrightarrow v_1) \vee (v_1' \Leftrightarrow v_1 \oplus v_2)$, *as shown in Figure 4.3. Note that the approximate transition relation has more transition than the abstract transition relation, e.g., the transition from state 01 to 00, and the transition from state 11 to state 01. Moreover, each transition of the abstract transition relation exists in the approximate transition relation.*

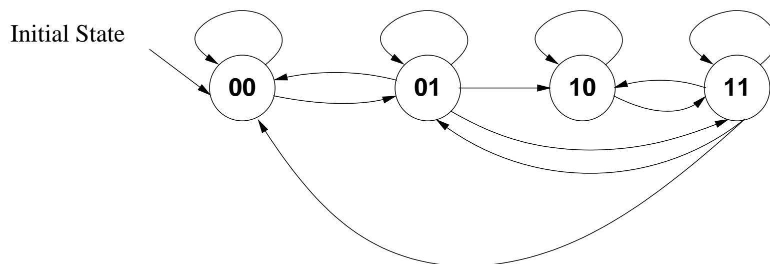

Figure 4.3: Approximation to the abstract state machine of Figure 4.2(B) obtained by pre-quantifying invisible variable v_3.

4.2.3 Bounded Model Checking in Abstraction-Refinement

Given an abstract model $\hat{M}$ and a safety formula ϕ, we run the usual BDD based symbolic model checking algorithm to determine if $\hat{M} \models \phi$. Suppose that the model checker produces an abstract path counterexample $\bar{s}_m = \langle \hat{s}_0, \hat{s}_1, \ldots, \hat{s}_m \rangle$. To check whether this counterexample holds on the concrete model M or not, we symbolically simulate M beginning with the initial state $I(s_0)$ using a fast SAT checker. At each stage of the symbolic simulation, we constrain the values of visible variables only according to the counterexample produced. The equation for symbolic simulation is:

$$(I(s_0) \wedge (h(s_0) = \hat{s}_0)) \wedge (R(s_0, s_1) \wedge (h(s_1) = \hat{s}_1)) \wedge \ldots \wedge (R(s_{m-1}, s_m) \wedge (h(s_m) = \hat{s}_m)) \tag{4.5}$$

Each $h(s_i)$ is just a projection of the state s_i onto visible variables. If this propositional formula is satisfiable, then we can successfully simulate the counterexample on the concrete machine to conclude that $M \not\models \phi$. The satisfiable assignments to invisible variables, along with the assignments to visible variables that model checking produces give a valid counterexample on the concrete machine.

If this formula is not satisfiable, the counterexample is *spurious* and the abstraction needs refinement. Assume that the counterexample can be simulated up to the abstract state $\hat{s}_f$, but not up to $\hat{s}_{f+1}$ ([23,25]). Thus Formula 4.6 is satisfiable while Formula 4.7 is *not* satisfiable, as shown in Figure 4.4.

$$(I(s_0) \wedge (h(s_0) = \hat{s}_0)) \wedge (R(s_0, s_1) \wedge (h(s_1) = \hat{s}_1)) \wedge \ldots \wedge (R(s_{f-1}, s_f) \wedge (h(s_f) = \hat{s}_f)) \tag{4.6}$$

$$(I(s_0) \wedge (h(s_0) = \hat{s}_0)) \wedge (R(s_0, s_1) \wedge (h(s_1) = \hat{s}_1)) \wedge \ldots \wedge (R(s_f, s_{f+1}) \wedge (h(s_{f+1}) = \hat{s}_{f+1})) \tag{4.7}$$

Using the terminology introduced in [23], we call the abstract state $\hat{s}_f$ a *failure*

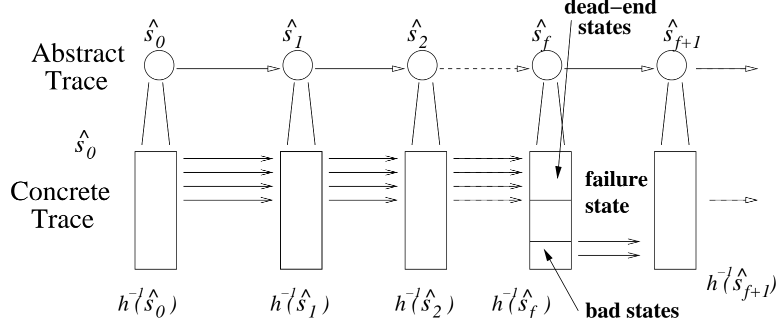

Figure 4.4: A spurious counterexample showing failure state [25]. No concrete path can be extended beyond failure state.

state. The abstract state $\hat{s}_f$ contains many concrete states. All the concrete states contained in $\hat{s}_f$ are given by all possible valuations of invisible variables, keeping the same values for visible variables. The concrete states in $\hat{s}_f$ reachable from the initial states following the spurious counterexample are called the *dead-end* states. The concrete states in $\hat{s}_f$ that have a reachable set in $\hat{s}_{f+1}$ are called *bad* states. Because the dead-end states and the bad states are part of the same abstract state, we get the spurious counterexample. The refinement step then is to separate dead-end states and bad states by making a small subset of invisible variables visible. It is easy to see that the set of dead-end states are given by the values of state variables in the fth step for all satisfying solutions to Equation 4.6. Note that in symbolic simulation formulas, we have a copy of each state variable for each time frame.

We do this symbolic simulation using the SAT checker Chaff [61]. We assume that there are concrete transitions which correspond to each abstract transition from $\hat{s}_i$ to $\hat{s}_{i+1}$, where $0 < i \leq f$. It is fairly straightforward to extend our algorithm to handle spurious abstract transitions. In this case, the set of *bad* states is not empty. Since $\bar{s}_f$ is the shortest prefix that is unsatisfiable, there must be information passed through the invisible registers at time frame f in order for the SAT solver to prove

the counterexample is spurious. Specifically, the SAT solver implicitly generates constraints on the invisible registers at time frame f based on either the last abstract transition or the prefix $\bar{s}_f$. Obviously the intersection of these two constraints on those invisible registers is empty. Thus the set of invisible registers that are constrained in time frame f during the SAT process is sufficient to separate *dead-end* states and *bad* states after refinement. Therefore, our algorithm limits the refinement candidates to the registers that are constrained in time frame f.

Equation 4.5 is exactly like symbolic simulation with Bounded Model Checking. The only difference is that the values of visible state variables at each step are constrained to the counterexample values. Since the original input variables to the system are unconstrained, we also constrain their values according to the abstract counterexample. This puts many constraints on the SAT formula. Hence, the SAT checker is able to prune the search space significantly. We rely on the ability of Chaff to identify important variables in this SAT check to separate dead-end and bad states, as described in the next section. In the abstraction refinement framework of [55], bounded model checking up to the length of the abstract counterexample is used without putting any constraints on the simulation. Thus, the ability to simulate the concrete state machine symbolically is central to abstraction refinement frameworks.

Refinement Strategies

Refinement for our abstraction based on partitioning state variables into visible and invisible variables corresponds to moving a small subset of invisible variables to visible variables. For our example, making the variable v_3 visible refines the abstraction, in fact, giving us the original transition relation. We proposed in [19] the following two refinement strategies for refinement. The first strategy relies on the fact that the

variables that get more backtracks during the unsatisfiability of a spurious counterexample, and those that appear in the conflict clauses are likely to be important. The second strategy formally analyses the conflicts generated during the unsatisfiability, and derives the variables important. This is similar to the unsatisfiability proofs.

4.2.4 Refinement Based on Scoring Invisible Variables

We score invisible variables based on two factors, first, the number of times a variable gets backtracked to and, second, the number of times a variable appears in a conflict clause. Note that we have to adjust the first score by an exponential factor based on the decision level a variable is at, as the variable at the root node can get a maximum of just two back tracks, while a variable at the decision level dl can potentially get 2^{dl} backtracks globally. Every time the SAT procedure backtracks to an invisible variable at decision level dl, we add the following number to the *backtrack_score* of that variable.

$$2^{\frac{|\mathcal{I}|-dl}{c}}$$

We use c as a normalizing constant. For example, if $c = |\mathcal{I}|/10$, then the backtrack score ranges from $2^0 = 1$ for $dl = |\mathcal{I}|$ to 2^{10} for $dl = 0$.

For computing the second score, we just keep a global counter *conflict_score* for each variable and increment the counter for each variable appearing in any conflict clause. The method used for identifying conflict clauses from conflict graphs greatly affects SAT performance. As shown in [76], we use the most effective method called the *first unique implication point* (1UIP) for identifying conflict clauses. We then use weighted average of these two scores to derive the final score as follows.

$$w_1 \cdot \mathit{backtrack_score} + w_2 \cdot \mathit{conflict_score} \tag{4.8}$$

Note that the second factor is very similar to the decision heuristic VSIDS used in Chaff. The difference is that Chaff uses these per variable *global scores* to arrive at *local decisions* (of the next branching variable), while we use them to derive *global information* about important variables. Therefore, we do not periodically divide the variable scores as Chaff does for giving more weight to the recent history.

We also have to be careful to guide Chaff not to decide on the intermediate variables introduced while converting various formulas to CNF form, which is the required input format for SAT checkers. This is done automatically in our method.

4.2.5 Refinement Based on Conflict Dependency Graph

The choice of which invisible registers to make visible is the key to the success of the refinement algorithm. Ideally, we want this set of registers to be small and still be able to prevent the spurious trace. The set of registers appearing in all the conflict graphs during the checking of the counterexample could prevent the spurious trace, as all the reasons for unsatisfiability have been removed. However, this set can be very large. We will show here that it is unnecessary to consider all conflict graphs.

Dependencies Between Conflict Graphs

We call the implication graph associated with a conflict a *conflict graph*. At least one conflict clause is generated from a conflict graph.

Definition 7 *Given two conflict graphs A and B, if at least one of the conflict clauses generated from A labels one of the edges in B, then we say that conflict B* ***directly***

depends *on conflict A.*

In other words, conflict B directly depends on conflict A if we used at least one conflict clauses derived from the conflict A to arrive at the conflict B.

For example, consider the conflicts depicted in Figure 4.5. Suppose that at a certain stage of the SAT checking, conflict graph A is generated. This produces the conflict clause $\omega_9 = (\neg x_9 + x_{11} + \neg x_{15})$. We are using the first UIP (1UIP) learning strategy [76] to identify the conflict clause here. This conflict clause can be rewritten as $x_9 \wedge \neg x_{11} \rightarrow \neg x_{15}$. In the other conflict graph B, clause ω_9 labels one of the edges, and forces variable x_{15} to be 0. Hence, we say that conflict graph B directly depends on conflict graph A.

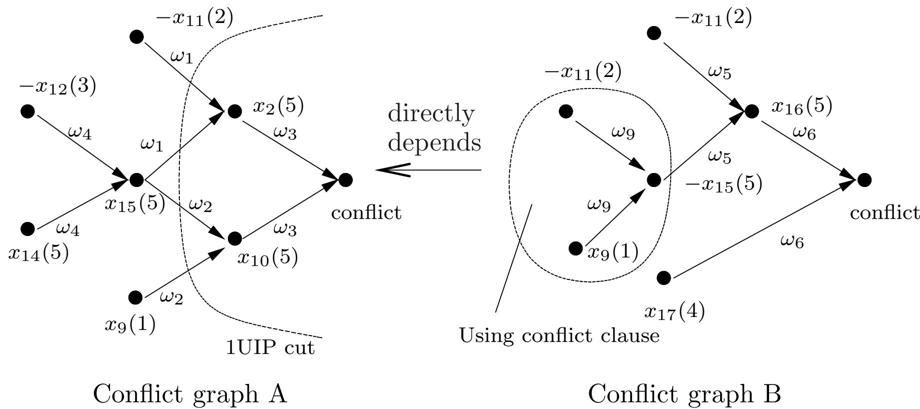

Figure 4.5: Two dependent conflict graphs. Conflict B depends on conflict A, as the conflict clause ω_9 derived from the conflict graph A produces conflict B.

Given the set of conflict graphs generated during satisfiability checking, we construct the *unpruned conflict dependency graph* as follows:

- **Vertices** of the unpruned dependency graph are all conflict graphs created by the SAT algorithm.

- **Edges** of the unpruned dependency graph are direct dependencies.

Figure 4.6 shows an unpruned conflict dependency graph with five conflict graphs. A conflict graph B depends on another conflict graph A, if vertex A is reachable from vertex B in the unpruned dependency graph. In Figure 4.6, conflict graph E depends on conflict graph A. When the SAT algorithm detects unsatisfiability, it terminates with the last conflict graph corresponding to the last conflict. The subgraph of the unpruned conflict dependency graph on which the last conflict graph depends is called the *conflict dependency graph.* Formally,

Definition 8 *The **conflict dependency graph** is a subgraph of the unpruned dependency graph. It includes the last conflict graph and all the conflict graphs on which the last one depends.*

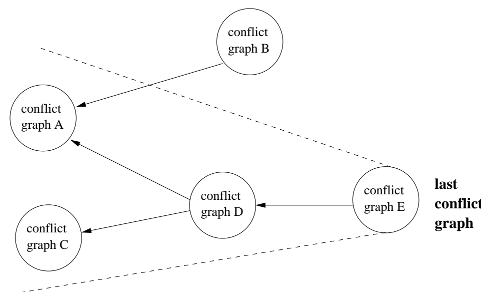

Figure 4.6: The unpruned dependency graph and the dependency graph (within dotted lines)

In Figure 4.6, conflict graph E is the last conflict graph, hence the conflict dependency graph includes conflict graphs A, C, D, E. Thus, the conflict dependency graph can be constructed from the unpruned dependency graph by any directed graph traversal algorithm for reachability. Typically, many conflict graphs can be pruned away in this traversal, so that the dependency graph becomes much smaller than the unpruned dependency graph. Intuitively, all SAT decision strategies are based

on heuristics. For a given SAT problem, the initial set of decisions/conflicts a SAT solver comes up with may not be related to the final unsatisfiability result. Our dependency analysis helps to remove that irrelevant reasoning.

Generating Conflict Dependency Graph Based on Zchaff

We have implemented the conflict dependency analysis algorithm on top of zchaff [76], which has a powerful learning strategy called first UIP (1UIP). Experimental results from [76] show that 1UIP is the best known learning strategy. In 1UIP, only one conflict clause is generated from each conflict graph, and it only includes those implications that are closer to the conflict. Refer to [76] for the details. We have built our algorithms on top of 1UIP, and we restrict the following discussions to the case that only one conflict clause is generated from a conflict graph. Note here that the algorithms can be easily adapted to other learning strategies.

After SAT terminates with unsatisfiability, our pruning algorithm starts from the last conflict graph. Based on the clauses contained in this conflict graph, the algorithm traverses other conflict graphs that this one depends on. The result of this traversal is the pruned dependency graph.

Identifying Important Variables

The dependency graph records the reasons for unsatisfiability. Therefore, only the variables appearing in the dependency graph are important. Instead of collecting all the variables appearing in any conflict graph, those in the dependency graph are sufficient to disable the spurious counterexample.

Suppose $\bar{s}_{f+1} = \langle \hat{s}_0, \hat{s}_1, \ldots, \hat{s}_{f+1} \rangle$ is the shortest prefix of a spurious counterexample that can not be simulated on the concrete machine. Recall that $\hat{s}_f$ is the

failure state. During the satisfiability checking of $\bar{s}_{f+1}$, we generate an unpruned conflict dependency graph. When Chaff terminates with unsatisfiability, we collect the clauses from the pruned conflict dependency graph. Some of the literals in these clauses correspond to invisible registers at time frame f. Only those portions of the circuit that correspond to the clauses contained in the pruned conflict dependency graph are necessary for the unsatisfiability. Therefore, the candidates for refinement are the invisible registers that appear at time frame f in the conflict dependency graph.

Refinement Minimization

The set of refinement candidates identified from conflict analysis is usually not minimal, i.e., not all registers in this set are required to invalidate the current spurious abstract counterexample. To remove those that are unnecessary, we have adapted the greedy refinement minimization algorithm in [72]. The algorithm in [72] has two phases. The first phase is the addition phase, where a set of invisible registers that suffices to disable the spurious abstract counterexample is identified. In the second phase, a minimal subset of registers that is necessary to disable the counterexample is identified. Their algorithm tries to see whether removing a newly added register from the abstract model still disables the abstract counterexample. If that is the case, this register is unnecessary and is no longer considered for refinement. In our case, we only need the second phase of the algorithm. The set of refinement candidates provided by our conflict dependency analysis algorithm already suffices to disable the current spurious abstract counterexample. Since the first phase of their algorithm takes at least as long as the second phase, this should speed up our minimization algorithm considerably.

4.3 Reparameterization in Abstraction-Refinement

In abstraction-refinement framework, it is relatively straightforward to use reparameterization algorithm based symbolic simulation. In proof based abstraction refinement by McMillan *et al.* [55], a specific counterexample is not simulated on the concrete machine. Instead, a BMC of a given depth is done. In this case, the reparameterization algorithm can be used in BMC as described in previous Section 3.3. On the other hand, in CEGAR, a counterexample $\bar{s}_m = \langle \hat{s}_0, \hat{s}_1, \ldots, \hat{s}_m \rangle$ just assigns Boolean values to a subset of state variables at each step. Suppose along the length of the counterexample, reparameterization is invoked a total of l times at steps $m_1, m_2, \ldots, m_l$, such that $0 < m_1 < m_2 < \ldots \leq m$. Let $(f_1^{m_i}(I^{m_i}), \ldots, f_n^{m_i}(I^{m_i}))$ be the old parametric representation. Let $(h_1^{m_i}(P^{m_i}), \ldots, h_n^{m_i}(P^{m_i}))$ be the new parametric representation at step m_i. Let S^{m_i} be the set of states represented by it. To determine if the counterexample is spurious, we simulate the abstract counterexample by adding $\hat{s}_0$ constraints to the initial state. Then we proceed to add $\hat{s}_1, \hat{s}_2, ...$ constraints to the symbolic simulation as described in section 3.3.5. These constraints are just assignments of values, and hence are easy to add in the symbolic simulation. When we reach the step m_1, the process is repeated considering $\hat{s}_{m_1}$ as constraints on the reparameterized state. Also, at each of the steps m_i, we check to see if the set of states S^{m_i} is empty or not. This can be done by checking if the SAT formula

$$\hat{s}_{m_i}^1 = f_1^{m_i}(I^{m_i}) \wedge \hat{s}_{m_i}^2 = f_2^{m_i}(I^{m_i}) \ldots \hat{s}_{m_i}^n = f_n^{m_i}(I^{m_i}) \tag{4.9}$$

has any satisfiable assignments or not. Here, $\hat{s}_{m_i}^j$ denotes the assignment to the jth state variable by the abstract counterexample in step number m_i. If Equation 4.9 is satisfiable, then we know that the counterexample is real and we proceed to build the real counterexample as described in the previous section. If not, we need to identify refinement information from the failed SAT instance.

For identifying refinement information, we can use the heuristics of [19]. However, there is one important difference. Equation 4.9 does not contain state variables for all information steps. The state variables that appear in the formula are from step m_{i-1} to step m_i only. However, as reported in the previous subsection titled "Identifying Important Variables", just looking at a part of the failed counterexample (often just the failure state) provides useful refinement information. Therefore, I hope that the refinement information extracted from the partial SAT instance will be useful. I want to evaluate the quality of refinement information that we get from such SAT instances by extensive experimentation.

4.4 Experimental Results for Refinement

We embed the symbolic simulation algorithm with SAT-based reparametrization into the abstraction refinement framework described in the last section. The symbolic simulation algorithm is used to replace BMC as means of simulating abstract counterexamples. The refinement information is extracted from the full simulation run. In contrast to that, the proposed algorithm with symbolic simulation extracts refinement information only from the last segment of the counterexample simulation. This may result in refinement information of lower quality. Note that both algorithms are just refinement heuristics, and none guarantees the elimination of the spurious counterexample.

Both methods use a BDD-based model checker for the verification of the abstract model. The model checker is based on NuSMV and uses dynamic variable ordering. Apart from deriving refinement information, the initial variable orders for the BDD-based model checker are also derived from the analysis of failed counterexample. In the very first iteration of the abstraction refinement loop, no variable orders are

provided to NuSMV.

Table 4.1 lists the circuits that we used for the experiments, and provides some characteristics of the circuits. The circuits are from three different classes. The D and M series circuits are processor benchmarks. The IU circuits are models of the picoJava microprocessor from Synopsys, and the s-series circuits are ISCAS89 sequential benchmarks.

The D, M and IU series benchmarks already come with properties. However, there are no properties available for the ISCAS89 circuits. We used random simulation to infer reasonable properties for these circuits. The property verified for the s3271 circuit is $\mathbf{AG}\,\mathbf{AF}(\bigvee_{i=0}^{6} ManFinal_i)$, for s13207 the property is $\mathbf{AG}\,\neg(g12 \wedge g1229 \wedge g1325 \wedge 1391 \wedge g1431 \wedge g972 \wedge g182)$, for s15850 the property is $\mathbf{AG}\,\neg(g109 \wedge g878 \wedge g901)$, and for s38417, the property is $\mathbf{AG}\,\neg(g222 \wedge g342)$. We also experimented with other ISCAS89 circuits, however, the length of the longest counterexample to simulate on these circuits was either too short to be of interest, or the time taken by the SAT-based simulation was too small a fraction of the total time.

We performed our experiments on a machine with dual AMD Athlon MP 1800+ processors and 3GB memory. The reparameterization is done as soon as the size of the SAT instance for the simulation exceeds 700MB. The total amount of memory was limited to 2.5GB.

Table 4.2 compares the abstraction refinement with refinement based simulation against the abstraction refinement without the refinement based simulation from [19]. The refinement technique used and all other parameters were the same in both sets of experiments. The only difference is the algorithm used for simulation.

The columns marked “sym” are for the new algorithm, while the columns marked ”fmcad” are for the old algorithm. The set marked “# refn” compares the number of

circuit	# latches	# inputs	counterexample length
D6	161	16	20
D18	498	247	28
D19	285	49	32
D20	532	30	14
M3	334	155	true
M4	744	95	true
M5	316	104	true
IUp1	4494	361	true
IUp2	4494	361	true
IUp3	4494	361	true
s3271	116	26	true
s13207	669	31	true
s15850	597	14	true
s38417	1636	28	true

Table 4.1: Circuits used for abstraction-refinement experiment.

refinement iterations required, the set marked "|reg|" compares the number of latches in the final abstract model, the set marked "max |CE|" compares the length of the longest counterexample encountered, the set marked "sim. time" compares the time spent in the simulation of abstract counterexamples over all refinement iterations, and the set marked "total time" compares the total time to prove the property or to disprove it. The last column marked "# rep" lists the total number of reparameterizations done across various simulations for the circuit. Verification was not complete for circuits when the numbers are in bold typeface with an accompanying symbol. The run times are given in seconds.

ckt	# refn		|reg|		max |CE|		sim. time		total time		# rep
	fmcad	sym	fmcad	sym	fmcad	sym	fmcad	sym	fmcad	sym	
D6	48	48	39	39	20	20	438	362	845	718	23
D18	142	127	253	253	28	28	3598	2740	9873	8349	56
D19	37	49	103	112	32	32	4348	1329	14528	12087	95
D20	74	74	265	265	14	14	1359	338	2794	2192	23
M3	58	**42**†	128	**87**†	54	**54**†	4378	**2088**†	15306	>**21600**†	3
M4	173	**94**†	336	**184**†	44	**39**†	15540	**4776**†	20327	>**21600**†	21
M5	7	11	30	30	6	10	3427	2902	8653	10312	3
IUp1	**8**‡	13	**12**‡	19	**72**‡	72	**3390**‡	1295	**4877**‡	4063	117
IUp2	6	6	13	13	22	22	1298	605	2498	1335	16
IUp3	**17**⋆	32	**19**⋆	41	**52**⋆	67	> **21600**⋆	3022	> **21600**⋆	5836	325
s3271	32	32	38	38	48	48	117	96	198	174	3
s13207	15	15	23	23	43	43	2231	1035	4066	2454	13
s15850	8	8	18	18	56	36	1643	669	2998	2108	8
s38417	19	19	29	29	53	53	1347	462	1655	1077	14

Table 4.2: Comparison of SAT based reparameterization against plain SAT based simulation in abstraction-refinement framework.

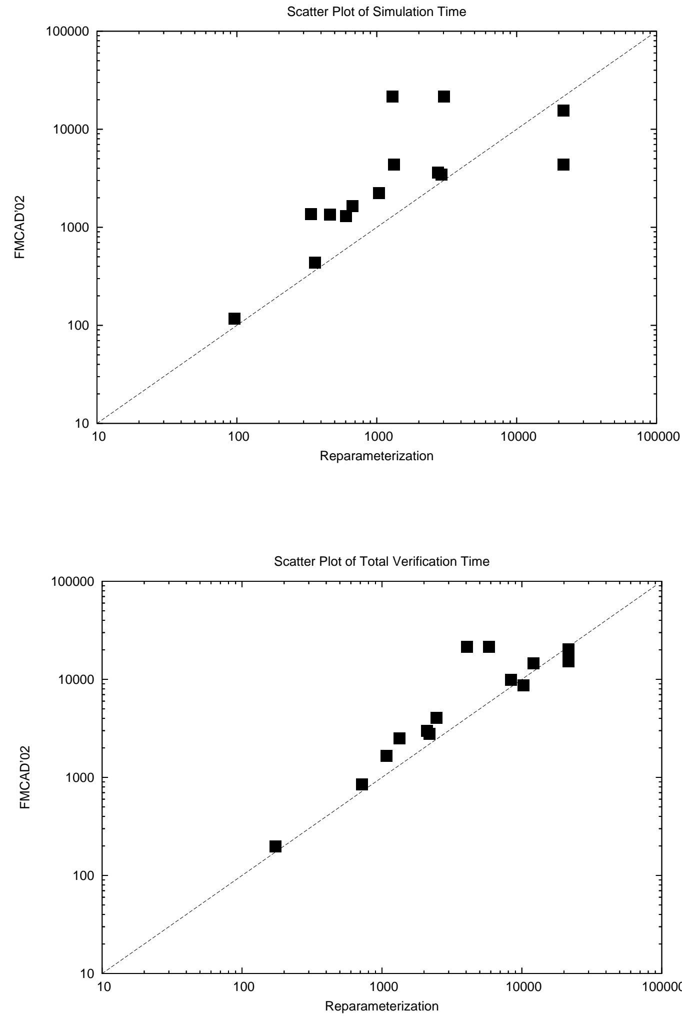

Figure 4.7: Scatter plots of simulation time and total time. A point above the $y = x$ line (diagonal) is a win for the new algorithm, and a point below the line is a win for the FMCAD02 algorithm.

In the table, † denotes that the model checking of abstract model timed out, ‡ denotes that the simulation of counterexample failed due to memory limit, and $\star$ denotes that the simulation of counterexample timed out.

In Figure 4.7, we show the scatter plots of the simulation time and the total model checking time for both techniques. The horizontal axis is for the new simulation algorithm, while the old algorithm is represented by the vertical axis. Thus, a point

above the $y = x$ line (diagonal) is a win for the new algorithm, and a point below the line is a win for the original algorithm. For the failed instances, we used the time value 21600 in the scatter plots.

The new simulation algorithm yields useful refinement information in most experiments, and the improvement in run-time is due to the faster simulation. The large circuits IUp1 and IUp3 fail to verify with the original simulation algorithm, but can be verified with the new technique. The simulation using SAT-based BMC exceeds the memory bound for IUp1 and the time bound for IUp3. The difference between IUp1 and IUp3 is due to the fact that there is only one very long counterexample for IUp1, while for IUp3 there are multiple long counterexamples. The sum of the time required to simulate all the counterexamples exceeds the time bound.

However, the medium-sized circuits M3 and M4 show negative results. These circuits fail to verify within the time limit of 6 hours because the BDD-based model checking of abstract model times out. We examined the failure of the new algorithm for the circuits M3 and M4. For the M4 circuit, the new set of latches obtained from the truncated simulation using the new technique was different from that obtained by the original algorithm. Thus, the failure is caused by the low quality of the refinement information.

For the M3 circuit the set of latches computed by the new algorithm is exactly the same as computed by the BMC-based algorithm. However, we analyze the failed counterexample simulation to derive variable orders for the BDDs used for verifying the abstract model. The BDD variable orders obtained by the new method were different from those obtained by the old method, and cause the BDD-based model checker to fail. When we used the variable orders derived by the old method, the abstract model checking in the new method was successful for 6 more refinement iterations, after which the model checking of abstract model checking failed due to a

different set of latches being found as refinement.

4.5 Summary

Using experiments on large industrial circuits, we show that the use of symbolic simulation with SAT-based reparametrization within the Counterexample Guided Abstraction Refinement (CEGAR) framework can yield significant performance improvements and enables the verification of larger circuits.

However, the results also show that in certain instances, the SAT-based reparametrization provides insufficient refinement information, and thus, performs worse than BMC. The new technique is therefore not clearly dominant over the old technique, and the user should be given a choice of both techniques.

Future research should investigate criteria that can predict the success of either simulation technique and automated ways to decide which technique should be used. We will also investigate the performance impact using different refinement algorithms.

Chapter 5

Conclusions and Future Directions

In this thesis, I have attempted to address the capacity challenges to formal verification on multiple fronts. Beginning at the core of model checking and state reachability, I proposed advances to the BDD based image computation. Where BDDs are unsuitable, especially when the design contains thousands of variables, SAT offers a promise. To that effect, I proposed a SAT-enumeration based algorithm for image computation. Moving up from the core that is image computation, I examine symbolic simulation, which forms the basis of modern verification techniques like abstraction-refinement, and bounded model checking. I proposed a novel SAT based approach to a specific kind of function decomposition called parametric representation. The algorithm aims at reducing the size of the function representation during symbolic simulation, which allows one to explore deeper traces than before. Moving up next, two critical applications of the reparameterization algorithm for symbolic simulation were attempted. I used the reparameterization algorithm for BMC and to simulate abstract counterexamples in automated abstraction-refinement.

The promise of quantification scheduling is to keep disjointly decomposed BDDs as much separate as possible when computing images and pre-images. To that effect,

I proposed various linear and non-linear quantification scheduling algorithms. These algorithms advance the state of the art in BDD based image computation. The work still continues though. The techniques presented for linear quantification scheduling rely on heuristics, and therefore, there may exist a class or classes of problems on which they works poorly. However, just as BDD variable ordering is essentially intractable, and hence one must rely on heuristics, the problem of quantification scheduling is also in the same state. Most often, simple variable orderings based on static circuit information might be sufficient in practice, just like the BDD variable orders. A promising direction to investigate is a combination of static and dynamic variable orders. The techniques presented are amenable to incorporating stating ordering. The interplay of BDD variable orders and quantification orders also is interrelated, and needs to be examined.

Existential quantification of a subset of variables from a Boolean function is the basis of image computation algorithm. Existential quantification can be carried out by enumerating satisfying assignments to a Boolean formula. I proposed an efficient algorithm to carry out such enumeration on top of modern SAT solvers. The algorithm relies on an efficient data structure to store enumerated cubes, and on the cube enlargement procedure, that tries to make a single satisfying assignment as general as possible. The approach does have some limitations though. The cube representation is still a clausal representation, and there exist a class of functions where clausal representation is expensive. For that class, one should seek a non-clausal representation. Building an enumerating SAT solver that uses non-clausal representation should be an important development. The work ultimately leads to the problem of solving quantified Boolean formulas (QBF), existential quantification being a very specific kind of the QBF problem, for which we have still not had a breakthrough as we did for SAT. Reachability by forward image computation is doing a breadth-first

search (BFS) for finding counterexamples. The SAT based image computation can be expanded to do a depth-first search (DFS), or a mix of DFS and and BFS. The searches can also be done in a backward manner, as opposed to forward manner, once the basic technique of SAT-enumeration is in place.

The main component of my thesis is SAT-based reparameterization for symbolic simulation. When formulas representing state sets grow large in symbolic simulation, reparameterization is used to re-encode the set-state, to reduce the size of the representation. Reparameterization uses the SAT-based existential quantification described earlier. One obvious application of reparameterization is in simulating long traces for bounded model checking (BMC). I showed that the technique scales well for deep BMC runs. The reparameterization algorithm works for both functional representation, as well as non-functional representation of transition relations. There are avenues for further improvements. The reparameterization algorithm uses a particular kind of decomposition. One can however examine different kinds of decompositions, which would lead to different reparameterization algorithms. However, the basic framework of reparameterization using existential quantification should still apply. The type of decomposition that I used also allows for canonical representation, modulo the variables orders. That brings us to an exploration of various variable orderings for reparameterization, as different variables orders lead to different parametric representations. Finally, the SAT-based reparameterization presented is still a Boolean technique. A natural and a very powerful extension of the algorithm would be word-level reparameterization.

The final part of the thesis presented another prominent use of symbolic simulation. In automated SAT-based CEGAR, long counterexample traces need to be simulated on large transition systems to determine the validity of one or more abstract counterexamples. Using reparameterization, we are able to simulate long counterex-

ample traces. One however loses on the refinement information obtained from a spurious counterexample, that does not simulate on the concrete transition system. Without reparameterization, the whole trace is simulated by the SAT solver, and all the time frames beginning from the initial time frame are available for analysis. With reparameterization, only the suffix of the abstract counterexample, from where the reparameterization was done last, is available for analysis. This might lead to sub-optimal refinement. Future research should concentrate on improving the analysis of failed counterexamples for better refinement of abstract models. Research should also focus on adaptively choosing the plain symbolic simulation or simulation with reparameterization for abstraction-refinement purposes.

In summary, my proposed techniques combat the state-explosion problem at various levels, beginning at the image computation all the way up to abstraction refinement. I hope to have advanced the state of the art in state space analysis for formal verification.

Appendix A

Proof of Theorem 1

It is easy to see that for a given permutation σ of rows, we can compute λ in polynomial time ($O(n \cdot m)$) and check if $\lambda \leq r$.

To show that $\lambda - OPT$ is NP-hard, we reduce a known NP-complete problem called *optimal linear arrangement (OLA)* [32, page 200] to $\lambda - OPT$. An instance of OLA consists of a graph $G(V, E)$ and a positive integer K. The question is whether there exists a permutation f of V such that $\sum_{(u,v)\in E} |f(u) - f(v)| \leq K$. The reduction consists of constructing a dependence matrix D and a number r such that $(V, E), K$ is a solution of OLA iff D, r is a solution to $\lambda - OPT$. An example of a reduction is given in figure A.1.

Formally, D has $|V|$ rows corresponding to the vertices of $G(V, E)$, and $|E|$ columns corresponding to the edges of $G(V, E)$. For any edge $e_k = (v_i, v_j)$, set $d_{ik} = d_{jk} = 1$ and set all other d_{ij}'s to 0. Thus, in each column there are two occurences of the symbol 1. We set $r = \frac{K+n}{n \cdot m}$. Trivially we obtain the following

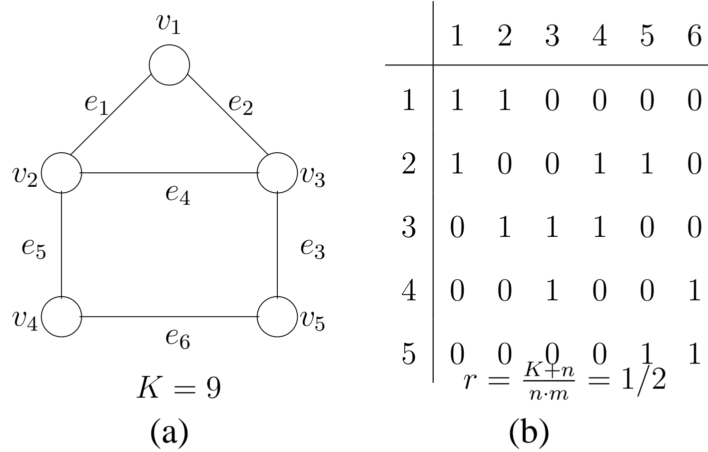

	1	2	3	4	5	6
1	1	1	0	0	0	0
2	1	0	0	1	1	0
3	0	1	1	1	0	0
4	0	0	1	0	0	1
5	0	0	0	0	1	1

Figure A.1: (a) An instance of Optimal Linear Arrangement, (b) its reduction to $\lambda - OPT$. The permutation v_1, v_2, v_3, v_5, v_4 is a solution to both.

equivalence:

$$
\begin{aligned}
\frac{\sum_{1 \leq j \leq n}(h_j - l_j + 1)}{n \cdot m} &\leq r \\
\Leftrightarrow \sum_{1 \leq j \leq n}(h_j - l_j + 1) &\leq r \cdot (n \cdot m) \\
\Leftrightarrow \sum_{1 \leq j \leq n}(h_j - l_j + 1) &\leq K + n
\end{aligned}
$$

Let σ be a permutation of the vertices of V. Note that σ simultaneously is a permutation of the rows of D. We have to show that σ is a solution of $G(V, E), K$ iff σ is a solution of D, r.

The important observation is that because of the construction of D, the only non-zero entries in each column j correspond to the two vertices of the edge $e_j = (u, v)$. Therefore, we conlude that $h_j - l_j = |\sigma(u) - \sigma(v)|$. Continuing the above equivalence we obtain

$$
\begin{aligned}
\sum_{1 \leq j \leq n} |\sigma(u) - \sigma(v)| + n &\leq K + n \\
\Leftrightarrow \sum_{(u,v) \in E} |f(u) - f(v)| &\leq K
\end{aligned}
$$

Appendix B

Proof of Theorem 3

We provide a proof of Theorem 3 in this section. We prove that the parametric representation that we get from the algorithm OrderedReparam is equivalent to the original representation. As usual, $\bar{v} = (v_1, \ldots, v_n) \in \mathcal{S}_n$ denotes an assignment to n variables $V = \{v_1, \ldots, v_n\}$, $\bar{\iota} \in \mathcal{W}^k$ denotes an assignment to variables I^k, and $\bar{p} = (p_1, \ldots, p_n) \in \mathcal{P}_n$ denotes an assignment to variables $P = \{p_1, \ldots, p_n\}$. We use $\mathcal{X}_n$ to denote the set of states described by the representation $(f_1(\bar{\iota}), f_2(\bar{\iota}), \ldots, f_n(\bar{\iota}))$ and $\mathcal{Y}_n$ to denote the set of states given by the new parametric form $(h_1(\bar{p}), h_2(\bar{p}), \ldots, h_n(\bar{p}))$. These clearly are subsets of $\mathcal{S}_n$. We will often drop the subscripts from $\mathcal{S}_n, \mathcal{P}_n, \mathcal{X}_n$, and $\mathcal{Y}_n$ when it is clear that the sets are constructed from n length vectors. Moreover, when it is clear what the arguments to a function are, we will often drop the arguments for brevity. We would also like to remind the reader of the important equations 3.4, 3.5, 3.6, 3.7 and 3.8.

We will prove this theorem in two parts. First, we prove that $\mathcal{X} \subseteq \mathcal{Y}$, and then we prove that $\mathcal{Y} \subseteq \mathcal{X}$.

$\boxed{\mathcal{X} \subseteq \mathcal{Y}}$.

If $\mathcal{X} = \emptyset$, then obviously $\mathcal{X} \subseteq \mathcal{Y}$. Otherwise, let $\bar{v}$ be an arbitrary element of $\mathcal{X}$. Then by definition of $\mathcal{X}$, there exists an assignment $\bar{\iota} \in \mathcal{W}^k$ such that $f_1(\bar{\iota}) = v_1 \wedge \ldots \wedge f_n(\bar{\iota}) = v_n$. In order to show that $\bar{v} \in \mathcal{Y}$, we have to provide an assignment $\bar{p} \in \mathcal{P}$ such that $h_1(\bar{p}) = v_1 \wedge \ldots \wedge h_n(\bar{p}) = v_n$.

We will prove the existence of such $(p_1, p_2, \ldots, p_n)$ by induction on n. Formally, we establish the following by induction on n.

$$\forall \bar{v} \in \mathcal{X}_n . \exists \bar{p} \in \mathcal{P}_n . h_1(\bar{p}) = v_1 \wedge \ldots \wedge h_n(\bar{p}) = v_n.$$

Base Case: $n = 1$

By definition,

$$\rho_i(p_1, \ldots, p_{i-1}, \bar{\iota}) = (f_1(\bar{\iota}) = h_1(p_1)) \wedge \ldots (f_{i-1}(\bar{\iota}) = h_{i-1}(p_1, \ldots, p_{i-1})).$$

Hence it is vacuously true that $\rho_1(\bar{\iota})$ is 1 for any input vector $\bar{\iota}$, or formally $\forall \iota \in \mathcal{W}^k . \rho_1(\bar{\iota}) = 1$. Therefore,

$$\begin{aligned} h_1^\alpha &= \forall \bar{\iota} \in \mathcal{W}^k . (\rho_1(\bar{\iota}) \Rightarrow f_1(\bar{\iota}) = \alpha) \\ &= \forall \bar{\iota} \in \mathcal{W}^k (f_1(\bar{\iota}) = \alpha), \end{aligned}$$

for both $\alpha = 0$ and $\alpha = 1$. Thus, h_i^α evaluates to constant 0 or 1 as it has no arguments.

There are two cases to consider, depending on whether v_1 is 1 or 0.

Case 1: $v_1 = 1$.

Since there is an input vector $\bar{\iota}$ for which $f_1(\bar{\iota}) = 1$, the first bit v_1 is not forced to 0. Therefore, h_1^0, the condition under which v_1 is forced to 0, has to be false. Since h_1^1, h_1^0, and h_1^c are mutually exclusive, only one of them is 1 and the other two are

0. Thus, there are two possibilities left. Either $h_1^1 = 1$ or $h_1^c = 1$. If $h_1^1 = 1$, then $h_1(p_1) = h_1^1 \vee p_1 \cdot h_1^c = 1$ for any p_1. On the other hand, if $h_1^c = 1$, then $h_1(p_1) = p_1$, so we choose $p_1 = 1$. Then $h_1(p_1) = p_1 \Rightarrow h_1(p_1) = 1$.

Case 2: $v_1 = 0$.

Since there is an input vector $\bar{\imath}$ for which $f_1(\bar{\imath}) = 0$, the first bit v_1 is not forced to 1. Therefore, h_1^1, the condition under which v_1 is forced to 1, has to be false. As h_1^1, h_1^0, and h_1^c are mutually exclusive, only one of them is 1 and the other two are 0. Thus, there are two possibilities left. Either $h_1^0 = 1$ or $h_1^c = 1$. If $h_1^c = 0$, then $h_1(p_1) = h_1^1 \vee p_1 \cdot h_1^c = 0$ for any p_1. On the other hand, if $h_1^c = 1$, then $h_1(p_1) = p_1$, so we choose $p_1 = 0$. Then $h_1(p_1) = p_1 \Rightarrow h_1(p_1) = 0$.

Both cases establish the base case of the induction.

Induction Step: $n \rightarrow n+1$

The induction hypothesis is

$$\forall \bar{v} \in \mathcal{X}_n . \exists \bar{p} \in \mathcal{P}_n . h_1(\bar{p}) = v_1 \wedge \ldots \wedge h_n(\bar{p}) = v_n .$$

Here, $\mathcal{X}_n$ and $\mathcal{P}_n$ are used to emphasize that $\bar{v}$ and $\bar{p}$ are assignments to n variables. We have to prove that

$$\forall \bar{v} \in \mathcal{X}_{n+1} . \exists \bar{p} \in \mathcal{P}_{n+1} . h_1(\bar{p}) = v_1 \wedge \ldots \wedge h_{n+1}(\bar{p}) = v_{n+1} .$$

Let $\bar{v} = (v_1, \ldots, v_{n+1}) \in \mathcal{X}_{n+1}$. Then by definition of $\mathcal{X}_{n+1}$, there exists an $\bar{\imath} \in \mathcal{W}^k$ such that $f_1(\bar{\imath}) = v_1 \wedge \ldots \wedge f_{n+1}(\bar{\imath}) = v_{n+1}$. According to the induction hypothesis, there exists $(p_1, \ldots, p_n)$ such that $h_1(p_1) = v_1 \wedge \ldots \wedge h_n(p_1, p_2, \ldots, p_n) = v_n$. We will extend this assignment by p_{n+1} such that $h_{n+1}(p_1, \ldots, p_{n+1}) = v_{n+1}$. By definition, h_{n+1}^1, h_{n+1}^0 and h_{n+1}^c depend only on $p_1, \ldots, p_n$. So the particular assignment $(p_1, \ldots, p_n)$ assigns specific values to these three functions. They are also mutually

exclusive. We also have

$$\begin{aligned}\rho_{n+1}(p_1,\ldots,p_n,\bar{\iota}) &= (f_1(\bar{\iota})=h_1(p_1))\wedge\ldots(f_n(\bar{\iota})=h_n(p_1,\ldots,p_n))\\ &= 1\text{, by induction hypothesis}\end{aligned}$$

Moreover, by definition,

$$h^{\alpha}_{n+1}(p_1,p_2,\ldots,p_n) = \forall\bar{\iota}\in\mathcal{W}^k.(\rho_{n+1}(p_1,\ldots,p_n,\bar{\iota})\Rightarrow f_{n+1}(\bar{\iota})=\alpha)$$

for both $\alpha=1$ and $\alpha=0$. Thus, if there is at least one input vector for which ρ_{n+1} evaluates to 1 and f_{n+1} evaluates to $\neg\alpha$, then $h^{\alpha}_{n+1}=0$. For the specific $\bar{\iota}$ we are considering, we have shown that $\rho_{n+1}=1$.

As in the base case, we have two cases when v_{n+1} is either 0 or 1.

Case 1: $v_{n+1}=1$.

Since there exists an $\bar{\iota}$ (the one we are considering) for which $\rho_i(p_1,\ldots,p_n,\bar{\iota})=1$ and $f_{n+1}(\bar{\iota})=1$ hold, h^0_{n+1}, the condition under which f_{n+1} is forced to 0, is false (or 0). As h^0_{n+1},h^1_{n+1} and h^c_{n+1} are mutually exclusive, there are two sub-cases to consider. If $h^1_{n+1}=1$, then $h_{n+1}(p_1,\ldots,p_{n+1})=h^1_{n+1}\vee p_{n+1}\cdot h^c_{n+1}=1$ for any p_{n+1}. On the other hand, if $h^c_{n+1}=1$, then $h_{n+1}(p_1,\ldots p_{n+1})=p_{n+1}$. In that case, we choose $p_{n+1}=1$. Then $h_{n+1}(p_{n+1})=p_{n+1}\Rightarrow h_{n+1}(p_{n+1})=1$.

Case 2: $v_{n+1}=0$.

Since there exists an $\bar{\iota}$ (the one we are considering) for which $\rho_i(p_1,\ldots,p_n,\bar{\iota})=1$ and $f_{n+1}(\bar{\iota})=0$ hold, h^1_{n+1}, the condition under which f_{n+1} is forced to 1, is false (or 0). As h^0_{n+1},h^1_{n+1} and h^c_{n+1} are mutually exclusive, there are two sub-cases to consider. If $h^0_{n+1}=1$, then $h_{n+1}(p_1,\ldots,p_{n+1})=h^1_{n+1}\vee p_{n+1}\cdot h^c_{n+1}=0$ for any p_{n+1}. On the other hand, if $h^c_{n+1}=1$, then $h_{n+1}(p_1,\ldots p_{n+1})=p_{n+1}$. In that case, we choose $p_{n+1}=0$. Then $h_{n+1}(p_{n+1})=p_{n+1}\Rightarrow h_{n+1}(p_{n+1})=0$.

So in both cases, we can choose p_{n+1} such that h_{n+1} evaluates to v_{n+1}.

Thus, the vector $\bar{p} = (p_1, p_2, \ldots, p_n, p_{n+1})$ has the desired property $h_1(\bar{p}) = v_1 \wedge \ldots \wedge h_{n+1}(\bar{p}) = v_{n+1}$. This holds for $p_1, \ldots, p_n$ by the induction hypothesis, and for p_{n+1} by the arguments above. This establishes the induction step.

By induction, we have provided an assignment $\bar{p}$ such that $\bar{h}(\bar{p}) = \bar{v}$ for a given $\bar{v} \in \mathcal{X}$. Thus $\bar{v} \in \mathcal{Y}$, hence $\mathcal{X} \subseteq \mathcal{Y}$.

$\boxed{\mathcal{Y} \subseteq \mathcal{X}}$.

If $\mathcal{Y} = \emptyset$, then the relation obviously holds. Otherwise, suppose $\bar{v} \in \mathcal{Y}$. Then by definition of $\mathcal{Y}$, there exists $\bar{p} \in \mathcal{P}$ such that $h_1(\bar{p}) = v_1 \wedge \ldots \wedge h_n(\bar{p}) = v_n$. In order to show that $\bar{v} \in \mathcal{X}$, we have to provide an assignment $\bar{\imath}$ such that $f_1(\bar{\imath}) = v_1 \wedge \ldots \wedge f_n(\bar{\imath}) = v_n$. However, instead of giving just one such input vector $\bar{\imath}$, we will compute the largest set $\mathcal{J}^k \subseteq \mathcal{W}^k$ of input vectors such that any input vector in $\mathcal{J}^k$ will have the desired property. Formally, we will prove the following stronger claim by induction on n:

$$\forall \bar{v} \in \mathcal{Y}. \exists \mathcal{J}^k \subseteq \mathcal{W}^k. \left[\mathcal{J}^k \neq \emptyset \wedge \mathcal{J}^k = \left\{ \bar{\imath} \in \mathcal{W}^k | \bigwedge_{i=1}^{n} f_i(\bar{\imath}) = v_i \right\} \right]$$

Thus, we provide a non empty set of input vectors $\mathcal{J}^k \subseteq \mathcal{W}^k$ such that for every input vector in $\mathcal{J}^k$, the function vector $\bar{f}(\bar{\imath})$ will evaluate to the state vector $\bar{v}$, and for every input vector that is not in $\mathcal{J}^k$, at least one function $f_i(\bar{\imath})$ will not match the value of the bit v_i. Mathematically, we want $\mathcal{J}^k$ to satisfy the following three conditions:

(I) $\mathcal{J}^k \neq \emptyset$

(II) $\forall \bar{\imath} \in \mathcal{J}^k. \bar{f}(\bar{\imath}) = \bar{v}$

(III) $\forall \bar{\imath} \notin \mathcal{J}^k. \bar{f}(\bar{\imath}) \neq \bar{v}$

Any $\bar{\imath}$ from $\mathcal{J}^k$ will suffice for our purpose. In condition (III), the type of $\bar{\imath}$ was

implicitly assumed to be $\bar{\iota} \in \mathcal{W}^k$, thus, $\bar{\iota} \notin \mathcal{J}^k$ means $\bar{\iota} \in \mathcal{W}^k \setminus \mathcal{J}^k$. Throughtout the rest of the proof, we will not explicitly denote that $\bar{\iota} \in \mathcal{W}^k$ and continue to use $\iota \notin \mathcal{J}^k$ notation.

The reason for proving a stronger invariant is as follows. In the first part of the proof, we could construct the parameter vector $(p_1, p_2, \ldots, p_n)$ incrementally. In this case, however, we have to provide a complete input vector $\bar{\iota}$ for each bit such that the same input vector gives the values $h_1(p_1), h_2(p_1, p_2), \ldots$, to the state bits. If we provide some input vector $\bar{\iota}_1$ such that $f_1(\bar{\iota}_1) = h_1(p_1)$, it may very well be the case that when we go to the next bit, it $f_2(\bar{\iota}_1) \neq h_2(p_2, p_2)$. So we have to come up with another input vector $\bar{\iota}_2$ such that $f_1(\bar{\iota}_2) = h_1(p_1)$ and $f_2(\bar{\iota}_2) = h_2(p_1, p_2)$. This means we have to revisit the previous state bits, not a desirable situation. Instead, we begin with the largest set of input vectors that satisfy the equality for the first bit, and then gradually keep on removing those input vectors that violate the equalities for later bits. The heart of the proof is then to show that in this process, we do not end up without any input vector at all.

Base Case: $n = 1$

By definition, we have $\forall \bar{\iota} \in \mathcal{W}^k.\rho_1(\bar{\iota}) = 1$. Therefore, we conclude $h_1^\alpha = (\forall \iota \in \mathcal{W}^k.f_1(\bar{\iota}) = \alpha), \alpha \in \{0, 1\}$ from definition of h_i^α. Since h_1^1, h_1^0 and h_1^c are mutually exclusive, only one of them is 1 and the rest are 0. We have two cases depending on whether $v_1 = 0$ or $v_1 = 1$.

Case 1: $v_1 = 1$.

Since $v_1 = h_1(p_1)$ which is equal to $h_1^1 \vee p_1 \cdot h_1^c$, we have two sub-cases to consider: If $h_1^1 = 1$, then $\forall \bar{\iota} \in \mathcal{W}^k.f_1(\bar{\iota}) = 1$, as $\rho_1 = 1$. In this case, $\mathcal{J}^k = \mathcal{W}^k$ and $\mathcal{J}^k$ is obviously non empty. Moreover, conditions (II) and (III) are also clearly satisfied by $\mathcal{J}^k$.

On the other hand, if $p_1 = 1$ and $h_1^c = 1$, then this implies that $h_1^0 = 0$. We choose $\mathcal{J}^k = \{\bar{\iota} \in \mathcal{W}^k \mid f_1(\bar{\iota}) = 1\}$ to satisfy condition (II). $\mathcal{J}^k$ is non empty, since there exist at least one $\bar{\iota}$ such that $f_1(\bar{\iota}) = 1$, due to $h_1^0 = 0$. Moreover, $f_1(\bar{\iota}) \neq 1$ for any $\bar{\iota} \notin \mathcal{J}^k$ by definition. Thus, $\mathcal{J}^k$ also satisfies condition (III).

Case 2: $v_1 = 0$.

Since $v_1 = h_1(p_1)$, which is equal to $h_1^1 \vee p_1 \cdot h_1^c$, we have $h_1^1 = 0$ and either $h_1^c = 0$ or $p_1 = 0$. So there are two sub-cases to consider: If $h_1^c = 0$, then $h_1^0 = 1$. As $\rho_1 = 1$, this implies that $\forall \bar{\iota} \in \mathcal{W}^k . f_1(\bar{\iota}) = 0$. In this case, $\mathcal{J}^k = \mathcal{W}^k$ and $\mathcal{J}^k$ is obviously non empty. Moreover, conditions (II) and (III) are also clearly satisfied by $\mathcal{J}^k$.

On the other hand, if $h_1^c = 1$, this implies that $p_1 = 0$, we choose $\mathcal{J}^k = \{\bar{\iota} \in \mathcal{W}^k \mid f_1(\bar{\iota}) = 0\}$ to satisfy condition (II). $\mathcal{J}^k$ is non empty, since there exist at least one $\bar{\iota}$ such that $f_1(\bar{\iota}) = 0$, due to $h_1^1 = 0$. Moreover, $f_1(\bar{\iota}) \neq 0$ for any $\bar{\iota} \notin \mathcal{J}^k$ by definition. Therefore, $\mathcal{J}^k$ also satisfies condition (III).

Thus, in both cases, we have found a $\mathcal{J}^k$ with the desired properties.

Induction Step : $n \to n+1$

The induction hypothesis is that

$$\forall \bar{v} \in \mathcal{Y}_n . \exists \mathcal{J}^k \subseteq \mathcal{W}^k . \left[\mathcal{J}^k \neq \emptyset \wedge \mathcal{J}^k = \left\{ \bar{\iota} \in \mathcal{W}^k | \bigwedge_{i=1}^{n} f_i(\bar{\iota}) = v_i \right\} \right]$$

We need to prove this for $n+1$, i.e.,

$$\forall \bar{v} \in \mathcal{Y}_{n+1} . \exists \mathcal{K}^k \subseteq \mathcal{W}^k . \left[\mathcal{K}^k \neq \emptyset \wedge \mathcal{K}^k = \left\{ \bar{\iota} \in \mathcal{W}^k | \bigwedge_{i=1}^{n+1} f_i(\bar{\iota}) = v_i \right\} \right]$$

For clarity, we use $\mathcal{J}^k$ for the induction hypothesis and $\mathcal{K}^k$ for the claim. Suppose we are given $\bar{v} = (v_1, v_2, \ldots, v_{n+1}) \in \mathcal{Y}_{n+1}$. By the induction hypothesis, there exists a non empty $\mathcal{J}^k$ such that $\forall \bar{\iota} \in \mathcal{J}^k . f_1(\bar{\iota}) = v_1 \wedge \ldots \wedge f_n(\bar{\iota}) = v_n$. We provide a non empty $\mathcal{K}^k \subseteq \mathcal{J}^k$ such that $\forall \bar{\iota} \in \mathcal{K}^k . f_{n+1}(\bar{\iota}) = v_{n+1}$ and $\forall \bar{\iota} \in \mathcal{J}^k \setminus \mathcal{K}^k . f_{n+1}(\bar{\iota}) \neq v_{n+1}$.

Then, since $\mathcal{K}^k \subseteq \mathcal{J}^k$, we already have $\forall \bar{\iota} \in \mathcal{K}^k . f_1(\bar{\iota}) = v_1 \wedge \ldots \wedge f_n(\bar{\iota}) = v_n$. Therefore, $\mathcal{K}^k$ satisfies condition (II). If $\bar{\iota} \notin \mathcal{K}^k$, then there are two cases depending on whether $\bar{\iota}$ is in $\mathcal{J}^k$ or not. If $\bar{\iota}$ is in $\mathcal{J}^k$, then the function f_{n+1} disagrees with v_{n+1}. Otherwise, induction hypothesis gives us that at least one of $f_i(\bar{\iota})$ disagrees with v_i for $i \leq n$. Thus, $\mathcal{K}^k$ satisfies condition (III) as well.

We find the subset $\mathcal{K}^k$ of $\mathcal{J}^k$ as follows.

Since we have $\bar{v} \in \mathcal{Y}_{n+1}$, there is an assignment $\bar{p} = (p_1, p_2, \ldots, p_{n+1})$ such that $h_1(\bar{p}) = v_1 \wedge \ldots h_{n+1}(\bar{p}) = v_{n+1}$. Before commencing our inductive proof, we need to establish that $h^{\alpha}_{n+1} = \forall \bar{\iota} \in \mathcal{J}^k . f_{n+1}(\bar{\iota}) = \alpha$. Note that for all input vectors $\bar{\iota} \in \mathcal{J}^k$, $\rho_{n+1}(p_1, p_2, \ldots, p_n, \bar{\iota}) = 1$ by definition of ρ_{n+1} and by induction hypothesis. Moreover, $\forall \bar{\iota} \notin \mathcal{J}^k . \rho_{n+1}(p_1, p_2, \ldots, p_n, \bar{\iota}) = 0$. We will use these facts in the derivation next.

$$
\begin{aligned}
h^{\alpha}_{n+1} &= \forall \bar{\iota} \in \mathcal{W}^k . \left(\rho_{n+1} \Rightarrow f_{n+1}(\bar{\iota}) = \alpha\right) \\
&= \Big(\forall \bar{\iota} \in \mathcal{J}^k . \left(\rho_{n+1} \Rightarrow f_{n+1}(\bar{\iota}) = \alpha\right)\Big) \bigwedge \\
&\quad \Big(\forall \bar{\iota} \notin \mathcal{J}^k . \left(\rho_{n+1} \Rightarrow f_{n+1}(\bar{\iota}) = \alpha\right)\Big) \\
&= \Big(\forall \bar{\iota} \in \mathcal{J}^k . \left(1 \Rightarrow f_{n+1}(\bar{\iota}) = \alpha\right)\Big) \bigwedge \\
&\quad \Big(\forall \bar{\iota} \notin \mathcal{J}^k . \left(0 \Rightarrow f_{n+1}(\bar{\iota}) = \alpha\right)\Big) \\
&= \Big(\forall \bar{\iota} \in \mathcal{J}^k . \left(f_{n+1}(\bar{\iota}) = \alpha\right)\Big) \bigwedge 1 \\
\text{Thus, } h^{\alpha}_{n+1} &= \forall \bar{\iota} \in \mathcal{J}^k . f_{n+1}(\bar{\iota}) = \alpha.
\end{aligned}
$$

Since h^1_{n+1}, h^0_{n+1} and h^c_{n+1} are mutually exclusive, only one of them is 1 and the other two are 0. We have two cases depending on whether $v_{n+1} = 0$ or $v_{n+1} = 1$.

<u>Case 1: $v_{n+1} = 1$.</u>

Since $v_{n+1} = h_{n+1}(\bar{p})$, which is equal to $h^1_{n+1} \vee p_{n+1} \cdot h^c_{n+1}$, we have two sub-cases

to consider. If $h^1_{n+1} = 1$, then $\forall \bar{\iota} \in \mathcal{J}^k . f_{n+1}(\bar{\iota}) = 1$, as $\rho_{n+1} = 1$. In this case, $\mathcal{K}^k = \mathcal{J}^k$ and $\mathcal{K}^k$ is non empty since $\mathcal{J}^k$ is. $\mathcal{K}^k$ also satisfies condition (II) as the first n functions match the first n bits by induction and the last function matches the last bit 1 by the argument above. If $\bar{\iota} \notin \mathcal{K}^k$, then $\bar{\iota} \notin \mathcal{J}^k$, and at least one of $f_1, f_2, \ldots, f_n$ does not match the value of the corresponding bit. Thus, condition (III) is also satisfied by $\mathcal{K}^k$.

On the other hand, if $h^c_{n+1} = 1$ and $p_{n+1} = 1$, then this implies that $h^0_{n+1} = 0$. We choose $\mathcal{K}^k = \{\bar{\iota} \in \mathcal{J}^k \mid f_{n+1}(\bar{\iota}) = 1\}$ to satisfy condition (II). $\mathcal{K}^k$ is non empty, since there exist at least one $\bar{\iota} \in \mathcal{J}^k$ such that $f_{n+1}(\bar{\iota}) = 1$, due to $h^0_{n+1} = 0$. For $\bar{\iota} \notin \mathcal{K}^k$, if $\bar{\iota} \in \mathcal{J}^k$, then $f_{n+1}(\bar{\iota}) \neq 1$. Otherwise, $\bar{\iota} \notin \mathcal{J}^k$, and inductive hypothesis gives us at least one $f_i, 1 \leq i \leq n$ such that $f_i(\bar{\iota}) \neq v_i$. Thus, $\mathcal{K}^k$ also satisfies condition (III).

Case 2: $v_{n+1} = 0$.

Since $v_{n+1} = h_{n+1}(\bar{p})$, which is equal to $h^1_{n+1} \vee p_{n+1} \cdot h^c_{n+1}$, we have $h^1_{n+1} = 0$ and either $h^c_{n+1} = 0$ or $p_{n+1} = 0$. Thus, we have two sub-cases to consider. If $h^c_{n+1} = 0$, then $h^0_{n+1} = 1$, so $\forall \bar{\iota} \in \mathcal{J}^k . f_{n+1}(\bar{\iota}) = 0$. In this case, $\mathcal{K}^k = \mathcal{J}^k$ and $\mathcal{K}^k$ is non empty since $\mathcal{J}^k$ is. $\mathcal{K}^k$ also satisfies condition (II) as the first n functions match the first n bits by induction and the last function matches the last bit 1 by the argument above. If $\bar{\iota} \notin \mathcal{K}^k$, then $\bar{\iota} \notin \mathcal{J}^k$, and at least one of $f_1, f_2, \ldots, f_n$ does not match the value of the corresponding bit. Thus, condition (III) is also satisfied by $\mathcal{K}^k$.

On the other hand, if $h^c_{n+1} = 1$, then $p_{n+1} = 0$ and we choose $\mathcal{K}^k = \{\bar{\iota} \in \mathcal{J}^k \mid f_{n+1}(\bar{\iota}) = 0\}$ to satisfy condition (II). $\mathcal{K}^k$ is non empty, since there exist at least one $\bar{\iota} \in \mathcal{J}^k$ such that $f_{n+1}(\bar{\iota}) = 0$, due to $h^1_{n+1} = 0$. For $\bar{\iota} \notin \mathcal{K}^k$, if $\bar{\iota} \in \mathcal{J}^k$, then $f_{n+1}(\bar{\iota}) \neq 0$. Otherwise, $\bar{\iota} \notin \mathcal{J}^k$, and inductive hypothesis gives us at least one $f_i, 1 \leq i \leq n$ such that $f_i(\bar{\iota}) \neq v_i$. Thus, $\mathcal{K}^k$ also satisfies condition (III).

Therefore, in both cases, we have found a $\mathcal{J}^k$ with the desired properties.

Hence, by the induction principle, we can always provide a $\mathcal{J}^k$ such that $\forall \bar{\iota} \in \mathcal{J}^k . \bar{f}(\bar{\iota}) = \bar{v}$. We can choose any $\bar{\iota}$ from $\mathcal{J}^k$. Therefore, $\bar{v} \in \mathcal{X}$, hence $\mathcal{Y} \subseteq \mathcal{X}$.

QED.

Appendix C

Proof of Theorem 4

in the proof, we will sometimes use subscripts n or $n+1$ to the symbols $\mathcal{X}, \mathcal{Y}, \mathcal{P}$, etc., to emphasize the length of the vectors that constitute these sets. We need to establish the following first.

$$\begin{aligned}
h_i^{\alpha} &= \forall t \in \mathcal{S}^{k+1}.\, (\rho_i \Rightarrow (t(k)_i = \alpha))\,, \text{ where } \alpha \text{ is either 0 or 1} \\
&= (\forall t \in \mathcal{T}_k.\, (\rho_i \Rightarrow (t(k)_i = \alpha))) \bigwedge (\forall t \notin \mathcal{T}_k.\, (\rho_i \Rightarrow (t(k)_i = \alpha))) \\
&= (\forall t \in \mathcal{T}_k.\, (\rho_i \Rightarrow (t(k)_i = \alpha))) \bigwedge (\forall t \notin \mathcal{T}_k.\, (0 \Rightarrow (t(k)_i = \alpha))) \\
&= (\forall t \in \mathcal{T}_k.\, (\rho_i \Rightarrow (t(k)_i = \alpha))) \bigwedge 1 \\
&= \forall t \in \mathcal{T}_k.(\rho_i \Rightarrow (t(k)_i = \alpha)).
\end{aligned}$$

$\boxed{\mathcal{X} \subseteq \mathcal{Y}}$

If $\mathcal{X} = \emptyset$, then obviously $\mathcal{X} \subseteq \mathcal{Y}$. Otherwise, let $\bar{v}$ be an arbitrary element of $\mathcal{X}$. Then by definition of $\mathcal{X}$, there exists a valid trace $t \in \mathcal{T}_k$ such that $t(k)_1 = v_1 \wedge \ldots \wedge t(k)_n = v_n$. In order to show that $\bar{v} \in \mathcal{Y}$, we have to provide an assignment $\bar{p} \in \mathcal{P}$ such that $h_1(\bar{p}) = v_1 \wedge \ldots \wedge h_n(\bar{p}) = v_n$.

We will prove the existence of such $(p_1, p_2, \ldots, p_n)$ by induction on n. Formally,

we establish the following by induction on n.

$$\forall \bar{v} \in \mathcal{X}_n . \exists \bar{p} \in \mathcal{P}_n . h_1(\bar{p}) = v_1 \wedge \ldots \wedge h_n(\bar{p}) = v_n .$$

Base Case: $n = 1$

By definition,

$$\rho_i(p_1, \ldots, p_{i-1}, t) = \tau(t) \wedge (t(k)_1 = h_1(p_1)) \wedge \ldots (t(k)_{i-1} = h_{i-1}(p_1, \ldots, p_{i-1})).$$

It is vacuously true that $\rho_1(t)$ is 1 for any valid trace t, or formally $\forall t \in \mathcal{T}_k . \rho_1(t) = 1$. Therefore,

$$\begin{aligned} h_1^{\alpha} &= \forall t \in \mathcal{T}_k . (\rho_1(t) \Rightarrow t(k)_1 = \alpha) \\ &= \forall t \in \mathcal{T}_k . (t(k)_1 = \alpha), \end{aligned}$$

for both $\alpha = 0$ and $\alpha = 1$. Thus, h_i^{α} evaluates to constant 0 or 1 as it has no arguments.

There are two cases to consider, depending on whether v_1 is 1 or 0. Suppose $v_1 = 1$. Since there exists a valid trace t for which $t(k)_1 = 1$, the first bit v_1 is not forced to 0. Therefore, h_1^0, the condition under which v_1 is forced to 0, has to be false. Since h_1^1, h_1^0, and h_1^c are mutually exclusive, only one of them is 1 and the other two are 0. Thus, there are two possibilities left. Either $h_1^1 = 1$ or $h_1^c = 1$. If $h_1^1 = 1$, then $h_1(p_1) = h_1^1 \vee p_1 \cdot h_1^c = 1$ for any p_1. On the other hand, if $h_1^c = 1$, then $h_1(p_1) = p_1$, so we choose $p_1 = 1$. Then $h_1(p_1) = p_1 \Rightarrow h_1(p_1) = 1$. The case $v_1 = 0$ is similar. Both cases establish the base case of the induction.

Induction Step: $n \rightarrow n + 1$

The induction hypothesis is

$$\forall \bar{v} \in \mathcal{X}_n . \exists \bar{p} \in \mathcal{P}_n . h_1(\bar{p}) = v_1 \wedge \ldots \wedge h_n(\bar{p}) = v_n .$$

Here, $\mathcal{X}_n$ and $\mathcal{P}_n$ are used to emphasize that $\bar{v}$ and $\bar{p}$ are assignments to n variables. We have to prove that

$$\forall \bar{v} \in \mathcal{X}_{n+1}.\exists \bar{p} \in \mathcal{P}_{n+1}.h_1(\bar{p}) = v_1 \wedge \ldots \wedge h_{n+1}(\bar{p}) = v_{n+1}.$$

Let $\bar{v} = (v_1, \ldots, v_{n+1}) \in \mathcal{X}_{n+1}$. Then by definition of $\mathcal{X}_{n+1}$, there exists a $t \in \mathcal{T}_k$ such that $t(k)_1 = v_1 \wedge \ldots \wedge t(k)_{n+1} = v_{n+1}$. According to the induction hypothesis, there exists $(p_1, \ldots, p_n)$ such that $h_1(p_1) = v_1 \wedge \ldots \wedge h_n(p_1, p_2, \ldots, p_n) = v_n$. We will extend this assignment by p_{n+1} such that $h_{n+1}(p_1, \ldots, p_{n+1}) = v_{n+1}$. By definition, h^1_{n+1}, h^0_{n+1} and h^c_{n+1} depend only on $p_1, \ldots, p_n$. Thus, the assignment $(p_1, \ldots, p_n)$ assigns specific values to these three functions. They are also mutually exclusive. We also have

$$\begin{aligned} \rho_{n+1}(p_1, \ldots, p_n, t) &= \tau(t) \wedge (t(k)_1 = h_1(p_1)) \wedge \ldots (t(k)_n = h_n(p_1, \ldots, p_n)) \\ &= \tau(t), \text{ since } v_i = t(k)_i \text{ and by the induction hypothesis} \end{aligned}$$

Moreover, by definition,

$$h^\alpha_{n+1}(p_1, p_2, \ldots, p_n) \quad = \quad \forall t \in \mathcal{T}_k.(\rho_{n+1}(p_1, \ldots, p_n, t) \Rightarrow t(k)_{n+1} = \alpha)$$

for both $\alpha = 1$ and $\alpha = 0$. Thus, if there is at least one valid trace for which ρ_{n+1} evaluates to 1 and $t(k)_{n+1}$ evaluates to $\neg\alpha$, then $h^\alpha_{n+1} = 0$. For the specific valid trace t we are considering, we have shown that $\rho_{n+1} = 1$.

As in the base case, we have two cases when v_{n+1} is either 0 or 1. We will just show the case $v_1 = 1$. Since there exists a valid trace t (the one we are considering) for which $\rho_i(p_1, p_2, \ldots, p_n, t) = 1$ and $t(k)_{n+1} = 1$ hold, h^0_{n+1}, the condition under which $t(k)_{n+1}$ is forced to 0, is false (or 0). As h^0_{n+1}, h^1_{n+1} and h^c_{n+1} are mutually exclusive, there are two sub-cases to consider. If $h^1_{n+1} = 1$, then $h_{n+1}(p_1, \ldots, p_{n+1}) = h^1_{n+1} \vee p_{n+1} \cdot h^c_{n+1} = 1$ for any p_{n+1}. On the other hand, if $h^c_{n+1} = 1$, then $h_{n+1}(p_1, \ldots p_{n+1}) = p_{n+1}$. In that case, we choose $p_{n+1} = 1$. Then $h_{n+1}(p_{n+1}) = p_{n+1} \Rightarrow h_{n+1}(p_{n+1}) = 1$. The case

$v_1 = 0$ is similar. So in both cases, we can choose p_{n+1} such that h_{n+1} evaluates to v_{n+1}.

Thus, the vector $\bar{p} = (p_1, p_2, \ldots, p_n, p_{n+1})$ has the desired property $h_1(\bar{p}) = v_1 \wedge \ldots \wedge h_{n+1}(\bar{p}) = v_{n+1}$. This holds for $p_1, \ldots, p_n$ by the induction hypothesis, and for p_{n+1} by the arguments above. This establishes the induction step. Thus, we have provided an assignment $\bar{p}$ such that $\bar{h}(\bar{p}) = \bar{v}$ for a given $\bar{v} \in \mathcal{X}$. Thus $\bar{v} \in \mathcal{Y}$, hence $\mathcal{X} \subseteq \mathcal{Y}$.

$\boxed{\mathcal{Y} \subseteq \mathcal{X}}$

If $\mathcal{Y} = \emptyset$, then the relation obviously holds. Otherwise, suppose $\bar{v} \in \mathcal{Y}$. Then by definition of $\mathcal{Y}$, there exists $\bar{p} \in \mathcal{P}$ such that $h_1(\bar{p}) = v_1 \wedge \ldots \wedge h_n(\bar{p}) = v_n$. In order to show that $\bar{v} \in \mathcal{X}$, we have to provide a valid trace t such that $t(k)_1 = v_1 \wedge \ldots \wedge t(k)_n = v_n$. However, instead of giving just one such trace t, we will compute the largest set $\mathcal{J}_k \subseteq \mathcal{T}_k$ of traces such that any trace in $\mathcal{J}_k$ will have the desired property. Formally, we will prove the following stronger claim by induction on n:

$$\forall \bar{v} \in \mathcal{Y}. \exists \mathcal{J}_k \subseteq \mathcal{T}_k. [\mathcal{J}_k \neq \emptyset \wedge \mathcal{J}_k = \{t \in \mathcal{T}_k | t(k) = \bar{v}\}]$$

Thus, we provide a non-empty set of valid traces $\mathcal{J}_k \subseteq \mathcal{T}_k$ such that for every trace t in $\mathcal{J}_k$, the last state in t is $\bar{v}$, and for every trace that is not in $\mathcal{J}_k$, at least one bit $t(k)_i$ does not match the value of the bit v_i. Mathematically, we want $\mathcal{J}_k$ to satisfy the following three conditions: **(I)** $\mathcal{J}_k \neq \emptyset$, **(II)** $\forall t \in \mathcal{J}_k . t(k) = \bar{v}$, and, **(III)** $\forall t \notin \mathcal{J}_k . t(k) \neq \bar{v}$. Any t from $\mathcal{J}_k$ will suffice for our purpose.

The reason for proving a stronger invariant is as follows. In the first part of the proof, we could construct the parameter vector $(p_1, p_2, \ldots, p_n)$ incrementally. In this case, however, we have to provide a complete valid trace t for each state bit such that the same trace has the values $h_1(p_1), h_2(p_1, p_2), \ldots$, etc., for the last state bits. If we provide some valid trace t' such that $t'(k)_1 = h_1(p_2)$, it may very well be the case

that when we go to the next bit, $t'(k)_2 \neq h_2(p_2, p_2)$. So we have to come up with another trace t'' such that $t''(k)_1 = h_1(p_1)$ and $t''(k)_2 = h_2(p_1, p_2)$. Instead, we begin with the largest set of traces that satisfy the equality for the first bit and then keep on removing those traces that violate the equalities for later bits. The heart of the proof is then to show that in this process, we do not end up without any trace.

Base Case: $n = 1$

By definition, we have $\forall t \in \mathcal{T}_k.\rho_1(t) = 1$. Therefore, we conclude $h_1^\alpha = (\forall t \in \mathcal{T}_k.t(k)_1 = \alpha), \alpha \in \{0, 1\}$ from the definition of h_i^α. Since h_1^1, h_1^0 and h_1^c are mutually exclusive, only one of them is 1 and the rest are 0. We have two cases depending on whether $v_1 = 0$ or $v_1 = 1$. As before, we'll just show one case $v_1 = 0$. Since $v_1 = h_1(p_1)$, which is equal to $h_1^1 \vee p_1 \cdot h_1^c$, we have $h_1^1 = 0$ and either $h_1^c = 0$ or $p_1 = 0$. So there are two sub-cases to consider: If $h_1^c = 0$, then $h_1^0 = 1$. As $\forall t \in \mathcal{T}_k.\rho_1(t) = 1$, this implies that $\forall t \in \mathcal{T}_k.t(k)_1 = 0$. In this case, $\mathcal{J}_k = \mathcal{T}_k$ and $\mathcal{J}_k$ is obviously non empty as we have assumed that the set of valid traces of length k is non-empty. Moreover, conditions (II) and (III) are also clearly satisfied by $\mathcal{J}_k$. On the other hand, if $h_1^c = 1$, this implies that $p_1 = 0$, we choose $\mathcal{J}_k = \{t \in \mathcal{T}_k \mid t(k)_1 = 0\}$ to satisfy condition (II). $\mathcal{J}_k$ is non-empty, since there exist at least one valid trace t such that $t(k)_1 = 0$, due to $h_1^1 = 0$. Moreover, $t(k)_1 \neq 0$ for any $t \notin \mathcal{J}_k$ by definition. Therefore, $\mathcal{J}_k$ also satisfies condition (III).

The case $v_1 = 1$ is similar. Thus, in both cases, we have found a $\mathcal{J}_k$ with the desired properties.

Induction Step : $n \to n + 1$

The induction hypothesis is that

$$\forall \bar{v} \in \mathcal{Y}_n.\exists \mathcal{J}_k \subseteq \mathcal{T}_k.\left[\mathcal{J}_k \neq \emptyset \wedge \mathcal{J}_k = \{t \in \mathcal{T}_k | t(k) = \bar{v}\}\right]$$

We need to prove this for $n+1$, i.e.,

$$\forall \bar{v} \in \mathcal{Y}_{n+1}.\exists \mathcal{K}_k \subseteq \mathcal{T}_k.\, [\mathcal{K}_k \neq \emptyset \wedge \mathcal{K}_k = \{t \in \mathcal{T}_k | t(k) = \bar{v}\}]$$

For clarity, we use $\mathcal{J}_k$ for the induction hypothesis and $\mathcal{K}_k$ for the claim. Suppose we are given $\bar{v} = (v_1, v_2, \ldots, v_{n+1}) \in \mathcal{Y}_{n+1}$. By the induction hypothesis, there exists a non-empty $\mathcal{J}_k$ such that $\forall t \in \mathcal{J}_k.t(k)_1 = v_1 \wedge \ldots \wedge t(k)_n = v_n$. We will provide a non-empty $\mathcal{K}_k \subseteq \mathcal{J}_k$ such that $\forall t \in \mathcal{K}_k.t(k)_{n+1} = v_{n+1}$ and $\forall t \in \mathcal{J}_k \setminus \mathcal{K}_k.t(k)_{n+1} \neq v_{n+1}$. Then, since $\mathcal{K}_k \subseteq \mathcal{J}_k$, we already have $\forall t \in \mathcal{K}_k.t(k)_1 = v_1 \wedge \ldots \wedge t(k)_n = v_n$. Therefore, $\mathcal{K}_k$ satisfies condition (II). If $t \notin \mathcal{K}_k$, then there are two cases depending on whether t is in $\mathcal{J}_k$ or not. If t is in $\mathcal{J}_k$, then $t(k)_{n+1}$ disagrees with v_{n+1}. Otherwise, induction hypothesis gives us that at least one of $t(k)_i$ disagrees with v_i for $i \leq n$. Thus, $\mathcal{K}_k$ satisfies condition (III) as well.

We find $\mathcal{K}_k$ as follows.

Since $\bar{v} \in \mathcal{Y}_{n+1}$, there is an assignment to parameters $\bar{p} = (p_1, \ldots, p_{n+1})$ such that $h_1(\bar{p}) = v_1 \wedge \ldots h_{n+1}(\bar{p}) = v_{n+1}$. Before commencing our inductive proof, we need to establish that $h^{\alpha}_{n+1} = \forall t \in \mathcal{J}_k.t(k)_{n+1} = \alpha$. Note that for all traces $t \in \mathcal{J}_k$, $\rho_{n+1}(p_1, p_2, \ldots, p_n, t) = 1$ by definition of ρ_{n+1} and by induction hypothesis. Moreover, $\forall t \notin \mathcal{J}_k.\rho_{n+1}(p_1, p_2, \ldots, p_n, t) = 0$. We will use these facts in the derivation next.

$$\begin{aligned}
h^{\alpha}_{n+1} &= \forall t \in \mathcal{T}_k.\, (\rho_{n+1} \Rightarrow (t(k)_{n+1} = \alpha)) \\
&= (\forall t \in \mathcal{J}_k.\, (\rho_{n+1} \Rightarrow (t(k)_{n+1} = \alpha))) \bigwedge (\forall t \notin \mathcal{J}_k.\, (\rho_{n+1} \Rightarrow (t(k)_{n+1} = \alpha))) \\
&= (\forall t \in \mathcal{J}_k.\, (1 \Rightarrow (t(k)_{n+1} = \alpha))) \bigwedge (\forall t \notin \mathcal{J}_k.\, (0 \Rightarrow (t(k)_{n+1} = \alpha))) \\
&= (\forall t \in \mathcal{J}_k.\, (t(k)_{n+1} = \alpha)) \bigwedge 1 \\
&= \forall t \in \mathcal{J}_k.(t(k)_{n+1} = \alpha).
\end{aligned}$$

Since h^1_{n+1}, h^0_{n+1} and h^c_{n+1} are mutually exclusive, only one of them is 1 and the other two are 0. We have two cases depending on whether $v_{n+1} = 0$ or $v_{n+1} = 1$. We will only show the case $v_{n+1} = 0$. Since $v_{n+1} = h_{n+1}(\bar{p})$, which is equal to $h^1_{n+1} \vee p_{n+1} \cdot h^c_{n+1}$, we have $h^1_{n+1} = 0$ and either $h^c_{n+1} = 0$ or $p_{n+1} = 0$. Thus, we have two sub-cases to consider. If $h^c_{n+1} = 0$, then $h^0_{n+1} = 1$, so $\forall t \in \mathcal{J}_k.t(k)_{n+1} = 0$. In this case, $\mathcal{K}_k = \mathcal{J}_k$ and $\mathcal{K}_k$ is non-empty since $\mathcal{J}_k$ is. On the other hand, if $h^c_{n+1} = 1$, then $p_{n+1} = 0$ and we choose $\mathcal{K}_k = \{t \in \mathcal{J}_k \mid t(k)_{n+1} = 0\}$ to satisfy condition (II). $\mathcal{K}_k$ is non-empty, since there exist at least one $t \in \mathcal{J}_k$ such that $t(k)_{n+1} = 0$, due to $h^1_{n+1} = 0$. The case $v_1 = 1$ is similar. Therefore, in both cases, we have found a $\mathcal{J}_k$ with the desired properties.

Hence, by the induction principle, we can always provide a $\mathcal{J}_k$ such that $\forall t \in \mathcal{J}_k.t(k) = \bar{v}$. We can choose any t from $\mathcal{J}_k$. Therefore, $\bar{v} \in \mathcal{X}$, hence $\mathcal{Y} \subseteq \mathcal{X}$.

QED.

Bibliography

[1] Mark D. Aagaard, Robert B. Jones, and Carl-Johan H. Seger. Formal verification using parametric representations of boolean constraints. In *Proceedings of Design Automation Conference (DAC'99)*, pages 402–407. ACM Press, June 1999.

[2] Nina Amla, Xiaoqun Du, Andreas Kuehlmann, Robert P. Kurshan, and Kenneth L. McMillan. An analysis of sat-based model checking techniques in an industrial environment. In *CHARME*, pages 254–268, 2005.

[3] Felice Balarin and Alberto L. Sangiovanni-Vincentelli. An iterative approach to language containment. In *Conference on Computer Aided Verification (CAV 1993)*, pages 29–40, 1993.

[4] C. J. P. B'elisle. Convergence theorems for a class of simulated annealing algorithms. *Journal of Applied Probability*, 29:885–892, 1992.

[5] Armin Biere, Alessandro Cimatti, Edmund M. Clarke, M. Fujita, and Yunshan Zhu. Symbolic model checking using SAT procedures instead of BDDs. In *Proceedings of the Design Automation Conference (DAC'99)*, pages 317–320, 1999.

[6] Armin Biere, Alessandro Cimatti, Edmund M. Clarke, Ofer Strichman, and Yunshan Zhu. *Bounded Model Checking*, volume 58, chapter 3, pages 118–146. Academic Press, 2003.

[7] Armin Biere, Alexandro Cimatti, Edmund M. Clarke, and Yunshan Zhu. Symbolic model checking without BDDs. In *Proceedings of Tools and Algorithms for the Analysis and Construction of Systems (TACAS'99)*, number 1579 in LNCS, 1999.

[8] Jonathan Bowen. Formal methods virtual library. Online. http://vl.fmnet.info/.

[9] R. S. Boyer and J. S. Moore. *A Computational Logic Handbook*. Academic Press, New York, NY, USA, 1988.

[10] Randal E. Bryant. Graph-based algorithms for Boolean function manipulation. *IEEE Transactions on Computers*, C-35(8):677–691, August 1986.

[11] T. N. Bui and C. Jones. Finding good approximate vertex and edge partitions is NP-hard. *Information Processing Letters*, 42:153–159, 1992.

[12] J. R. Burch, E. M. Clarke, and D. E. Long. Representing circuits more efficiently in Symbolic Model Checking. In *28th ACM/IEEE Design Automation Conference*, 1991.

[13] J. R. Burch, E. M. Clarke, and D. E. Long. Symbolic Model Checking with partitioned transition relations. In A. Halaas and P. B. Denyer, editors, *Proceedings of the International Conference on Very Large Scale Int egration*, Edinburgh, Scotland, August 1991.

[14] J. R. Burch, E. M. Clarke, K. L. McMillan, and D. L. Dill. Sequential circuit verification using symbolic model checking. In *27th ACM/IEEE Design Automation Conference*, 1990.

[15] Pankaj Chauhan, Edmund M. Clarke, Somesh Jha, Jim Kukula, Tom Shiple, Helmut Veith, and Dong Wang. Non-linear quantification scheduling in image computation. In *Proceedings of ICCAD'01*, pages 293–298, November 2001.

[16] Pankaj Chauhan, Edmund M. Clarke, Somesh Jha, Jim Kukula, Helmut Veith, and Dong Wang. Using combinatorial optimization methods for quantification scheduling. In Tiziana Margaria and Tom Melham, editors, *Proceedings of CHARME'01*, volume 2144 of *LNCS*, pages 293–309, September 2001.

[17] Pankaj Chauhan, Edmund M. Clarke, and Daniel Kroening. A SAT based algorithm for reparameterization in symbolic simulation. Technical Report CMU-CS-03-191, Carnegie Mellon University, School of Computer Science, 2003.

[18] Pankaj Chauhan, Edmund M. Clarke, and Daniel Kroening. Using SAT based image computation for reachability analysis. Technical Report CMU-CS-03-151, Carnegie Mellon University, School of Computer Science, 2003.

[19] Pankaj Chauhan, Edmund M. Clarke, Samir Sapra, James Kukula, Helmut Veith, and Dong Wang. Automated abstraction refinement for model checking large state spaces using SAT based conflict analysis. In *Proceedings of FM-CAD'02*, volume 2517 of *LNCS*, pages 33–50, November 2002.

[20] A. Cimatti, E. M. Clarke, F. Giunchiglia, and M. Roveri. NuSMV: A new Symbolic Model Verifier. In N. Halbwachs and D. Peled, editors, *Proceedings of the International Conference on Computer-Aided Verification (CAV 1999)*, number 1633 in Lecture Notes in Computer Science, pages 495–499. Springer, July 1999.

[21] E. M. Clarke and E. A. Emerson. Synthesis of synchronization skeletons for branching time temporal logic. In *Logic of Programs: Workshop*, volume 131 of *Lecture Notes in Computer Science*. Springer-Verlag, Yorktown Heights, NY, May 1981.

[22] E. M. Clarke, E. A. Emerson, and A. P. Sistla. Automatic verification of finite-state concurrent systems using temporal logic specifications. *ACM Transactions on Programming Languages and Systems*, 8(2):244–263, 1986.

[23] E. M. Clarke, O. Grumberg, S. Jha, Y. Lu, and H. Veith. Counterexample-guided abstraction refinement. In E. A. Emerson and A. P. Sistla, editors, *Conference on Computer Aided Verification (CAV 2000)*, volume 1855 of *LNCS*, pages 154–169, July 2000.

[24] E. M. Clarke, O. Grumberg, and D. Peled. *Model Checking*. MIT Press, 2000.

[25] Edmund Clarke, Anubhav Gupta, James Kukula, and Ofer Strichman. SAT based abstraction-refinement using ILP and machine learning techniques. In *Conference on Computer Aided Verification (CAV 2002)*, 2002.

[26] Edmund Clarke, Somesh Jha, Yuan Lu, and Helmut Veith. Tree-like counterexamples in model checking. In *Proceedings of the 17th Annual IEEE Symposium on Logic in Computer Science (LICS'02)*, 2002.

[27] Edmund Clarke, Daniel Kroening, Joel Ouaknine, and Ofer Strichman. Computational challenges in bounded model checking. *Software Tools for Technology Transfer (STTT)*, 7(2):174–183, April 2005.

[28] Edmund M. Clarke, Daniel Kroening, Joël Ouaknine, and Ofer Strichman. Completeness and complexity of bounded model checking. In *VMCAI*, pages 85–96, 2004.

[29] Edmund M. Clarke and Jeannette M. Wing. Formal methods: State of the art and future directions. *ACM Computing Surveys*, 28(4):626–643, 1996.

[30] Olivier Coudert and Jean Christophe Madre. A unified framework for the formal verification of sequential circuits. In *Proc. Intl. Conf. on Computer-Aided Design (ICCAD)*, pages 78–82. IEEE Computer Society Press, November 1990.

[31] C.M. Fiduccia and R.M. Mattheyses. A linear time heuristic for improving network partitions. In *19th ACM/IEEE Design Automation Conference*, pages 175–181, 1982.

[32] Michael R. Garey and David S. Johnson. *Computers and Intractability: A Guide to the Theory of NP-Completeness*. W. H. Freeman & Co., 1979.

[33] D. Geist and I. Beer. Efficient Model Checking by automated ordering of transition relation partitions. In D. L. Dill, editor, *Sixth Conference on Computer Aided Verification (CAV 1994)*, volume 818 of *LNCS*, pages 299–310, Stanford, CA, USA, 1994. Springer-Verlag.

[34] Amit Goel. *A Unified Framework for Symbolic Simulation and Model Checking*. PhD thesis, Electrical and Computer Engineering, Carnegie Mellon University, 2003.

[35] Amit Goel and Randal E. Bryant. Set manipulation with boolean functional vectors for symbolic reachability analysis. In *Proceedings of Design Automation and Test in Europe (DATE'03)*, pages 10816–10821, 2003.

[36] Shankar G. Govindaraju and David L. Dill. Counterexample-guided choice of projections in approximate symbolic model checking. In *Proceedings of ICCAD'00*, San Jose, CA, November 2000.

[37] Alex Groce, Sagar Chaki, Daniel Kroening, and Ofer Strichman. Error explanation with distance metrics. *International Journal on Software Tools for Technology Transfer*, 8(3):229–247, June 2006.

[38] Aarti Gupta, Zijian Yang, Pranav Ashar, Lintao Zhang, and Sharad Malik. Partition-based decision heuristics for image computation using SAT and BDDs. In *Proc. of the Intl. Conf. on Computer-Aided Design (ICCAD)*, 2001.

[39] Aarti Gupta, Zijiang Yang, Pranav Ashar, and Anubhav Gupta. SAT-based image computation with application in reachability analysis. In Warren A. Hunt Jr. and Steven D. Johnson, editors, *Proceedings of FMCAD'00*, volume 1954 of *LNCS*, pages 354–371, November 2000.

[40] B. Hajek. A tutorial survey of theory and applications of simulated annealing. In *Proc. 24th IEEE Conf. Decision and Control*, pages 755–760, 1985.

[41] John Harrison. High-level verification using theorem proving and formalized mathematics. In *CADE-17: Proceedings of the 17th International Conference on Automated Deduction*, pages 1–6, London, UK, 2000. Springer-Verlag.

[42] Thomas A. Henzinger, Shaz Qadeer, and Sriram K. Rajamani. Decomposing refinement proofs using assume-guarantee reasoning. In *Proceedings of the International Conference on Computer-Aided Design (ICCAD)*, pages 245–252. IEEE Computer Society Press, 2000.

[43] Robert B. Jones. *Applications of symbolic simulation to the formal verification of microprocessors*. PhD thesis, Dept. of Electrical Engineering, Stanford University, 1999.

[44] Hyeong-Ju Kang and In-Cheol Park. SAT-based unbounded symbolic model checking. In *Proceedings of Design Automation Conference (DAC'03)*, pages 840–843, 2003.

[45] Brian Kernighan and S. Lin. An efficient heuristic procedure for partitioning graphs. *The Bell System Technical Journal*, pages 291–307, February 1970.

[46] S. Kirkpatrick, C. D. Gelatt Jr., and M. P. Vecchi. Optimization by simulated annealing. *Science*, 220:671–679, 1983.

[47] Donald E. Knuth. *The Art of Computer Programming*, volume 3: Sorting and Searching, chapter 6: Digital Searching, pages 495–512. Addison-Wesley, third edition, 1997.

[48] Daniel Kroening and Ofer Strichman. Efficient computation of recurrence diameters. In L. Zuck, P. Attie, A. Cortesi, and S. Mukhopadhyay, editors, *4th International Conference on Verification, Model Checking, and Abstract Interpretation*, volume 2575 of *Lecture Notes in Computer Science*, pages 298–309. Springer Verlag, January 2003.

[49] R. Kurshan. *Computer-Aided Verification of Co-ordinating Processes: The Automata-Theoretic Approach*. Princeton University Press, 1994.

[50] Shuvendu K. Lahiri, Randal E. Bryant, and Byron Cook. A symbolic approach to predicate abstraction. In *Proceedings of the International Conference on Computer-Aided Verification (CAV 2003)*, 2003.

[51] David E. Long. *Model checking, abstraction and compositional verification*. PhD thesis, Carnegie Mellon University, 1993. CMU-CS-93-178.

[52] Yuan Lu. *Automatic Abstraction in Model Checking*. PhD thesis, Department of Electrical and Computer Engineering, Carnegie Mellon University, Pittsburgh, PA 15213, Dec 2000. Available at http://www.cs.cmu.edu/ yuanlu/thesis.ps.

[53] Ken McMillan. Applying SAT methods in unbounded symbolic model checking. In Ed Brinksma and Kim Guldstrand Larsen, editors, *Proceedings of the International Conference on Computer-Aided Verification (CAV 2002)*, volume 2404 of *Lecture Notes in Computer Science*, pages 250–264. Springer, 2002.

[54] Kenneth L. McMillan. Interpolation and SAT-based model checking. In F. Somenzi and W. Hunt, editors, *Conference on Computer Aided Verification (CAV 2003)*, volume 2725 of *Lecture Notes in Computer Science*, pages 1–13. Springer, July 2003.

[55] Kenneth L. McMillan and Nina Amla. Automatic abstraction without counterexamples. In Hubert Garavel and John Hatcliff, editors, *Tools and Algorithms for the Construction and Analysis of Systems, 9th International Conference (TACAS 2003)*, volume 2619 of *Lecture Notes in Computer Science*, pages 2–17. Springer, 2003.

[56] N. Metropolis, A. W. Rosenbluth, M. N. Rosenbluth, A. H. Teller, and E. Teller. Equation of state calculations by fast computing machines. *Journal of Chemical Phyics*, 21(6):1087–1092, 1953.

[57] Maher Mneimneh and Karem Sakallah. SAT-based sequential depth computation. In *Proceedings of ASP-DAC*, January 2003.

[58] M. Oliver Möler and Rajeev Alur. Heuristics for hierarchical partitioning with application to model checking. In *Proceedings of CHARME*, 2001.

[59] In-Ho Moon, James H. Kukula, Kavita Ravi, and Fabio Somenzi. To split or to conjoin: The question in image computation. In *Proceedings of the 37th Design Automation Conference (DAC'00)*, pages 26–28, Los Angeles, June 2000.

[60] In-Ho Moon and Fabio Somenzi. Border-block triangular form and conjunction schedule in image computation. In Warren A. Hunt Jr. and Steven D. Johnson, editors, *Proceedings of the Formal Methods in Computer Aided Design (FMCAD'00)*, volume 1954 of *LNCS*, pages 73–90, November 2000.

[61] Matthew W. Moskewicz, Conor F. Madigan, Ying Zhao, Lintao Zhang, and Sharad Malik. Chaff: Engineering an efficient SAT solver. In *Proceedings of the Design Automation Conference (DAC'01)*, pages 530–535, 2001.

[62] Abelardo Pardo and Gary D. Hachtel. Incremental CTL model checking using BDD subsetting. In *Proceedings of the Design Automation Conference (DAC'98)*, pages 457–462, June 1998.

[63] Mukul R. Prasad, Armin Biere, and Aarti Gupta. A survey of recent advances in sat-based formal verification. *STTT*, 7(2):156–173, 2005.

[64] R.K. Ranjan, A. Aziz, B. Plessier, C. Pixley, and R.K. Brayton. Efficient BDD algorithms for FSM synthesis and verification. In *IEEE/ACM International Workshop on Logic Synthesis*, Lake Tahoe, 1995. IEEE/ACM.

[65] Richard Rudell. Espresso. Online. Available: http://www-cad.eecs.berkeley.edu/Software/software.html.

[66] Viktor Schuppan and Armin Biere. Efficient reduction of finite state model checking to reachability analysis. In *Proceedings of Software Tools for Technology Transfer*, 2003. Submitted for publication.

[67] Mary Sheeran, Satnam Singh, and Gunnar Stalmarck. Checking safety properties using induction and a SAT-solver. In Hunt and Johnson, editors, *Proc. Int. Conf. on Formal Methods in Computer-Aided Design (FMCAD'00)*, volume 1954 of *LNCS*, pages 108–125. Springer-Verlag, 2000.

[68] Shuo Sheng and Michael Hsiao. Efficient preimage computation using a novel success-driven atpg. In *Proceedings of Design Automation and Test in Europe (DATE'03)*, 2003.

[69] J. P. Marques Silva and K. A. Sakallah. GRASP: A new search algorithm for satisfiability. Technical Report CSE-TR-292-96, Computer Science and Engineering Division, Department of EECS, Univ. of Michigan, April 1996.

[70] H. Touati, H. Savoj, B. Lin, R. K. Brayton, and A. Sangiovanni-Vincentelli. Implicit enumeration of finite state machines using BDDs. In *Proceedings of the IEEE international Conference on Computer Aided Design (ICCAD)*, pages 130–133, November 1990.

[71] Jan van Leeuwen, editor. *Handbook of Theoretical Computer Science*, volume B: Formal Models and Sematics. Elsevier and MIT Press, 1990.

[72] Dong Wang, Pei-Hsin Ho, Jiang Long, James Kukula, Yunshan Zhu, Tony Ma, and Robert Damiano. Formal property verification by abstraction refinement with formal, simulation and hybrid engines. In *Proceedings of the DAC*, pages 35–40, 2001.

[73] Bwolen Yang. *Optimizing Model Checking Based on BDD Characterization*. PhD thesis, Carnegie Mellon University, Computer Science Department, May 1999.

[74] Jin Yang and Carl-Johan H. Seger. Generalized symbolic trajectory evaluation – abstraction in action. In *Proceedings of FMCAD'02*, volume 2517 of *LNCS*, pages 70–86, November 2002.

[75] Hantao Zhang. SATO: An efficient propositional prover. In *Proceedings of the Conference on Automated Deduction (CADE'97)*, pages 272–275, 1997.

[76] Lintao Zhang, Conor F. Madigan, Matthew W. Moskewicz, and Sharad Malik. Efficient conflict driven learning in a Boolean satisfiability solver. In *Proceedings of ICCAD'01*, November 2001.